DERIVED DISTRIBUTION OF WATER VOLUME ABOVE A GIVEN THRESHOLD DISCHARGE

by

SIU-ON CHAN

B.S., City College of New York
(1976)

SUBMITTED IN PARTIAL FULFILLMENT
OF THE REQUIREMENTS FOR THE
DEGREE OF

MASTER OF SCIENCE

at the

MASSACHUSETTS INSTITUTE OF TECHNOLOGY

June 1978

Signature redacted

Signature of Author..... .....
Department of Civil Engineering, March 22, 1978

Signature redacted

Certified by..... .....
Thesis Supervisor

Signature redacted

Accepted by.....
Chairman, Departmental Committee on Graduate Students
of the Department of Civil Engineering

DERIVED DISTRIBUTION OF WATER VOLUME ABOVE A GIVEN THRESHOLD DISCHARGE

by

SIU-ON CHAN

Submitted to the Department of Civil Engineering on March 1978, in partial fulfillment of the requirements for the degree of Master of Science.

ABSTRACT

The frequency distribution of the volume of water above a given threshold discharge is developed. This is done using basic and accessible information like the joint probability density function of rainfall intensity and duration together with expressions, to be derived, relating the volume of interest to rainfall intensity and duration. The resulting distribution function is in a closed analytical form containing only few climatological and physical parameters of a catchment. This distribution function will be of great value in the design of storage devices, flood control systems, and storm waters treatment facilities in urban areas.

Thesis Supervisor: Rafael L. Bras
Title: Assistant Professor of Civil Engineering

ACKNOWLEDGEMENTS

This work was partially supported by the National Science Foundation under contracts Nos. ENG 7611817 and ENG 7704999 and partially supported by my parents.

The author wishes to thank the many persons who made possible his graduate education.

He is very grateful to his parents, who guaranteed that he would not starve during his entire stay at MIT, and to Loraine, who brightened up many of his dark moments.

He is deeply indebted to Dr. Rafael L. Bras, his thesis and research supervisor, who provided him with ideas and guidance throughout the entire course of his work.

The author also wishes to express his sincere gratitude to Dr. Peter S. Eagleson, whose work provided much of the basis for his thesis.

Particular thanks are given to Mr. Dick K. Yue and Edward R. Johnson, research assistants, who provided many helpful suggestions in surmounting the mathematical difficulties of this work.

He also thanks Anne L. Clee, who patiently typed over two hundred and thirty-six equations in the thesis.

Lastly, special thanks go to Dr. Frank E. Perkins, Head of the Civil Engineering Department, who gave him an opportunity to live through one of his most treasurable experiences of his life here at MIT.

TABLE OF CONTENTS

LIST OF PRINCIPAL SYMBOLS

Note: 1) Subscripts c and s generally referred to the overland flow segment and the streamflow segment, respectively.

2) Symbols not included in the list are defined in the text wherever they are used.

3) In cases if a single notation represents more than one quantity in the text, it should be self-evident from the context to which it implies.

A, A_c	Catchment area (square miles)
A_r	Effective runoff contributing area (square miles)
A_s	Cross-sectional area of stream channel ($ft.^2$)
c, c_s	Wave velocity (ft./sec)
C	Runoff coefficient
d	Point total storm depth (inches)
d_A	Average areal rainfall depth (inches)
$E_2(\cdot)$	Exponential integral function of the second order
i_o	Average point rainfall intensity (inches/hour)
$\bar{i}_o$	Average areal rainfall intensity (inches/hour)
i_e	Average rainfall excess intensity (inches/hour)
K	Ratio of d_A to d
$K_1(\cdot)$	First order modified Bessel function of the second kind
L, L_c; L_s	Total length of a segment (ft.)
m, m_c; m_s	Parameter of kinematic wave model
n	Average number of storms per year Manning's roughness coefficient
q	Overland discharge at x_c (cfs/ft.)
q_L	Lateral discharge from overland flow segment to stream per unit length of stream (cfs/ft.)

Q_s	Stream discharge at x_s (cfs)
q_{th}, q_{th_c}; q_{th_s}	Threshold discharge (cfs/ft.)
t	Time variable
t_c, t_s	Time of concentration
t_*	Time of concentration of the combined catchment-stream direct runoff area
t_s^*	Time for a disturbance starts at $t = 0$, at $x_s = 0$ to reach $x_s = L_s$
t_r	Rainfall duration (hours)
t_{re}	Duration of rainfall excess (hours)
T_E	Recurrence interval of an annual exceedance series (years)
V_{th}, V_{th_c}; V_{th_s}	Volume of water above a given threshold discharge Flood-volume Exceedance volume Overflow volume ($ft.^3$)
x, x_c; x_s	Distance along a flow segment (ft.)
y_L	Depth of water at $x_c = L_c$
α, α_c; α_s	Parameter of kinematic wave model α_c($ft.^{1/3}$/sec), α_s(sec^{-1})
β	Parameter of distribution of rainfall intensity (hours/inch)
λ	Parameter of distribution of storm duration ($hour^{-1}$)
ϕ	Average potential loss rate Average infiltration rate (inches/hour)

LIST OF TABLES

LIST OF FIGURES

Chapter 1

INTRODUCTION

1.1 Urban Storm Drainage Problems and Solutions

Environmental pollution and local flooding in urban areas, due to the failure of urban storm drainage systems to handle storm runoff, have become a major problem in many cities of the United States. An urban drainage system may either be a combined (storm sewage and municipal sewage) sewer system, a separated sewer system, or a combination of the two. In a combined sewer system, the sewage is normally treated but in times of severe storms the discharge may exceed the intake capacity of the sewage treatment plant so that part of the sewage is discharged without treatment. This overflow sewage causes environmental pollution problems. In a separated sewer system, the municipal sewage has to be treated before discharging into receiving waters, while the storm sewage, known to be an important pollutant by itself, is usually discharged without going through any treatment. The American Public Works Association (APWA) (1967) estimated that as of 1962, of the 125 million people served by sewer systems, approximately 43.2 percent were served partially or totally by combined sewer systems.

During the past few decades, increased urbanization has substantially reduced the size of pervious surfaces in urban areas. New impervious surfaces such as roadways and roofs, together with developed commercial areas, may effectively increase the peak storm discharge to such an extent that frequent failure of the existing

drainage systems is not uncommon. This is particularly true in areas served only by combined sewers due to the increase of both municipal and storm sewage.

One of the solutions to the problem of environmental pollution and local flooding caused by increased storm sewage is the reconstruction of all the combined systems as separated systems. Municipal sewage will then always be treated before releasing into receiving waters, while storm sewage would hopefully not cause as many environmental pollution problems as the combined sewage overflows.

In the United States, cities such as Washington, D. C., New York, Philadelphia, Detroit, Milwaukee, Minneapolis and Chicago have invested huge sums of money in the examination of this problem. The consensus is that sewage separation is neither economically feasible nor practical. Cywin and Rosenkranz (1971) estimated the cost of reconstructing all the combined systems to separated systems in the United States would amount to 48 billion dollars in 1967. Granted that funds for reconstruction were available, it would still be doubtful whether storm water alone could be safely discharged at all, to say nothing of the construction nuisance and difficulties.

An alternate solution is the detention of part of the storm runoff by surface storage, or subsurface storage, or both, for later treatment. Provisions for storage can reduce peak runoff rates. Storage facilities can also prevent local flooding. While some cities are reconstructing a separate sewer system, others are constructing detention tanks, basins and underground storage tunnels. Table 1.1

Table 1.1

SUMMARY OF STORAGE COSTS FOR VARIOUS CITIES[a]
(Field and Lager, 1975)

Location (1)	Storage, in Millions of Gallons (2)	Capital Cost, in Dollars (3)	Storage Cost, in Dollars per Gallon (4)
Seattle, Wash.			
Control and monitoring system	-	3,500,000	-
Automated regulator station	-	3,900,000	-
	32.0	7,400,000	0.23
Minneapolis-St. Paul, Minn.	-	3,000,000	-
Chippewa Falls, Wisc.			
Storage	2.8	744,000	0.26
Treatment	-	186,000	-
Jamaica Bay, New York, N.Y.			
Basin	10.0	21,200,000	2.12
Basin and sewer	23.0	21,200,000	0.92
Humboldt Avenue, Milwaukee, Wisc.	4.0	3,010,000	0.50
Boston, Mass.			
Cottage Farm stormwater treatment station	1.3	6,200,000	4.74[b]
Chicago, Ill			
Storage basins	2,736.0	568,000,000	0.21
Collecting, tunnel, and pumping[c]	2,834.0	755,000,000	0.27
	5,570.0	1,323,000,000	0.24

[a] ENR = 2,000

[b] Includes pumping station, chlorination facilities and outfall.

[c] Includes 120 miles (193.1 km) of tunnels.

summarizes the storage costs for various cities.

The main advantage of building storage devices to attenuate flood peaks lies in its reduced cost. Cywin and Rosenkranz (1971) estimated that using storage devices and special wastewater treatment plants, it may be possible to reduce the cost of controlling overflows from 48 billion to 15 billion.

1.2 Distribution of the Overflow Volumes

In the construction of storage devices, some prior knowledge of the distribution of the volumes of the combined sewage overflow is necessary. If sufficient data of this overflow volume is available, an annual exceedance series or an annual maximum series may be used to describe its frequency distribution. Unfortunately, few historical data of this sort exist, mainly because it requires the knowledge of the entire hydrograph of a catchment while most streamflow gages record only the peak discharge.

An alternative approach is to make use of the more readily available historical rainfall data, together with some climatological and physical parameters of the catchment, as the inputs to a deterministic computer simulation model to generate a series of synthetic overflow volumes. The overflow volume in this case is referred to as the volume of water above a given threshold discharge (refer to Fig. 1.1). The threshold discharge corresponds, for example, to either the intake capacity of a sewage treatment plant or the intake capacity of a sewer system. The synthetic overflow volumes are then ranked and analyzed to

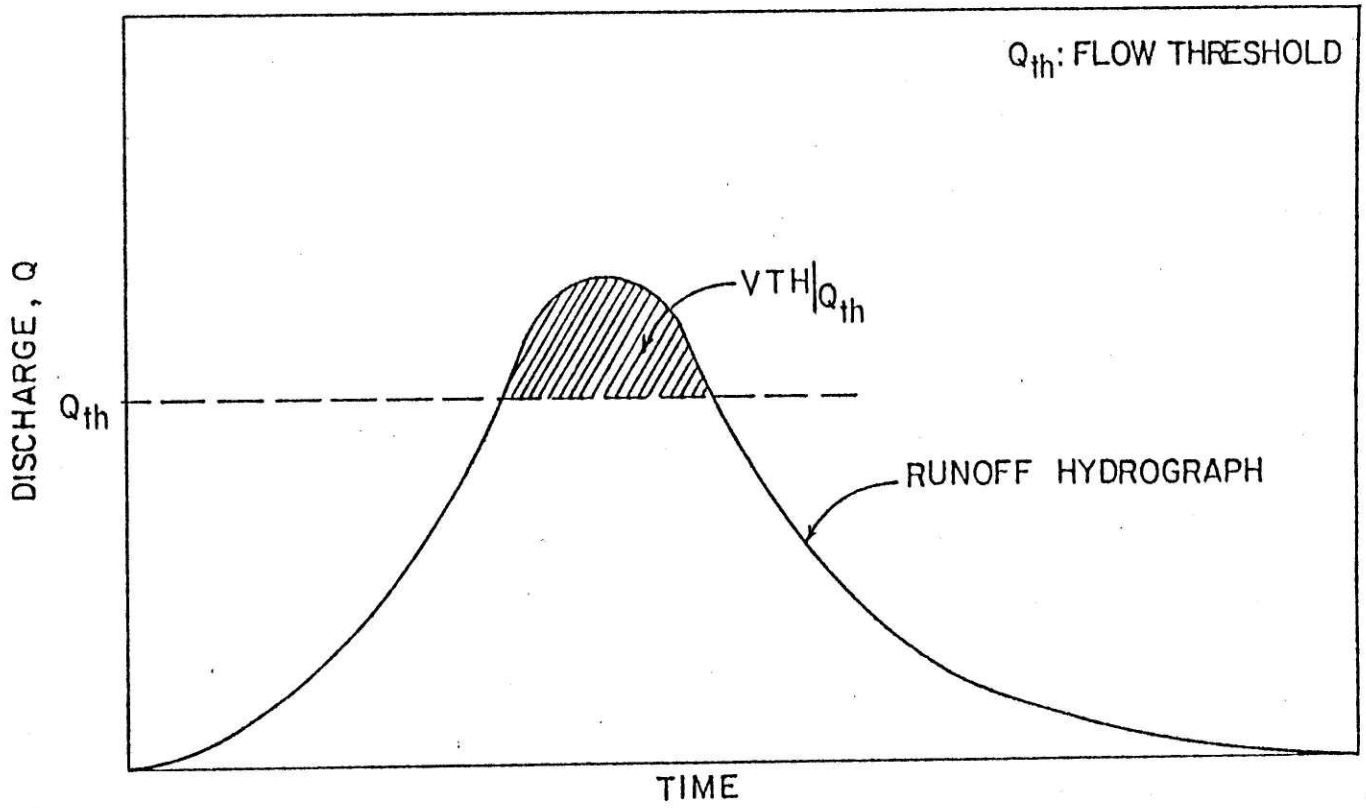

FIGURE 1.1: VOLUME ABOVE A GIVEN THRESHOLD DISCHARGE

obtain the annual exceedance series. If historical rainfall data is scarce, synthetic rainfall data may be generated by stochastic rainfall models, using the statistical parameters of the historical rainfall data as information for those stochastic models.

The main advantage of the simulation approach applied to urban areas is the inclusion of the effect of urbanization in the analysis of the overflow volume, which is reflected in the physical parameters of the catchment such as the roughness coefficient , the percentage of pervious surfaces, the infiltration rates, etc. (Bras and Perkins, 1975).

Fleming and Franz (1971), after studying eleven small watersheds (less than 20 square miles), concluded that the simulation approach is the most reliable mean for estimating flood frequency when compared to the rational method, the Potter's method and the method of regional frequency analysis. Perkins (1970), Bras and Perkins (1975) and Leclerc and Schaake (1972) have used the same approach with good results. Leclerc and Schaake (1973) also derived the frequency distribution of the volume of water above a given threshold discharge with the simulation method.

So far, the simulation approach seems to have a very promising future. More and more sophisticated models may be implemented and tested. Computer developments have undoubtedly provided a powerful tool for the hydrologist to unravel the 'black box' of hydrologic systems. But it has one main drawback, computer simulation is very costly.

Of course, the best approach should be one which is economical to use, easy to apply and with results comparable to the true

observations if historical data are available, or with results comparable to those obtained by the simulation approach if historical data are scarce. Such is the derived distribution technique (which will be fully described in Chapter 2). Using this technique, a closed-form, physically-based, analytical expression of the cumulative density function of the volume of water above a given threshold discharge may be derived.

Eagleson (1972), for the first time, used such an approach and derived a closed-form, analytical expression of the probability density function of peak discharges. The final expression contains only few climatic and physical parameters of the catchment. After comparing his derived flood frequency expression with observations from three natural catchments in Connecticut, he concluded that the agreement is good. Leclerc and Schaake (1972 and 1973) confirmed Eagleson's analytical results by simulation.

1.3 Objectives of This Work

The purpose of this work is to study the applicability of derived distribution technique in urban storm drainage problems. The theoretical physically-based distribution of the volume of water above a given threshold discharge will be derived. The resulting distribution function will be in a closed, analytical form with few hydrologic and basin parameters. A closed-form expression is very important to the general practitioner because it can provide a fast, easy, cheap and efficient mean to obtain the results without going through detailed, expensive computer simulation exercises. This resulting distribution

function will be of great value in the design of storage devices, flood control systems, and storm waters treatment facilities in urban areas.

Chapter 2

OVERLAND FLOW MODEL

2.1 Derived Distribution Technique

The derived distribution technique is well established in probability theory. It provides a tool to derive the density function of a dependent variable from random variables of which the joint density functions are known. The mechanics are as follows:

Let a random variable, x, be functionally related to y in the form

$$y = g(x) \tag{2.1}$$

If x has a probability density function given by $f_x(x_o)$, where x_o is a possible value of x, then the probability that x is less than some value, x_o, is given by

$$\text{Prob}(x < x_o) = \int_{-\infty}^{x_o} f_x(x_o)\, dx_o \tag{2.2}$$

Due to the randomness of x, y is also a random variable. For some monotonic, easily inverted functional relations, there is a one-to-one correspondence between x and y. Making use of the fact that the probability that y is between y_o and $y_o + dy_o$ is equal to the probability x is between x_o and $x_o + dx_o$, i.e.,

$$f_y(y_o)\, dy_o = f_x(x_o)\, dx_o \qquad \text{for } y_o = g(x_o)$$

$$\text{or } x_o = g^{-1}(y_o)$$

then it can be shown that

$$f_y(y_o) = f_x(x_o) \cdot \left|\frac{dx_o}{dy_o}\right| = f_x(g^{-1}(y_o)) \left|\frac{dg^{-1}(y_o)}{dy_o}\right| \qquad (2.3)$$

for some continuous, differentiable, monotonic functions as shown in Figure 2.1, after Benjamin & Cornell, 1970.

The cumulative probability of y is given by

$$\text{Prob}(y < y_o) = \int_{-\infty}^{y_o} f_y(y_o)\, dy_o \qquad (2.4)$$

Consider the simple case of two random variables, x_o, y_o. Assume z_o is functionally related to x_o, y_o as

$$z_o = h(x_o, y_o) \qquad (2.5)$$

and the density functions of x_o, y_o are known

$$f_{x,y}(x_o, y_o) = \left\{ \begin{array}{l} f_x(x_o) \cdot f_y(y_o) \\ f_{x|y}(x_o|y_o) \cdot f_y(y_o) \\ f_{y|x}(y_o|x_o) \cdot f_x(x_o) \end{array} \right\} \begin{array}{ll} \text{if } x_o, y_o & \text{independent} \\ \text{if } x_o, y_o & \text{dependent} \end{array} \qquad (2.6)$$

then,

$$\text{Prob}(z < z_o) = \int \int_{R_z} f_{x,y}(x, y)\, dxdy \qquad (2.7)$$

where R_z is the region in the space of x_o and y_o specified by $z_o = h(x_o, y_o)$ for which $z < z_o$.

In general, if y is a function of n random variables given by

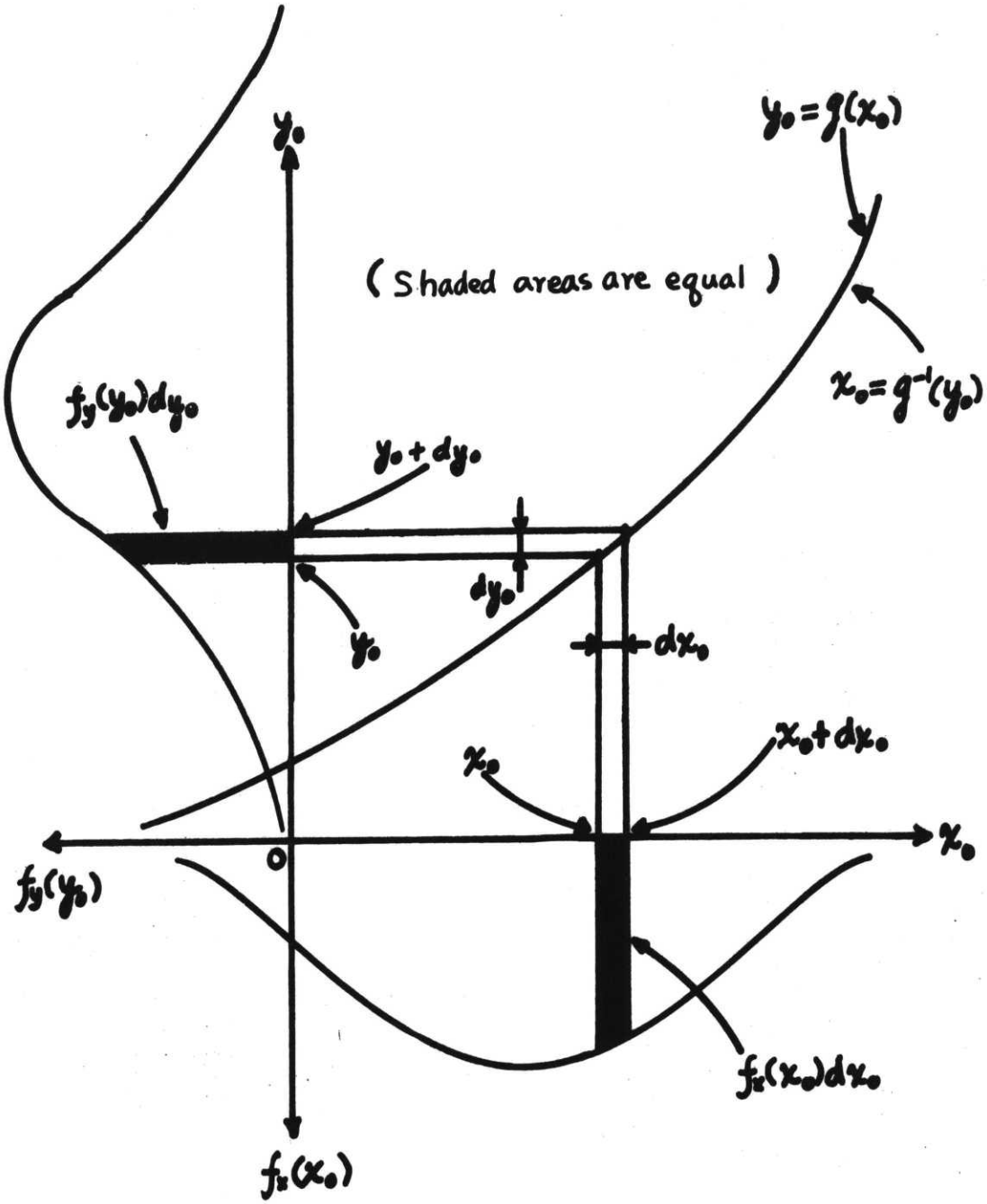

FIGURE 2.1: DIRECT DERIVATION OF PROBABILITY DENSITY FUNCTION
(BENJAMIN AND CORNELL, 1970)

$$y = g(x_1, x_2, \ldots, x_n) \tag{2.8}$$

then

$$\text{Prob}(y < y_o) = \int_{R_y} \ldots \int f_{x_1,x_2,\ldots,x_n}(x_1, x_2,\ldots,x_n)\, dx_1\, dx_2 \ldots dx_n \tag{2.9}$$

where $f_{x_1,x_2,\ldots,x_n}(\cdot)$ is the joint density function of the given n random variables and R_y is the region in the space of $(x_1, \ldots,x_n)$ specified by $y = g(x_1, x_2,\ldots,x_n)$ for which $y < y_o$.

In this work only the case with two random variables (average rainfall intensity and storm duration) is needed for the derivation of the distribution of the water volume above a given threshold discharge.

For simplicity, the water volume above a given threshold discharge, VTH, will be referred to as the flood-volume in this and the following chapters.

The method used in deriving the flood-volume distribution is shown in Figure 2.2.

2.2 Rainfall Model Chosen (Exponential Distributions)

A rainfall model is needed in order to derive the distribution of the flood-volume. Rainfall has to be considered a stochastic process for the derivation. Numerous distributions may be fitted to samples of storm exterior variables such as the average rainfall intensity, storm duration, storm total depth and time between storms. Eagleson, using hourly rainfall data (546 storms) at Boston, Massachusetts, found out

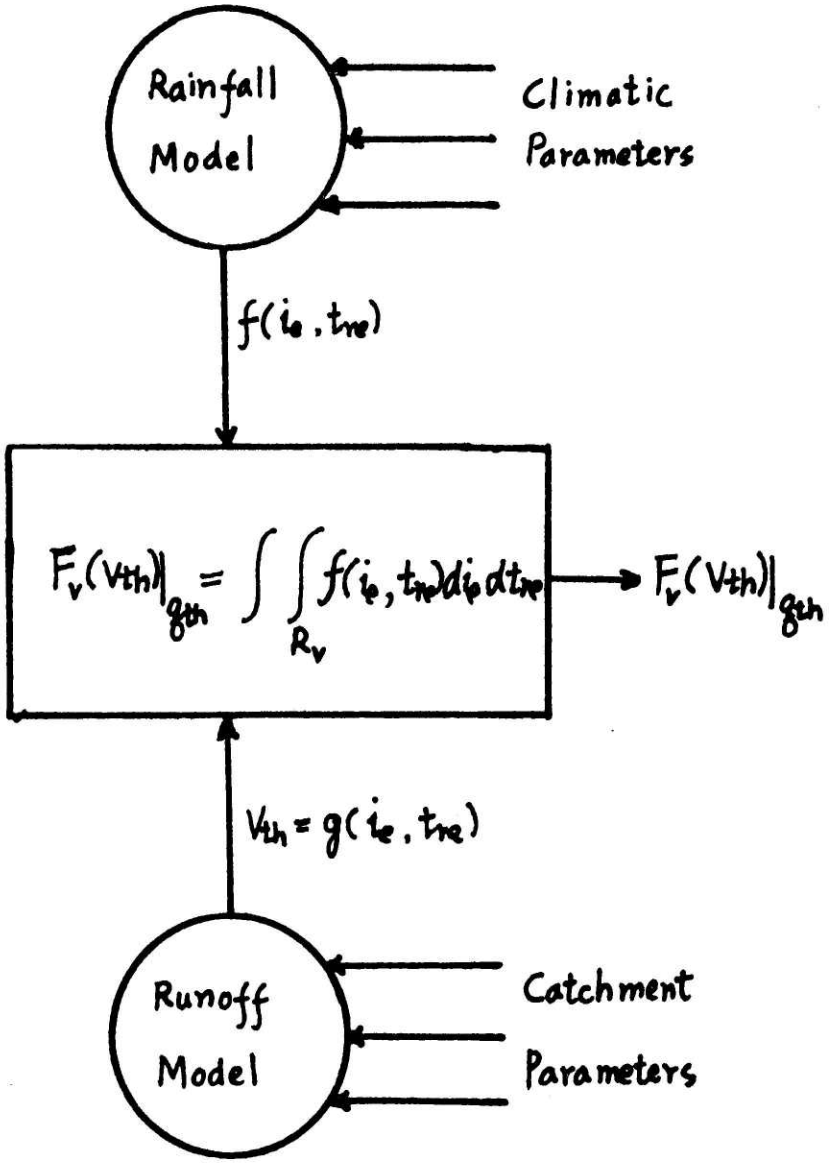

FIGURE 2.2: METHOD USED IN DERIVING THE FLOOD-VOLUME DISTRIBUTION

that the probability density functions of point rainfall intensity and storm duration may be fitted closely by an exponential function (Eagleson, 1972) as shown in Figure 2.3, 2.4. For computational reasons, he further approximated $f(d|t_r)$, the conditional probability density function of the total storm depth, d, given the storm duration, t_r, by an exponential function, which is a reasonable representation at large depths where flood events are important. The use of an exponential function for '$f(d|t_r)$' also implies the independence of point rainfall intensity and point storm duration. These exponential distributions will be used in this work as the stochastic rainfall models to derive the flood-volume distribution.

The derivation of the joint density function of rainfall excess, i_e, and duration of rainfall excess, t_{re}, follows Eagleson's approach (1972).

For point rainfall duration, t_r, and average point rainfall intensity, i_o,

$$f(t_r) = \lambda e^{-\lambda t_r} \tag{2.10}$$

$$f(i_o) = \beta e^{-\beta i_o} \tag{2.11}$$

where λ, β are climatic parameters which are assumed constants for a given catchment.

By definition,

$$i_o \equiv d/t_r \tag{2.12}$$

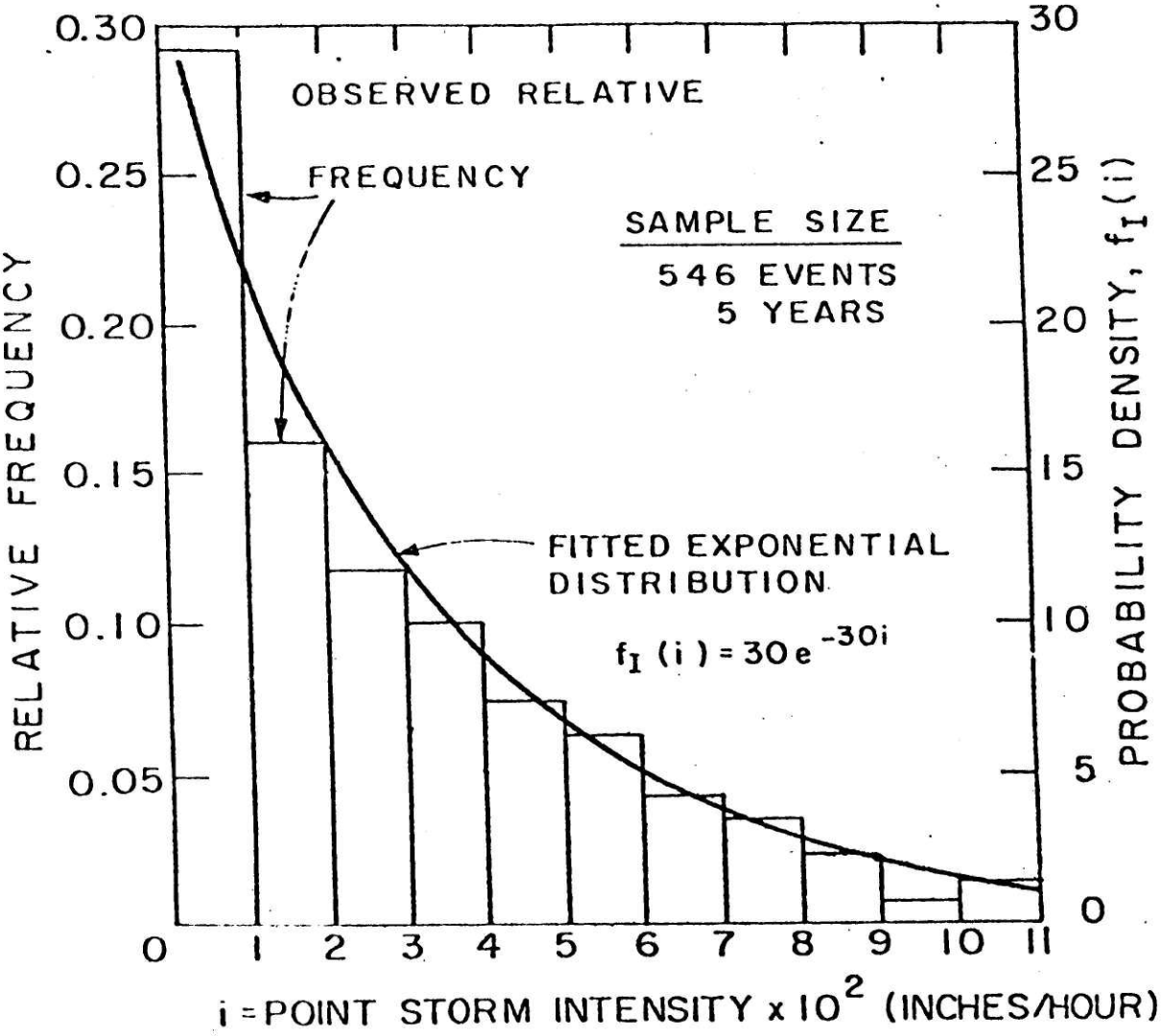

FIG.2.3: DISTRIBUTION OF POINT STORM INTENSITIES AT BOSTON, MASSACHUSETTS (EAGLESON, 1972)

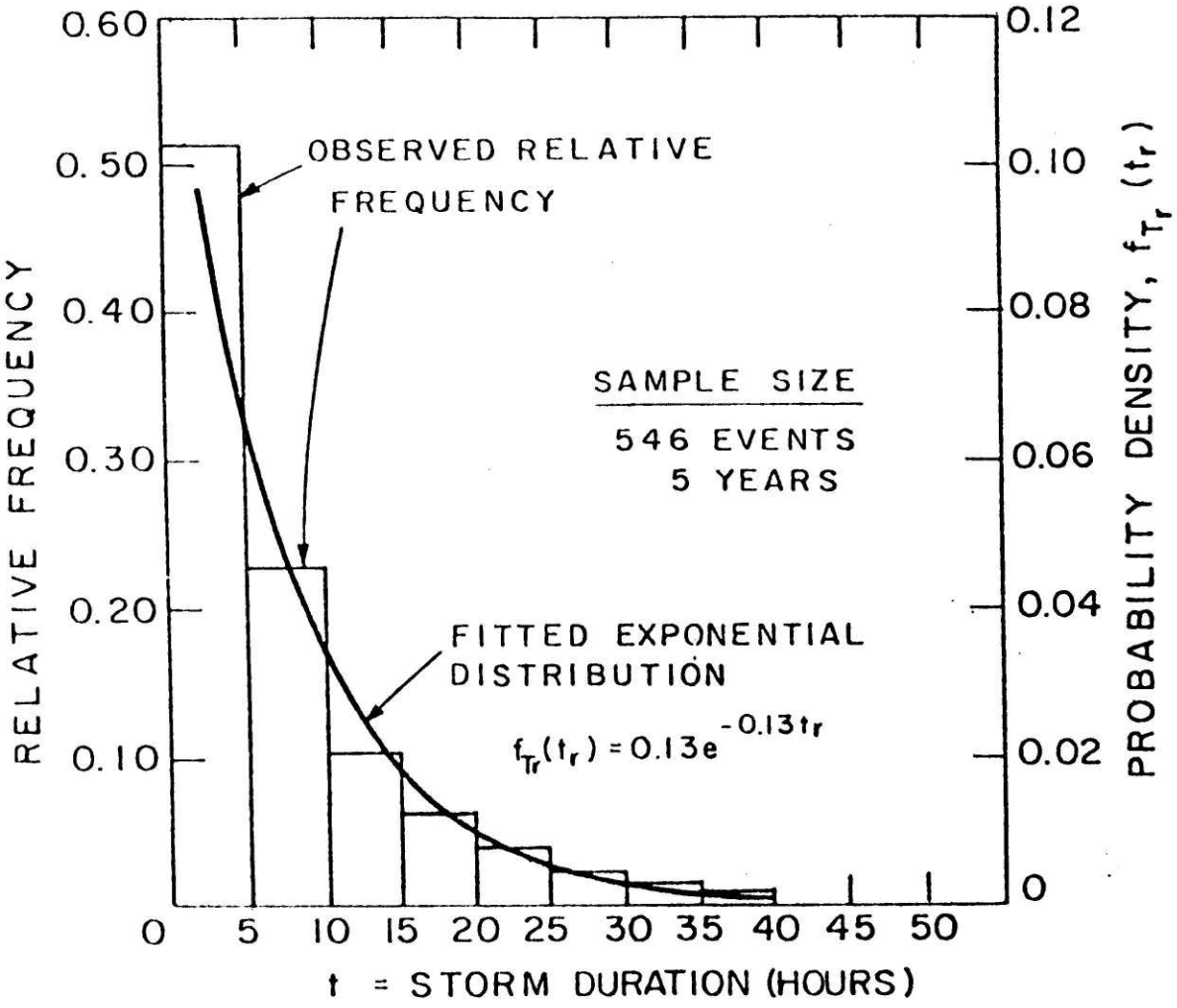

FIG.2.4: DISTRIBUTION OF STORM DURATIONS AT BOSTON, MASSACHUSETTS (EAGLESON,1972)

where d = point total storm depth.

The conditional distribution of depth given duration is taken as

$$f(d|t_r) = (\beta/t_r)\, e^{-\beta(d/t_r)} \tag{2.13}$$

From Equations (2.12) and (2.13), it can be shown that i_o and t_r are independent, as follows:

$$\begin{aligned} \text{Prob}(i_o < i_o'|t_r) &= \text{Prob}(\frac{d}{t_r} < i_o'|t_r) \\ &= \text{Prob}(d < i_o'\, t_r|t_r) \\ &= \int_o^{i_o'\, t_r} f(d|t_r)\, dd \\ &= \frac{\beta}{t_r} \int_o^{i_o'\, t_r} e^{-\frac{\beta}{t_r}\cdot d}\, dd \\ &= 1 - e^{-\beta i_o'} \end{aligned} \tag{2.14}$$

which implies

$$\begin{aligned} f(i_o|t_r) &= \frac{d}{di_o}(1 - e^{-\beta i_o}) \\ &= \beta e^{-\beta i_o} \end{aligned} \tag{2.15}$$

The above is identical to Equation (2.11), proving independence of i_o and t_r.

In order to reduce the average point rainfall depth, d, to the average areal rainfall depth, d_A, the following correction is made according to the U. S. Weather Bureau, as shown in Figure 2.5. The

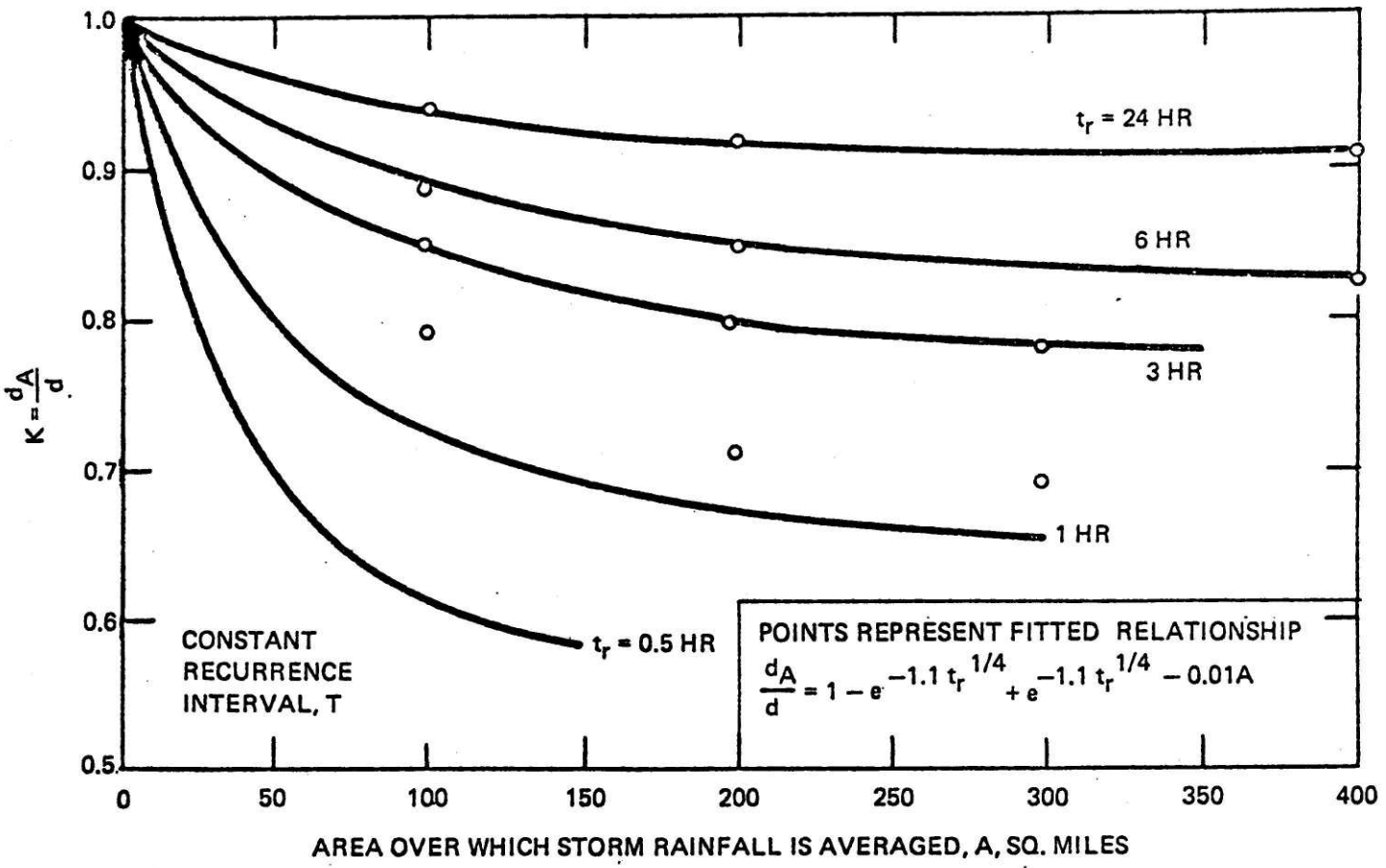

FIGURE 2.5 SPATIAL REDUCTION OF POINT RAINFALL INTENSITY

relationship is given by

$$\frac{d_A}{d} = 1 - \exp(-1.1\ t_r^{1/4}) + \exp(-1.1\ t_r^{1/4} - 0.01A) \qquad (2.16)$$

where A = area of catchments in square miles.

For urban areas where the area of the catchment is usually small (of the order of few square miles), it may be assumed that the runoff contributing area, A_r, is equal to the total area, A. In large basins, A_r is in fact a random variable taking values less than or equal to A. For an example on the inclusion of this randomness of A_r in the derivation, the reader is referred to Eagleson (1972).

The average areal rainfall intensity, $\bar{i}_o$, is by definition,

$$\bar{i}_o \equiv d_A/t_r \qquad (2.17)$$

From Equation (2.12)

$$\bar{i}_o = \left(\frac{d_A}{d}\right) i_o \qquad (2.18)$$

In order to simplify the mathematical manipulations, t_r in Equation (2.16) is replaced by its expected value, $1/\lambda$, and ' $\frac{d_A}{d}$ ' is given by its average value,

$$\frac{d_A}{d} = K = 1 - \exp(-1.1\ \lambda^{-1/4}) + \exp(-1.1\ \lambda^{-1/4} - 0.01A) \qquad (2.19)$$

and Equation (2.18) becomes

$$\bar{i}_o = K\ i_o$$

where K is a constant given the area of the catchment and

$$f(\bar{i}_o) \equiv f(\bar{i}_o|A) = \frac{\beta}{K} e^{-\beta \bar{i}_o/K} \quad , \qquad \bar{i}_o > 0 \tag{2.20}$$

Eagleson (1972) included infiltration effects as a spatially averaged potential loss rate, ϕ, subtracted from the average areal rainfall intensity for each storm period, i.e.,

$$\begin{aligned} i_e &= \bar{i}_o - \phi \quad , & \bar{i}_o &\geq \phi \\ &= 0 & \bar{i}_o &< \phi \end{aligned} \tag{2.21}$$

where i_e = areal average rainfall excess.

The density function of the rainfall excess, i_e, is given by

$$\begin{aligned} f(i_e) = f(\bar{i}_o|\bar{i}_o > \phi) &= f(\bar{i}_o)/\text{Prob}(\bar{i}_o > \phi) \\ &= \frac{\frac{\beta}{K} e^{-\frac{\beta}{K}\bar{i}_o}}{\int_{\phi}^{\infty} \frac{\beta}{K} e^{-\frac{\beta}{K}\bar{i}_o} d\bar{i}_o} \\ &= \frac{\frac{\beta}{K} e^{-\frac{\beta}{K}(i_e+\phi)}}{e^{-\frac{\beta}{K}\phi}} = \frac{\beta}{K} e^{-\frac{\beta}{K} i_e} \end{aligned} \tag{2.22}$$

The joint density of depth and duration, from Equations (2.10) and (2.13), is

$$\begin{aligned} f(d, t_r) &= f(d|t_r) \cdot f(t_r) \\ &= \frac{\beta\lambda}{t_r} \exp[-\frac{\beta}{t_r} \cdot d - \lambda t_r] \end{aligned} \tag{2.23}$$

Using Equations (2.19) and (2.23) results in

$$f(d_A, t_r) = \frac{\beta\lambda}{Kt_r} \exp(-\frac{\beta d_A}{Kt_r} - \lambda t_r) \tag{2.24}$$

The marginal probability density function of the rainfall excess duration, t_{re}, is then

$$f(t_{re}) = \frac{\int_{\phi t_r}^{\infty} f(d_A, t_r)\, dd_A}{\int_0^{\infty} dt_r \int_{\phi t_r}^{\infty} f(d_A, t_r)\, dd_A}$$

$$= \frac{\int_{\phi t_r}^{\infty} \frac{\beta\lambda}{Kt_r} \exp[-\frac{\beta d_A}{Kt_r} - \lambda t_r]\, dd_A}{\int_0^{\infty} \left[\int_{\phi t_r}^{\infty} \frac{\beta\lambda}{Kt_r} \exp[-\frac{\beta d_A}{Kt_r} - \lambda t_r]\, dd_A \right] dt_r}$$

$$= \frac{\lambda\, e^{-\frac{\beta}{K}\phi - \lambda t_r}}{e^{-\frac{\beta}{K}\phi}} = \lambda\, e^{-\lambda t_r} = f(t_r) \tag{2.25}$$

From Equations (2.15), (2.21) and (2.25), it is concluded that using this rainfall model implies the independence of rainfall excess, i_e, and its duration, t_{re}.

So finally the expression for the joint density function of i_e and t_{re} is

$$f(i_e, t_{re}) \equiv f(i_e, t_{re}|A)$$

$$= f(i_e|A) \cdot f(t_{re})$$

$$= \frac{\beta\lambda}{K} \exp[-\lambda t_{re} - \frac{\beta}{K} i_e] \tag{2.26}$$

The infiltration effect ϕ may be estimated as follows (Eagleson, 1972):

Let n = the average annual number of rainfall excess events

θ = the average annual number of independent rainfall events

P = the average annual point rainfall depth in inches

R = average annual runoff in inches

R_d = average annual direct runoff in inches

Defining

$$\Phi_1 = R/P \tag{2.27}$$

and

$$\Phi_2 = R_d/R \tag{2.28}$$

Then, on the average,

$$P\ \Phi_1\ \Phi_2 = n\ E[i_e\ t_{re}] \tag{2.29}$$

And in approximation

$$E[i_e\ t_{re}] \cong E[i_o\ t_r] = P/\theta \tag{2.30}$$

By equating (2.29) and (2.30),

$$\frac{n}{\theta} = \Phi_1\ \Phi_2 \tag{2.31}$$

But,

$$\frac{n}{\theta} = \int_{\phi}^{\infty} f(\bar{i}_o)\ d\bar{i}_o = e^{-\frac{\beta}{K}\phi} \tag{2.32}$$

Therefore,

$$e^{-\frac{\beta}{K}\phi} = \Phi_1 \Phi_2$$

and,

$$\phi = -\frac{K}{\beta} \ln(\Phi_1 \Phi_2) \qquad (2.33)$$

Wood (1976) discusses a procedure to consider the infiltration as a random variable.

Since for urban areas few records of the direct runoff, R_d, exist and the infiltration effect for urban areas is estimated by a different method in Chapter 3, no further discussion of the parameter ϕ is given. Nevertheless, the procedure is valuable for those studying runoff in large river basins, a topic Chapter 4 will be addressing.

2.3 Runoff Model, the Kinematic Wave Approximations

The validity of the application of the kinematic wave equations to overland flow and stream flow has been verified by numerous investigators (Lighthill and Whitham, 1955; Wooding, 1966; Eagleson, 1970; Harley, 1970; Bras, 1972; Leclerc and Schaake, 1973). The usefulness of this application lies in the fact that the kinematic wave equations require only few physical parameters of the catchment which may be obtained from topographic and soil maps. Once these parameters are known, the entire hydrograph for a specific input of rainfall intensity and duration can be predicted with reliable results.

Since the derivations of the kinematic wave equations are readily available from many sources (Eagleson, 1970), only a very brief account is given here.

The momentum equations for flow through a control volume which is fixed in inertial space (from Daily & Harleman, 1966) is given by

$$\vec{F}_s + \iiint_{C\Psi} \vec{B}\, \rho d\Psi = \iint_{CS} \vec{V}(\rho \vec{V} \cdot d\vec{A}) + \frac{\partial}{\partial t} \iiint_{C\Psi} \vec{V}(\rho\, d\Psi) \qquad (2.34)$$

and the conservation of mass equation

$$\iint_{CS} \vec{V}\, d\vec{A} + \frac{\partial}{\partial t} \iiint_{C\Psi} d\Psi = 0 \qquad (2.35)$$

where $\vec{F}_s$ = sum of surface forces acting on the control volume

$\vec{B}$ = sum of all body forces per unit mass

t = time

ρ = mass density of water

Ψ = volume

$\vec{V}$ = absolute fluid velocity

$d\vec{A}$ = directed area element, positive outward

$C\Psi$ = control volume

CS = control surface

Under the following assumptions,

1) Moderately wide rectangular channel (idealized overland flow conditions),

$$\frac{\text{Flow Depth (y)}}{\text{Channel Bottom Width (b)}} < 1$$

2) Small bottom slope, $\theta \cong \sin\theta \cong \tan\theta$

3) Velocity over a cross-section of the channel is uniform and the momentum distribution factor $\beta = 1$

4) The free surface over the cross-section is horizontal

5) The pressure distribution is hydrostatic

Equation (2.34) is reduced to

$$\frac{\partial V}{\partial t} + V \frac{\partial V}{\partial x} + g \frac{\partial y}{\partial x} = [i - f + \frac{2q_L}{b}] \frac{V}{y} - (1 + \frac{2y}{b}) \frac{\tau_o}{\rho y} + g\theta \qquad (2.36)$$

and Equation (2.35) becomes

$$\frac{\partial y}{\partial t} + V \frac{\partial y}{\partial x} + y \frac{\partial V}{\partial x} = i - f + \frac{2q_L}{b} \qquad (2.37)$$

where x = downstream direction (ft.)

i = rainfall intensity (ft./sec.)

f = infiltration rate (ft./sec.)

q_L = lateral inflow to stream per unit stream channel width (cfs/ft.)

τ_o = shear stress (LB/ft.^{2})

g = gravitational constant (ft./sec.^{2})

V = velocity in the x-direction (ft./sec.)

The terms in Equation (2.36) represent respectively (from left to right)the local acceleration, the convective acceleration, the surface elevation effects, the momentum contribution due to lateral inflow and rainfall, the bottom and wall shear and the acceleration due to bottom slope.

Under an order of magnitude analysis (Eagleson, 1970), considering the inflow, free surface slope and inertia terms as negligible in comparison with those of bottom slope and friction, Equation (2.36) is further reduced to

$$\tau_o = (\rho\ g)\ y\theta = \gamma\ y\ \sin\theta \tag{2.38}$$

where γ = weight of water per unit volume.

Equation (2.37) is rewritten as

$$\frac{\partial y}{\partial t} + \frac{\partial (Vy)}{\partial x} = i_e + \frac{2q_L}{b} \tag{2.39}$$

where $i_e = i - f$ = rainfall excess.

For the overland flow case, lateral inflow, q_L, is zero, leading to a continuity equation of the form,

$$\frac{\partial y}{\partial t} + \frac{\partial q}{\partial x} = i_e \tag{2.40}$$

where $q = Vy$ = flow per unit width of the overland flow channel (cfs/ft.)

Define

$$\tau_o = C_f(\rho\ \frac{V^2}{2}) \tag{2.41}$$

where C_f = function of the Reynolds number and the relative surface roughness.

Combining Equations (2.38) and (2.41),

$$V = \left(\frac{2\ \gamma\ y\ \sin\theta}{\rho\ C_f}\right)^{1/2} = \left(\frac{2g}{C_f}\right)^{1/2} S_o^{1/2}\ y^{1/2}$$

$$= C\ S_o^{1/2}\ y^{1/2} \qquad (2.42)$$

where $\frac{\gamma}{\rho} = g$ and $S_o = \sin\theta \cong \tan\theta \cong \theta$ and

$$C = \text{chezy coefficient} = \left(\frac{2g}{C_f}\right)^{1/2} \qquad (2.43)$$

If C_f is assumed to be a constant, then

$$q = Vy = \alpha y^{3/2} \qquad (2.44)$$

where

$$\alpha = CS_o^{1/2} = \left(\frac{2\ gS_o}{C_f}\right)^{1/2}$$

In general, including the effect of the possible variability of C_f,

$$q = \alpha y^m \qquad (2.45)$$

Using Manning's equation, it can be shown that α can also be expressed (for overland segments, turbulent flow condition) as

$$\alpha = \frac{1.49}{n}\ S_o^{1/2} \qquad \text{and} \qquad m = \frac{5}{3} \qquad (2.46)$$

where n = Manning's roughness coefficient ($ft.^{1/6}$)

For laminar overland flow

$$C_f = \frac{4}{R}$$

$$\alpha = \frac{g \sin\theta}{2\nu} \quad , \qquad \text{and} \qquad m = 3$$

where ν = kinematic viscosity of water

R = Reynolds number = $\frac{Vy}{\nu}$

Crawford and Linsley (1966) in simulating overland flow, considered both the laminar and the turbulent conditions. After some research, they decided to adopt the equations for the turbulent conditions.

Equation (2.40)

$$\frac{\partial y}{\partial t} + \frac{\partial q}{\partial x} = i_e$$

and Equation (2.45)

$$q = \alpha y^m$$

are referred to as the kinematic wave approximations for the overland flow case.

Solving (2.40) and (2.45) by the method of characteristics (Eagleson, 1970), the following results,

$$\frac{dq}{dt} = i_e \, c \tag{2.47}$$

$$\frac{dq}{dx} = i_e \tag{2.48}$$

$$\frac{dy}{dt} = i_e \tag{2.49}$$

$$\frac{dy}{dx} = i_e / c \tag{2.50}$$

Equations (2.47) to (2.50) are valid along the path given by the characteristic defined below,

$$\frac{dx}{dt} = c = \alpha m y^{m-1} \tag{2.51}$$

For overland flow (see Figure 2.6) the boundary conditions are

$$\begin{aligned} y = 0 \quad & 0 \leq x < L, \quad t = 0 \\ & x = 0, \quad t > 0 \end{aligned} \tag{2.52}$$

The solution to Equations (2.47) through (2.51) yields the following expressions applicable in two different cases (Eagleson, 1970)

Case 1: For the duration of rainfall excess, t_{re}, greater than the concentration time of the overland segment, t_c.

The concentration time, t_c, is defined as the time to the maximum discharge of the overland segment and is given by

$$t_c = \left(\frac{L\, i_e^{1-m}}{\alpha} \right)^{1/m} \tag{2.53}$$

For $t_c < t_{re} < \infty$ (see Figure 2.7)

The discharge per unit width of channel at x = L, q_L, is given by Equation (2.45),

$$q_L = \alpha y_L^m \quad , \qquad m = 5/3 \tag{2.54}$$

where y_L is the depth of water at x = L.

On the rising limb, y_L is given by

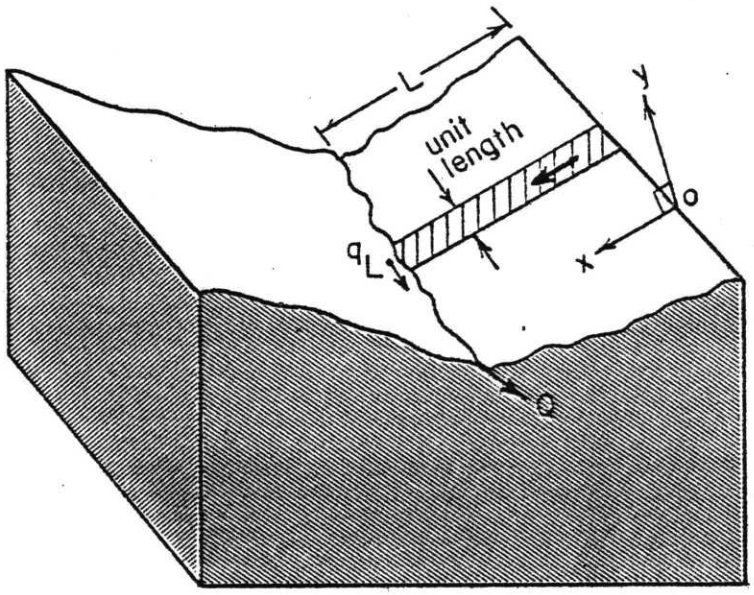

FIGURE 2.6: TYPICAL OVERLAND FLOW SEGMENT

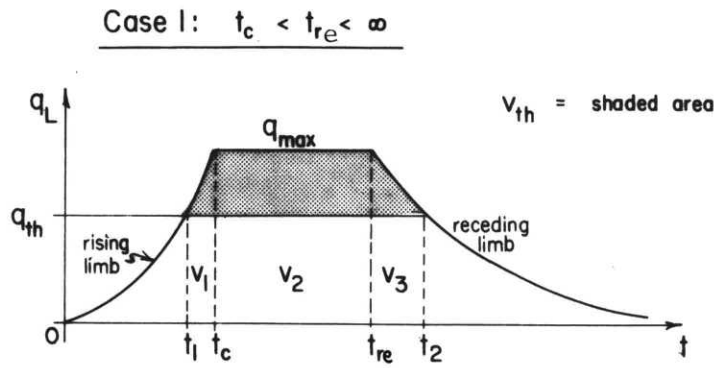

FIGURE 2.7: OVERLAND FLOW HYDROGRAPH FOR CASE 1

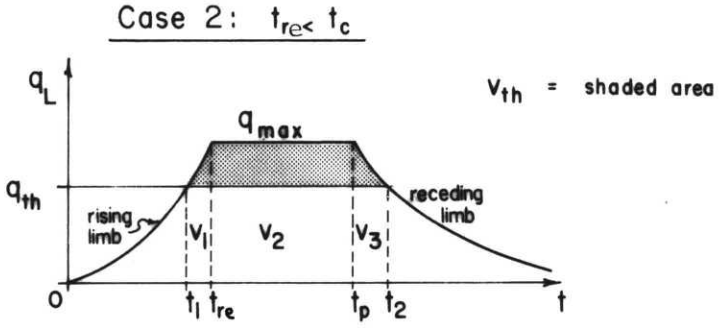

FIGURE 2.8: OVERLAND FLOW HYDROGRAPH FOR CASE 2

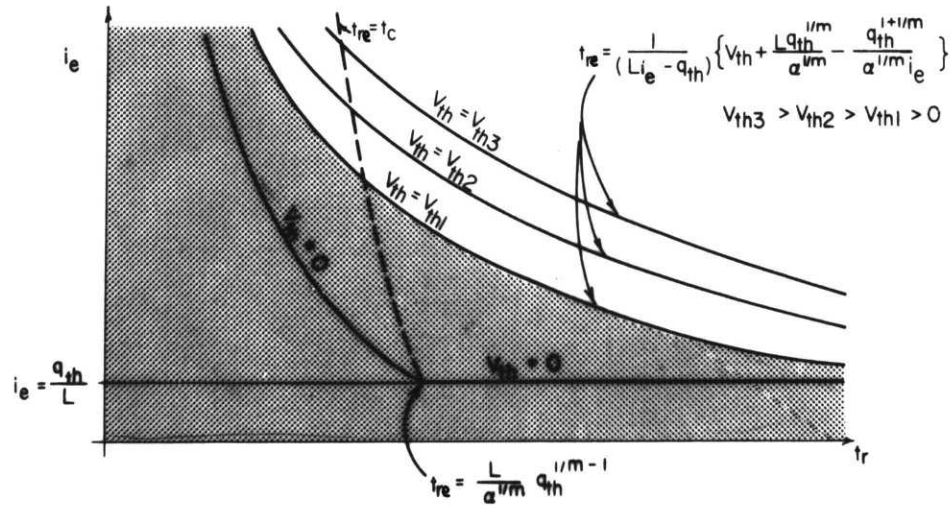

FIGURE 2.9: LINES OF CONSTANT EXCEEDANCE VOLUME AND REGION OF INTEGRATION FOR THE OVERLAND FLOW CASE

$$y_L = i_e t \quad , \qquad 0 < t \leq t_c \leq t_{re} \tag{2.55}$$

At maximum discharge,

$$y_L = \left(\frac{L\, i_e}{\alpha}\right)^{1/m} \qquad t_{re} \geq t \geq t_c \tag{2.56}$$

On the receding limb, y_L is given implicitly by

$$L = \alpha y_L^{m-1}[y_L/i_e + m(t - t_{re})] \quad , \qquad t > t_{re} \geq t_c \tag{2.57}$$

Case 2: For the duration of rainfall excess less than the concentration time of the overland segment.

For $t_{re} < t_c$ (see Figure 2.8)

Again,

$$q_L = \alpha y_L^m \tag{2.58}$$

On the rising limb, y_L is given by

$$y_L = i_e t \quad , \qquad 0 < t \leq t_{re} < t_c \tag{2.59}$$

For q_L constant at less than its maximum value,

$$y_L = i_e t_{re} \quad , \qquad t_c > t_{re} < t \leq t_p \tag{2.60}$$

where $(t_p - t_{re})$ is the time required for the initial disturbance to travel from its position, x_w, at time, t_{re}, to x = L. t_p is given by

$$t_p = t_{re} + (t_c^* - t_{re})/m \tag{2.61}$$

and

$$t_c^* = \frac{L}{\alpha y_{Lr}^{m-1}} \qquad \text{with} \qquad y_{Lr} = i_e \, t_{re} \tag{2.62}$$

On the receding limb, y_L is also given implicitly as

$$L = \alpha y_L^{m-1}[y_L/i_e + m(t - t_{re})] \tag{2.63}$$

These equations will be used to derive the expression of the flood-volume as shown in the shaded regions of Figures 2.7 and 2.8.

2.4 Expression for the Volume of Water above a Given Threshold Discharge (Flood Volume, VTH) for the Overland Flow Case

The analytical expression of the flood-volume for the two cases will be derived as follows:

Case 1: $t_c < t_{re} < \infty$ (Figure 2.7)

The equations defining this hydrograph are given by (2.53) through (2.57).

The flood-volume, from the figure, is given by

$$V_{th} = V_1 + V_2 + V_3 - V_4 \tag{2.64}$$

where

$$V_4 = q_{th}(t_2 - t_1) \tag{2.65}$$

Solving for t_1, using Equations (2.54) and (2.55),

$$t_1 = \frac{q_{th}^{1/m}}{\alpha^{1/m}\, i_e} \quad , \qquad 0 < t_1 < t_c \tag{2.66}$$

On the receding limb ($t_{re} < t_2 < \infty$), Equation (2.57) is rewritten as

$$t = t_{re} + \frac{1}{m}\left[\frac{L}{\alpha y^{m-1}} - \frac{y}{i_e}\right] \tag{2.67}$$

Since,

$$q_{th} = \alpha y_2^m \tag{2.68}$$

then

$$y_2 = \left(\frac{q_{th}}{\alpha}\right)^{1/m} \tag{2.69}$$

Substituting Equation (2.69) in (2.67) yields

$$t_2 = t_{re} + \frac{L}{m\alpha^{1/m}\, q_{th}^{1-1/m}} - \frac{q_{th}^{1/m}}{m\alpha^{1/m}\, i_e}$$

$$t_{re} < t_2 < \infty \tag{2.70}$$

With expressions for t_1, t_2 available, the evaluation of V_1, V_2, V_3 and V_4 follows:

$$V_1 = \int_{t_1}^{t_c} q_L(t)\, dt = \int_{t_1}^{t_c} \alpha(i_e\, t)^m\, dt$$

$$= \frac{\alpha\, i_e^m}{(m+1)}\,(t_c^{m+1} - t_1^{m+1}) \tag{2.71}$$

With t_c given by Equation (2.53) and t_1 by (2.66), then

$$V_1 = \frac{L^{1+1/m} i_e^{1/m}}{(m+1)\ \alpha^{1/m}} - \frac{q_{th}^{1+1/m}}{(m+1)\ \alpha^{1/m}\ i_e} \tag{2.72}$$

The maximum flow rate is

$$q_{max} = \alpha(i_e t_c)^m = L\ i_e \tag{2.73}$$

The second volume element is given by

$$V_2 = q_{max}(t_{re} - t_c) \tag{2.74}$$

After combining Equations (2.73), (2.74) and (2.53),

$$V_2 = L\ i_e\ t_{re} - \frac{L^{1+1/m} i_e^{1/m}}{\alpha^{1/m}} \tag{2.75}$$

The third volume element is given by

$$V_3 = \int_{t_{re}}^{t_2} \alpha\ y^m\ dt \tag{2.76}$$

Using Equation (2.67), differentiating both sides

$$dt = \left[\left(\frac{1-m}{m}\right) \frac{L}{\alpha}\ y^{-m} - \frac{1}{m i_e}\right] dy \tag{2.77}$$

At $t = t_{re}$, by Equation (2.67),

$$t_{re} = t_{re} + \frac{1}{m}\left[\frac{L}{\alpha y^{m-1}} - \frac{y}{i_e}\right]$$

or

$$y = \left(\frac{L\ i_e}{\alpha}\right)^{1/m} = i_e\ t_c \tag{2.78}$$

At $t = t_2$, by Equation (2.69)

$$y_2 = \left(\frac{q_{th}}{\alpha}\right)^{1/m}$$

From the above, Equation (2.76) becomes,

$$V_3 = \int_{y_1}^{y_2} \alpha y^m \left| \left(\frac{1-m}{m}\right) \frac{L}{\alpha} y^{-m} - \frac{1}{m i_e} \right| dy$$

where

$$y_1 = i_e t_c \quad , \quad y_2 = \left(\frac{q_{th}}{\alpha}\right)^{1/m} \tag{2.79}$$

Integrating,

$$V_3 = \left(\frac{1-m}{m}\right) \frac{L\, q_{th}^{1/m}}{\alpha^{1/m}} - \frac{q_{th}^{1+1/m}}{m(m+1)\alpha^{1/m}\, i_e} + \left(\frac{m}{m+1}\right) \frac{L^{1+1/m}\, i_e^{1/m}}{\alpha^{1/m}} \tag{2.80}$$

The fourth volume component is expanded as

$$\begin{aligned} V_4 &= q_{th}(t_2 - t_1) \\ &= q_{th}\, t_{re} + \frac{L\, q_{th}^{1/m}}{m\alpha^{1/m}} - \left(1 + \frac{1}{m}\right) \frac{q_{th}^{1+1/m}}{\alpha^{1/m}\, i_e} \end{aligned} \tag{2.81}$$

Finally, combining Equations (2.64), (2.72), (2.75), (2.80) and (2.81), factoring and cancelling terms, the flood-volume expression turns out to be quite simple

$$V_{th} = t_{re}(L\, i_e - q_{th}) + \frac{q_{th}^{1+1/m}}{\alpha^{1/m}\, i_e} - \frac{L\, q_{th}^{1/m}}{\alpha^{1/m}}$$

$$\text{for } t_c < t_{re} < \infty \tag{2.82}$$

which results from a simplification of

$$V_{th} = V_1 + V_2 + V_3 - V_4$$

$$= \frac{L^{1+1/m}\, i_e^{1/m}}{\alpha^{1/m}} \left[\frac{1}{m+1} - 1 + \frac{m}{m+1}\right] + t_{re}(L\, i_e - q_{th})$$

$$+ \frac{q_{th}^{1+1/m}}{\alpha^{1/m}\, i_e} \left[-\frac{1}{m+1} - \frac{1}{m(m+1)} + 1 + \frac{1}{m}\right] + \frac{L\, q_{th}^{1/m}}{\alpha^{1/m}} \left[\frac{1}{m} - 1 - \frac{1}{m}\right]$$

Case 2: $t_{re} < t_c$ (Figure 2.8)

The equations defining this hydrograph are given by (2.58) through (2.63).

The times at the threshold discharge, t_1 and t_2, are again given as in Case 1 by Equations (2.66) and (2.70) but with the limits, $0 < t_1 < t_{re}$ and $t_p < t_2 < \infty$.

The first volume component,

$$V_1 = \int_{t_1}^{t_{re}} \alpha(i_e\, t)^m\, dt$$

$$= \frac{\alpha\, i_e^{\,m}}{(m+1)}\, t_r^{m+1} - \frac{q_{th}^{1+1/m}}{(m+1)\, \alpha^{1/m}\, i_e} \qquad (2.83)$$

The second volume element takes the form

$$V_2 = q_{max}(t_p - t_{re}) \qquad (2.84)$$

where

$$t_p - t_{re} = \frac{1}{m}\left(\frac{L}{\alpha(i_e\, t_{re})^{m-1}} - t_{re}\right) \qquad (2.85)$$

from Equations (2.61) and (2.62). And,

$$q_{max} = \alpha(i_e\ t_{re})^m \tag{2.86}$$

from Equation (2.59).

Substituting Equations (2.85) and (2.86) in (2.82) results in

$$V_2 = \frac{L\ i_e\ t_{re}}{m} - \frac{\alpha}{m}\ i_e^m\ t_{re}^{m+1} \tag{2.87}$$

The third volume, using the change of variable as shown in Case 1, results in

$$\begin{aligned} V_3 &= \int_{t_{re}}^{t_2} \alpha\ y^m\ dt \\ &= \int_{y_1=i_e t_{re}}^{y_2=(q_{th}/\alpha)^{1/m}} \alpha y^m [(\tfrac{1-m}{m})\ \tfrac{L}{\alpha}\ y^{-m} - \tfrac{1}{m i_e}]\ dy \\ &= (\tfrac{1-m}{m})\ \frac{L\ q_{th}^{1/m}}{\alpha^{1/m}} - (\tfrac{1-m}{m})\ L\ i_e\ t_{re} - \frac{q_{th}^{1+1/m}}{m(m+1)\ \alpha^{1/m}\ i_e} \\ &\qquad + \frac{\alpha\ i_e^m\ t_r^{m+1}}{m(m+1)} \end{aligned} \tag{2.88}$$

The fourth volume component is expanded as

$$\begin{aligned} V_4 &= q_{th}(t_2 - t_1) \\ &= q_{th}\ t_{re} + \frac{L\ q_{th}^{1/m}}{m\alpha^{1/m}} - (1 + \tfrac{1}{m})\ \frac{q_{th}^{1+1/m}}{\alpha^{1/m}\ i_e} \end{aligned} \tag{2.89}$$

and the flood-volume expression, after combining (2.83), (2.87), (2.88) and (2.89) is

$$V_{th} = V_1 + V_2 + V_3 - V_4$$

$$= t_{re}^{m+1} \alpha i_e^m \left[\frac{1}{m+1} - \frac{1}{m} + \frac{1}{m(m+1)}\right] + t_{re}\left[\frac{L\, i_e}{m} - \left(\frac{1-m}{m}\right) L\, i_e - q_{th}\right]$$
$$+ \frac{q_{th}^{1+1/m}}{\alpha^{1/m}\, i_e}\left[-\frac{1}{m+1} - \frac{1}{m(m+1)} + \left(1 + \frac{1}{m}\right)\right]$$
$$+ \frac{L\, q_{th}^{1/m}}{\alpha^{1/m}}\left[\left(\frac{1}{m} - 1\right) - \frac{1}{m}\right]$$
$$= t_{re}(L\, i_e - q_{th}) + \frac{q_{th}^{1+1/m}}{\alpha^{1/m}\, i_e} - \frac{L\, q_{th}^{1/m}}{\alpha^{1/m}} \quad \text{for } 0 < t_{re} < t_c \tag{2.90}$$

which surprisingly is identical to the expression of V_{th} for Case 1.

Equations (2.82) and (2.90) define the regions of interest in the $i_e - t_{re}$ space.

For $t_{re} = t_c$, from Equation (2.53)

$$t_{re} = \left(\frac{L\, i_e^{1-m}}{\alpha}\right)^{1/m} \tag{2.91}$$

This is shown as a dashed line in Figure 2.9.

And for $t_{re} \lesseqgtr t_c$, from Equations (2.82), (2.90)

$$t_{re} = \frac{1}{(L\, i_e - q_{th})}\left\{V_{th} + \frac{L\, q_{th}^{1/m}}{\alpha^{1/m}} - \frac{q_{th}^{1+1/m}}{\alpha^{1/m}\, i_e}\right\} \tag{2.92}$$

which is shown in Figure 2.9 for constant flood-volumes, V_{th}, as a function of t_{re} and i_e.

In order to have non-zero V_{th}, the following conditions must be satisfied,

$$q_{th} < q_{max} = L\, i_e \quad \text{for} \quad t_{re} > t_c \tag{2.93}$$

therefore,

$$i_e > \frac{q_{th}}{L} \qquad \text{for} \qquad t_{re} > t_c \tag{2.94}$$

And

$$q_{th} < q_{max} = \alpha(i_e\ t_{re})^m \qquad \text{for} \qquad t_{re} < t_c \tag{2.95}$$

Therefore

$$t_{re} > \left(\frac{q_{th}}{\alpha}\right)^{1/m} \cdot \frac{1}{i_e} \qquad \text{for} \qquad t_{re} < t_c \tag{2.96}$$

Zero exceedance volumes then occur at

$$i_e = \frac{q_{th}}{L} \qquad \text{for} \qquad t_{re} > t_c \tag{2.97}$$

and

$$t_{re} = \left(\frac{q_{th}}{\alpha}\right)^{1/m} \cdot \frac{1}{i_e} \quad , \qquad \text{for} \qquad t_{re} < t_c \tag{2.98}$$

which are shown in Figure 2.9.

The shaded area in the figure defines regions of $V_{th} < (V_{th})_{given}$. With this region known, the derivation for the CDF of the flood-volumes may proceed.

2.5 Expression for the Cumulative Density Function (CDF) of the Volume of Water above a Given Threshold Discharge for the Overland Flow Case

2.5.1 Exact solution

The joint probability density function of i_e and t_{re} is, from

Equation (2.26),

$$f(i_e, t_{re}) = \frac{\beta\lambda}{K} \exp[- \lambda t_{re} - \frac{\beta}{K} i_e]$$

The CDF of the flood-volume, V_{th}, is then, from Equation (2.7)

$$F_V(V_{th})\Big|_{q_{th}} = \int \int_{R_V(i_e, t_{re})} f(i_e, t_{re}) \, d \, i_e \, d \, t_{re} \qquad (2.99)$$

where $R_V(i_e, t_{re})$ is the shaded region in Figure 2.9 for which V_{th} is less than a given value.

Equation (2.99) can be expanded (see Figure 2.9) into

$$F_V(V_{th})\Big|_{q_{th}} = \int_{i_{e_1}}^{\infty} \int_{t_{re_1}}^{t_{re_2}} f(i_e, t_{re}) \, d \, t_{re} \, d \, i_e + F_V(0) \qquad (2.100)$$

where

$$i_{e_1} = \frac{q_{th}}{L} \quad ; \qquad t_{re_1} = \frac{q_{th}^{1/m}}{\alpha^{1/m} \, i_e}$$

$$t_{re_2} = \frac{1}{(L \, i_e - q_{th})} \left\{ V_{th} + \frac{L \, q_{th}^{1/m}}{\alpha^{1/m}} - \frac{q_{th}^{1+1/m}}{\alpha^{1/m} \, i_e} \right\}$$

Integrating Equation (2.100) over t_{re} yields

$$F_V(V_{th})\Big|_{q_{th}} = \frac{\beta}{K} \int_{i_e = \frac{q_{th}}{L}}^{\infty} (e^w - e^u) \, d \, i_e + F_V(0) \qquad (2.101)$$

where

$$u = \frac{-C_1 V_{th}}{(C_2 i_e - q_{th})} - \frac{C_3}{i_e} - C_4 i_e$$

$$w = -\frac{C_3}{i_e} - C_4 i_e$$

for $(C_2 i_e - q_{th}) > 0$ (see Figure 2.9) and where

$$C_1 = F_1\lambda; \quad C_2 = F_2 L; \quad C_3 = F_3\lambda \left(\frac{q_{th}}{\alpha}\right)^{1/m}; \quad C_4 = F_4 \frac{\beta}{K}$$

F_1, F_2, F_3, F_4 are conversion factors to make units consistent.

Equation (2.101) is further expanded as

$$F_V(V_{th})\Big|_{q_{th}} = \frac{\beta}{K}\int_{i_e = \frac{q_{th}}{L}}^{\infty} e^w di_e - \frac{\beta}{K}\int_{i_e = \frac{q_{th}}{L}}^{\infty} e^u di_e + F_V(0)$$

$$= J_1 - J_2 + F_V(0) \qquad (2.102)$$

Closer examination of Equation (2.102) reveals the following properties:

When $V_{th} = 0$, $u = w$, which implies $J_1 = J_2$. Therefore,

$$F_V(0)\Big|_{q_{th}} = F_V(0), \quad \text{a finite impulse at } V_{th} = 0 \qquad (2.103)$$

When $V_{th} \to \infty$, $u \to -\infty$, therefore $J_2 \to 0$ and by definition $F_V(\infty)\Big|_{q_{th}} = 1$. Using Equation (2.102), then it is clear that

$$F_V(0) = 1 - J_1 = 1 - J_2\Big|_{V_{th} = 0} \qquad (2.104)$$

Substituting Equation (2.104) in (2.102) results in

$$F_V(V_{th})\Big|_{q_{th}} = 1 - J_2, \quad 0 \leq V_{th} < \infty \tag{2.105}$$

So it is clear that in order to obtain $F_V(V_{th})\Big|_{q_{th}}$, the only integral to be evaluated is J_2, where J_2 is given by

$$J_2 = \frac{\beta}{K} \int_{i_e = \frac{q_{th}}{L}}^{\infty} e^u di_e \tag{2.106}$$

The above integral has no exact analytical solution but a very good approximation can be obtained as will be shown in the following sections.

2.5.2 Approximate solution

From Equation (2.101) and (2.106), the expression for J_2 is

$$J_2 = C_4 \int_{i_e = \frac{q_{th}}{L}}^{\infty} \exp\left\{- \left| \frac{C_1 V_{th}}{C_2 i_e - q_{th}} + \frac{C_3}{i_e} + C_4 i_e \right| \right\} di_e \tag{2.107}$$

Let

$$C_2 i_e - q_{th} = x$$

then

$$i_e = (x + q_{th})/C_2 \quad ; \quad d i_e = \frac{dx}{C_2}$$

And Equation (2.107) becomes

$$J_2 = a_4 e^{-a_4 a_2} \int_0^{\infty} \exp - \left[\frac{a_1}{x} + \frac{a_3}{x+a_2} + a_4 x\right] dx \tag{2.108}$$

where

$$a_1 = C_1 V_{th}; \quad a_2 = q_{th}; \quad a_3 = C_3 C_2; \quad a_4 = \frac{C_4}{C_2}$$

Define,

$$f(x) = \frac{a_1}{x} + \frac{a_3}{x+a_2} + a_4 x \tag{2.109}$$

then, it is true that f(x) is bounded by

$$f_1(x) = \frac{a_1}{x} + a_4 x \leq f(x) \leq \frac{a_1 + a_3}{x} + a_4 x = f_2(x) \tag{2.110}$$

as shown in Figure 2.10.

The minimum points of the functions are also denoted in the figure.

Define,

$$\Delta_1 = XM - XL; \quad \Delta_2 = XU - XM; \quad \rho_1 = FM - FXL, \quad \rho_2 = FXU - FM \tag{2.111}$$

The minimum point of $f_1(x)$, by differentiation, is found to be

$$XL = (a_1/a_4)^{1/2}, \quad FXL = 2(a_1\ a_4)^{1/2} \tag{2.112}$$

and that for $f_2(x)$,

$$XU = [(a_1 + a_3)/a_4]^{1/2}, \quad FXU = 2[(a_1 + a_3)a_4]^{1/2} \tag{2.113}$$

As for the minimum point of f(x), setting the first derivative to zero yields

$$f'(x) = -\frac{a_1}{x^2} - \frac{a_3}{(x + a_2)^2} + a_4 = 0 \tag{2.114}$$

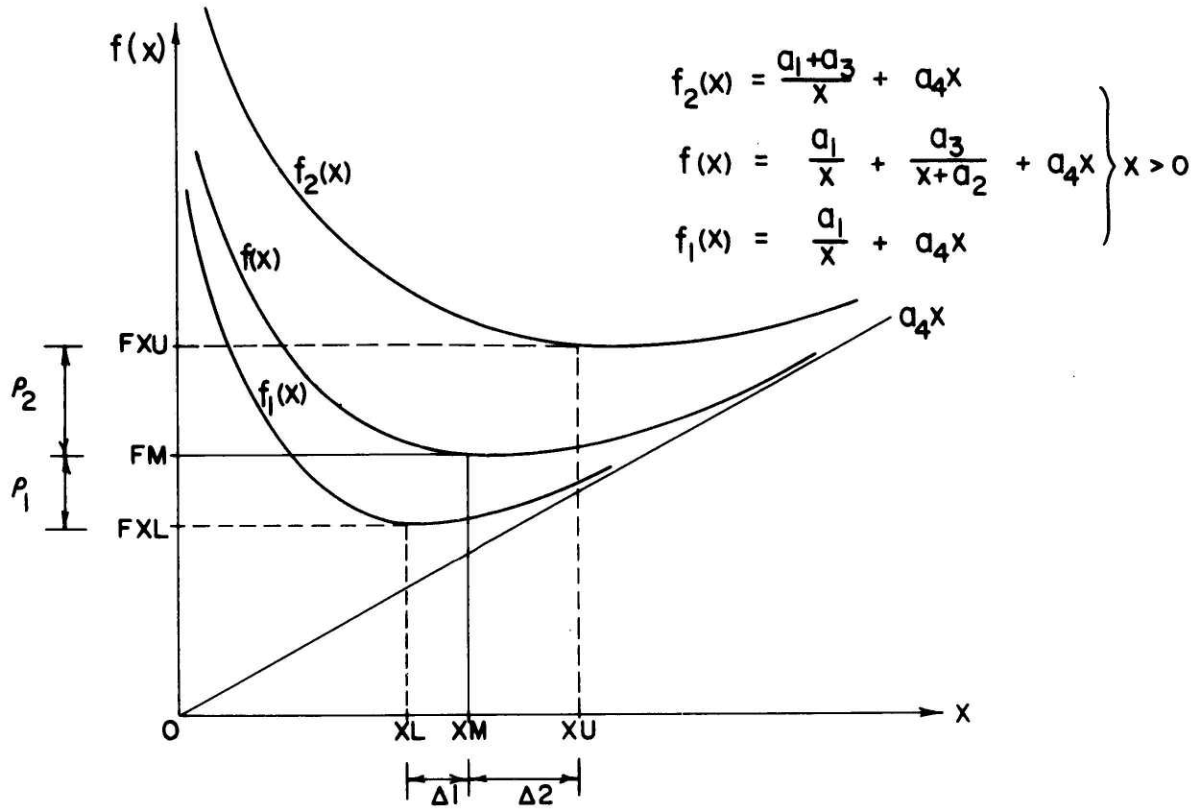

FIGURE 2.10: APPROXIMATIONS TO FUNCTION f(x)

$$f'(x) = -\frac{a_1}{x^2} - \frac{a_3}{(x+a_2)^2} + a_4 = 0$$

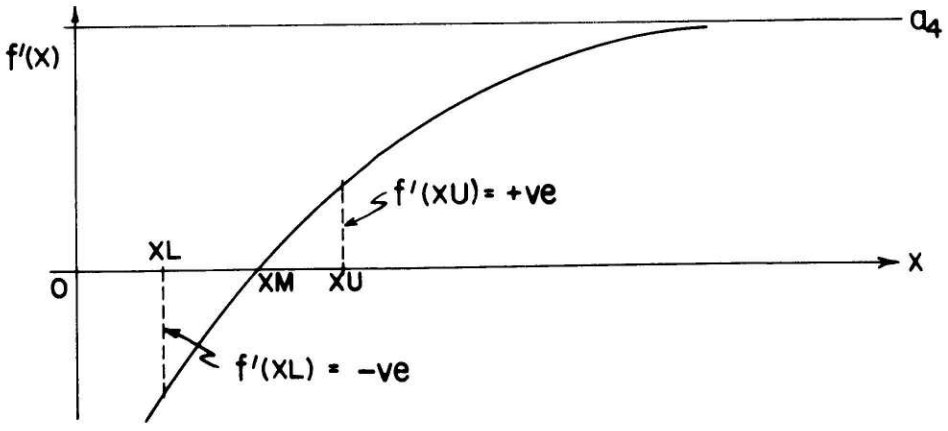

FIGURE 2.11: DERIVATIVE OF FUNCTION f(x)

which is a fourth degree polynomial equation. Since XM is bound by XL and XU as shown in Figure 2.11, and f'(x) is a very smooth function with f'(XL) = negative and f'(XU) = positive, a trial and error method would be the best mean for solving the equation, with an initial estimate of XM = (XL + XU)/2. Experiences show that in about three trials the value of f'(x) may be obtained to within 0.01 of the true value

Knowing XM, then

$$FM = \frac{a_1}{XM} + \frac{a_3}{(XM + a_2)} + a_4 XM \tag{2.115}$$

By translation, the minimum points of $f_1(x)$ and $f_2(x)$ can be forced to coincide with that of f(x), leading to closer bounds of f(x) as shown in Figure 2.12, with

$$f_1'(x) = \frac{a_1}{(x - \Delta_1)} + a_4(x - \Delta_1) + \rho_1 \tag{2.116}$$

and

$$f_2'(x) = \frac{a_1 + a_3}{(x + \Delta_2)} + a_4(x + \Delta_2) - \rho_2 \tag{2.117}$$

Using Equations (2.116) and (2.117), upper and lower bounds on J_2 can be established,

$$JU = a_4 e^{-a_4 a_2} \int_0^{\infty} e^{-f_2'(x)}\, dx \geq J_2 \geq a_4 e^{-a_4 a_2} \int_{\Delta_1}^{\infty} e^{-f_1'(x)}\, dx = JL \tag{2.118}$$

Extensive testing of Equation (2.118) with a wide range of values for parameters α, β, λ, L and q_{th} led to very good results in some ranges but bad in others. However, closer examination of the upper approximation, JU, led to excellent results.

The upper approximation, JU, from Equations (2.118) and (2.117) is

$$JU = a_4 e^{-a_4 a_2} \int_0^{\infty} \exp - \left\{ \frac{a_1 + a_3}{(x + \Delta_2)} + a_4(x + \Delta_2) - \rho_2 \right\} dx$$

$$= a_4 e^{-a_4 a_2 + \rho_2} \int_{\Delta_2}^{\infty} \exp - \left\{ \frac{a_1 + a_3}{z} + a_4 z \right\} dz \qquad (2.119)$$

where $z = x + \Delta_2$. Equation (2.119) can be rewritten as

$$JU = a_4 e^{-a_4 a_2 + \rho_2} \left\{ \int_0^{\infty} e^{-[\cdot]} dz - \int_0^{\Delta_2} e^{-[\cdot]} dz \right\} \qquad (2.120)$$

Integrating the first term inside brackets,

$$\int_0^{\infty} \exp - \left[\frac{a_1 + a_3}{z} + a_4 z \right] dz = 2\sqrt{(a_1 + a_3)/a_4}\; K_1\left[2\sqrt{(a_1 + a_3)\, a_4}\right] \qquad (2.121)$$

where $K_1(\cdot)$ = first order modified Bessel function of the second kind.

There is no exact closed-form expression for the second term inside the bracket of Equation (2.120). However,

$$f(z) = \frac{a_1 + a_3}{z} + a_4 z \qquad (2.122)$$

has a minimum at

$$z_{min} = \sqrt{(a_1 + a_3)/a_4} \qquad (2.123)$$

which is greater than Δ_2, since, from Equations (2.111) and (2.113)

$$\Delta_2 = XU - XM$$

$$= \sqrt{(a_1 + a_3)/a_4} - XM$$

Therefore, $\Delta_2 < z_{min}$ and since $0 < z < \Delta_2$, it is true that

$$\frac{a_1 + a_3}{z} > a_4 z \qquad \text{for} \qquad 0 < z < \Delta_2 \tag{2.124}$$

Using the above then

$$\phi = \int_0^{\Delta_2} \exp - \left\{\frac{a_1 + a_3}{z} + a_4 z\right\} dz$$

$$\cong \int_0^{\Delta_2} \exp - \frac{(a_1 + a_3)}{z} dz \tag{2.125}$$

Since JU overestimates J_2, neglecting $a_4 z$ in the integral slightly increases the value of ϕ, which may counter-balance the effect of overestimating J_2.

Let $z = (a_1 + a_3)y$, and $u = \frac{1}{y}$, then

$$\phi \cong (a_1 + a_3) \int_{\varepsilon}^{\infty} \frac{e^{-u}}{u^2} du$$

where $\varepsilon = \dfrac{a_1 + a_3}{\Delta_2}$. (2.126)

The above can easily be transformed into an exponential integral which is tabulated and available.

By letting $u = \varepsilon t$, then

$$\phi \cong (a_1 + a_3) \frac{1}{\varepsilon} \int_1^{\infty} \frac{e^{-\varepsilon t}}{t^2} dt$$

$$= \left(\frac{a_1 + a_3}{\varepsilon}\right) E_2(\varepsilon) \tag{2.127}$$

where $E_2(x) \equiv \int_1^{\infty} \frac{e^{-xt}}{t^2} dt$ = exponential integral function of the second order.

Substituting Equation (2.126) in (2.127),

$$\phi \cong \Delta_2 \, E_2\left[\frac{a_1 + a_3}{\Delta_2}\right] \tag{2.128}$$

Combining Equations (2.120), (2.121), (2.125) and (2.128) gives the final expression of JU as

$$JU = a_4 e^{-a_4 a_2 + \rho_2} \left\{2\sqrt{(a_1 + a_3)/a_4}\; K_1[2\sqrt{(a_1 + a_3)a_4}] - \Delta_2 \, E_2[(a_1 + a_3)/\Delta_2]\right\} \tag{2.129}$$

Finally, the expression for the cumulative density function of the flood-volume is given by Equations (2.105) and (2.108),

$$F_v(V_{th})\Big|_{q_{th}} = 1 - a_4 e^{-a_4 a_2} \int_0^\infty \exp - \left[\frac{a_1}{x} + \frac{a_3}{x + a_2} + a_4 x\right] dx \qquad 0 \leq V_{th} < \infty \tag{2.130}$$

which is approximated by

$$F_v(V_{th})\Big|_{q_{th}} \cong 1 - a_4 e^{-a_4 a_2 + \rho_2}\left\{2\sqrt{(a_1 + a_3)/a_4}\; K_1[2\sqrt{(a_1 + a_3)a_4}] - \Delta_2 \, E_2[(a_1 + a_3)/\Delta_2]\right\} \tag{2.131}$$

Numerical integration of Equation (2.130) and the approximate value of the CDF of flood-volume for a wide range of parameter values have been compared and the agreement between the two is excellent, with only a maximum error of about 4 hundredths when V_{th} approaches zero. As V_{th} increases from zero, the error decreases rapidly and the approximation becomes exact in the limit.

The range of parameter values tested is given below:

$0.1 < \alpha < 10$ ft.$^{1/3}$ sec.$^{-1}$; $0.5 < \beta < 70$ hr. in.$^{-1}$;

$0.02 < \lambda < 2$ hr.$^{-1}$; $50 < L < 1000$ ft.;

$1.76 \times 10^{-6} < q_{th} < 3.71 \times 10^{-2}$ cfs/ft.

which covers adequately the range of climatical and physical parameters of an urban catchment.

Equations (2.130) and (2.131) are plotted in Figures 2.13, 2.14, 2.15, with chosen parameters as shown. The excellent agreement between analytical approximation and numerical integration can be seen all through the figures.

Figure 2.13 shows the effect of varying the threshold discharge, q_{th}, while keeping all other parameters constant. As expected, the higher the threshold discharge, the higher the probability of zero volume. Higher q_{th} implies smaller flood-volume, or smaller probability of exceedance, $1 - F_V(V_{th})$. Therefore, the CDF of larger q_{th} envelopes those of smaller ones.

Figure 2.14 represents the effect of varying the kinematic wave parameter, α. A larger α leads to faster response and smaller concentration time. Therefore, higher α gives a higher flood-volume (with q_{th} fixed), which also implies a larger probability of exceedance, $1 - F_V(V_{th})$, or in other words, a smaller CDF.

Lastly, the effect of varying the overland flow length, L, is shown in Figure 2.15. A longer length leads to higher peak flows which implies a larger probability of exceedance, $1 - F_V(V_{th})$, or a smaller

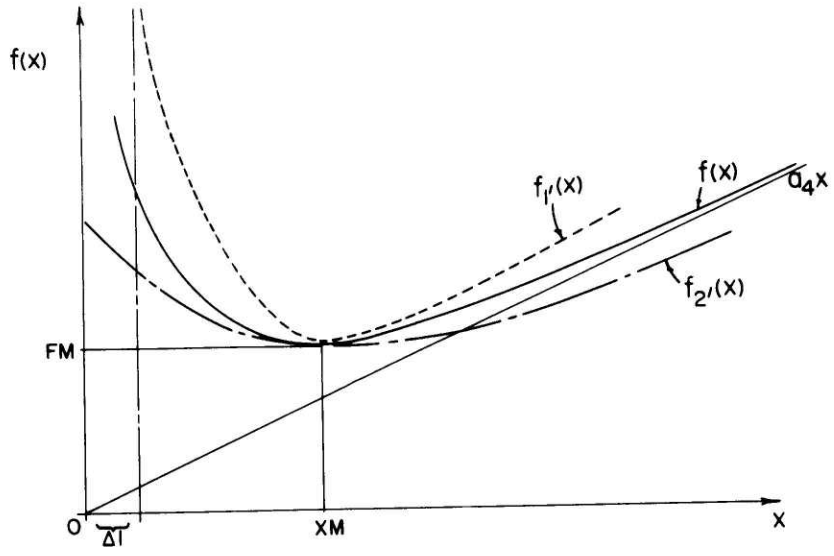

$$f(X) = \frac{a_1}{X} + \frac{a_3}{X+a_2} + a_4X$$

$$f_{1'}(X) = \frac{a_1}{(X-\Delta 1)} + a_4(X-\Delta 1) + \rho_1$$

$$f_{2'}(X) = \frac{a_1+a_3}{(X+\Delta 2)} + a_4(X+\Delta 2) - \rho_2$$

FIGURE 2.12: COMMON MINIMUM BOUNDS ON FUNCTION f(x)

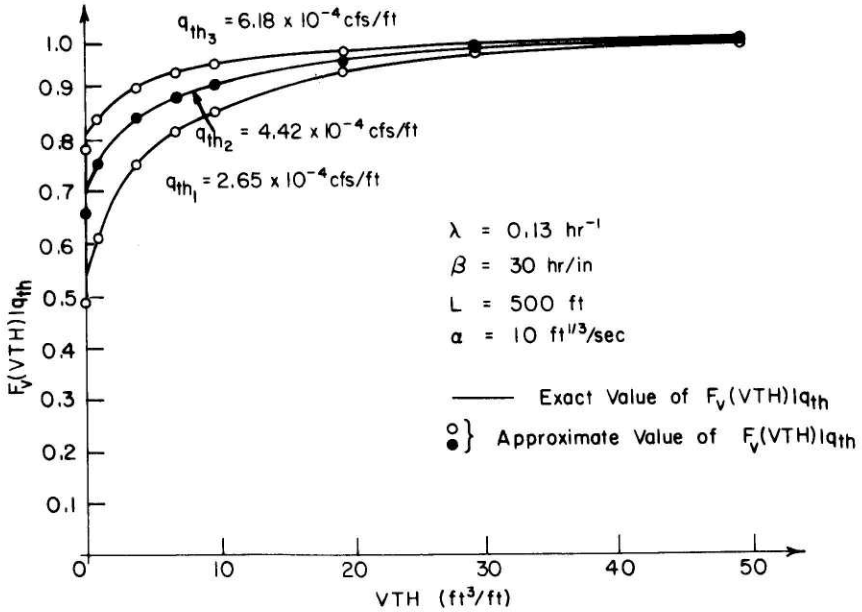

FIGURE 2.13: CUMULATIVE DISTRIBUTION OF FLOOD-VOLUME
(EFFECTS OF VARYING THRESHOLD DISCHARGE)

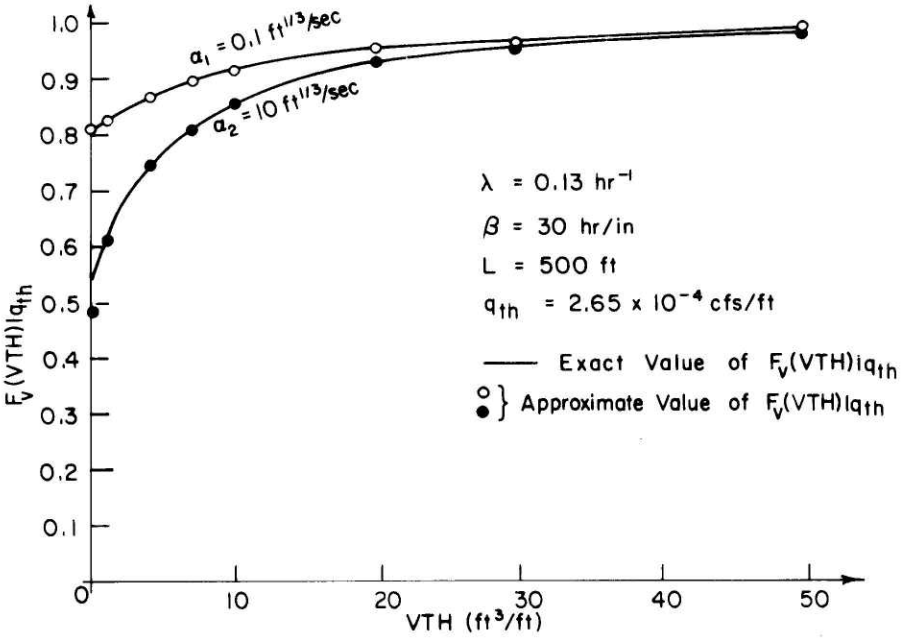

FIGURE 2.14: CUMULATIVE DISTRIBUTION OF FLOOD-VOLUME
(EFFECTS OF VARYING α)

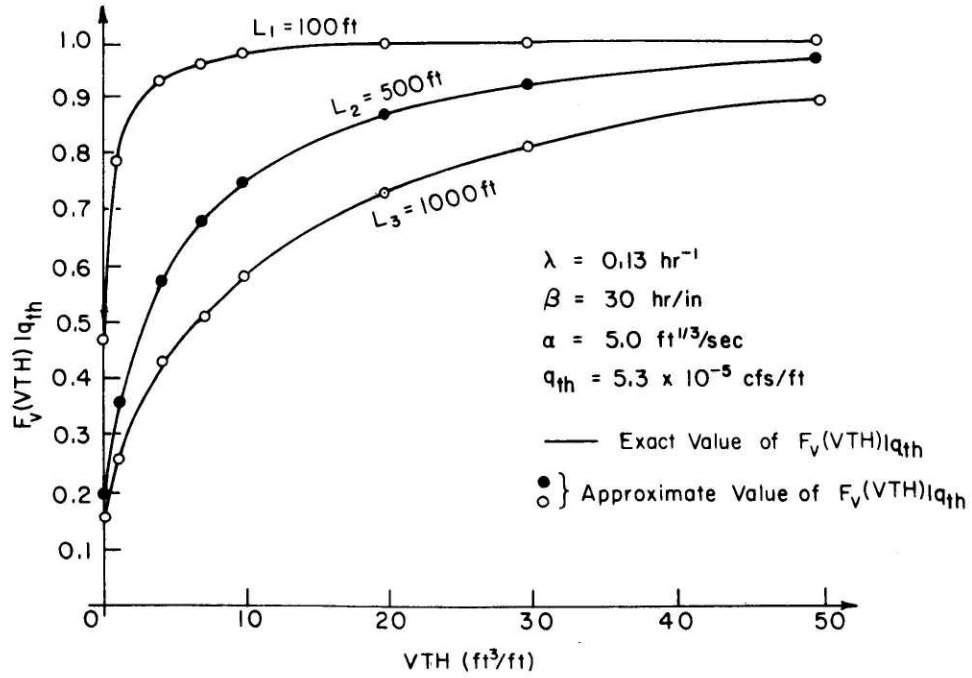

FIGURE 2.15: CUMULATIVE DISTRIBUTION OF FLOOD-VOLUME
(EFFECTS OF VARYING FLOW LENGTH)

CDF. As it is also shown in the figure, the greater the length, the smaller the probability of zero volume for a given q_{th}.

As it can be seen, the correctness of the expression of the CDF of flood-volume is confirmed in the above figures. The goodness of approximations is well-illustrated. The next chapter will demonstrate how this expression may be applied in the design of flood control systems in urban areas.

Chapter 3

APPLICATION OF THE FLOOD-VOLUME DISTRIBUTIONS TO AN URBAN CATCHMENT

3.1 Annual Exceedance Series of Flood-Volumes

The flood-volume distribution function derived in Chapter 2 gives a probabilistic statement of the occurrence of an event for all times. Traditional engineering usage obtains extreme value distributions for floods from annual exceedance series. These are expressed in function of the recurrence interval which is defined as the interval during which an event of a specified magnitude will be equaled or exceeded once on the average. The recurrence interval is expressed in years.

From Equation (2.131), the CDF of the flood-volume is given as

$$F_v(V_{th}) \cong 1 - a_4 e^{-a_4 a_2 + \rho_2} \left[2\sqrt{(a_1 + a_3)/a_4}\, K_1(2\sqrt{(a_1 + a_3)a_4} - \Delta_2 E_2 \left(\frac{a_1 + a_3}{\Delta_2} \right) \right] \qquad (2.131)$$

The exceedance probability of the flood-volume, $F_E(\cdot)$, is

$$F_E(VTH) \equiv \text{Prob}(V_{th} > VTH) = 1 - F_v(VTH) \qquad (3.1)$$

Define, N = number of years of observations of an event

n = average number of observations per year

nN = total number of observations

An event may represent storm depth, annual yield or flood-volume, etc. If the values (assumed independent) of observations of the event, flood-volume, are arranged in decreasing order of magnitude with order number **m** = 1 for the maximum value, m = nN for the minimum value, an ordered series may be formed with expected probability of exceedance given by

$$F_E(VTH_m) \equiv \text{Prob}(V_{th} \geq VTH_m) = \frac{m}{nN + 1} \tag{3.2}$$

For an annual exceedance series, only the N highest values from the nN values are to be considered. It is defined as

$$P_E(VTH_m) \equiv \text{Prob}(V_{th} \geq VTH_m)\Big|_{\substack{\text{Annual} \\ \text{basis}}} \equiv \frac{m}{N + 1} = \frac{1}{T_E} \tag{3.3}$$

where T_E is the recurrence interval in years on an annual exceedance basis. Dividing Equation (3.3) by Equation (3.2), where m is the same in both series, results in

$$\frac{P_E(VTH_m)}{F_E(VTH_m)} = \frac{nN + 1}{N + 1} = \left(\frac{1}{T_E}\right)\left(\frac{1}{F_E(VTH_m)}\right) \tag{3.4}$$

Since quite often N >> 1, then Equation (3.4) becomes

$$\left(\frac{1}{T_E}\right)\left(\frac{1}{F_E(VTH_m)}\right) \cong \frac{nN}{N} = n$$

or

$$\frac{1}{T_E} \cong n\ F_E(VTH_m) \tag{3.5}$$

The final expression of the annual exceedance series, after combining Equations (2.131),(3.1) and (3.5), leads to

$$\frac{1}{T_E} = na_4 e^{-a_4 a_2 + \rho_2} \left[2\sqrt{(a_1 + a_3)/a_4}\, K_1 [2\sqrt{(a_1 + a_3)a_4} - \Delta_2 E_2 \left(\frac{a_1 + a_3}{\Delta_2} \right) \right] \qquad (3.6)$$

3.2 Modeling an Urban Catchment (Lump Design)

3.2.1 Estimation of physical parameters of an urban catchment

An urban area may be ideally subdivided into a number of small catchments. Each catchment is characterized by a set of parameters such as length and width, slope of land, soil types, average infiltration rate, etc. Some of these parameters may be obtained from a topographic map, others might have to be estimated from collected data.

Of all the parameters to be estimated, the average infiltration rate is one of the most susceptible to uncertainty. A constant temporal-spatial average infiltration rate of an urban catchment composed of diverse soil types is extremely hard to estimate. Of course, such a constant is nothing but a convenient notation employed to account for a complex process which is not yet fully understood. In reality, such a constant never exists. In order to generalize different urban catchments, the average infiltration rate should be determined with little or no measurements of rainfall or runoff available. In other words, the average infiltration rate has to be estimated from the soil types and the degree of imperviousness of an urban catchment. It is here proposed

to assess the effect of infiltration by employing the runoff coefficient in the Rational Method. Instead of modeling the rainfall excess rate, i_e , by subtracting an average infiltration rate ϕ from the average areal rainfall intensity, $\bar{i}_o$, it is modeled as a percentage of the average areal rainfall intensity. That is

$$i_e = C\ \bar{i}_o \tag{3.7}$$

where C is the runoff coefficient in the Rational Method for estimating the peak discharge of small urban catchments. The rational equation is

$$Q_p = C\ i\ A \tag{3.8}$$

in which i = chosen uniform rainfall intensity of duration $t_r > t_c$

A = area of catchment

C = runoff coefficient

Q_p = peak discharge

t_c = concentration time

The runoff coefficient, C, is assumed to be a constant. A table for C is given in Appendix A. It ranges from 0.1 for a sandy soil to 0.95 for central business areas.

A composite runoff coefficient based on the percentage of different types of surface in an urban catchment is computed as:

$$C = \frac{\sum_i C_i\ A_i}{\sum_i A_i} \tag{3.9}$$

where C_i = runoff coefficient for the surface A_i.

Since extreme events are important in the frequency analysis of the flood-volume, the upper limits of C should always be used.

The catchment area is usually well-defined and obtainable from a topographic map using a planimeter. However, the shape of the catchment has to be modeled (Bras and Perkins, 1975) as rectangular block(s) in order to apply the kinematic wave routing uniformly over each segment. For a rectangular block,

$$A = L_c \, L_s \tag{3.10}$$

where A = catchment area

L_c = overland flow length

L_s = stream flow length

If the overland flow length is well-defined, L_s is computed as:

$$L_s = \frac{A}{L_c} \tag{3.11}$$

If the streamflow length is well defined, L_c is computed as

$$L_c = \frac{A}{L_s} \tag{3.12}$$

The kinematic wave parameter, α, is a function of Manning's roughness coefficient and the average slope of the surface. The average slope can be estimated from a contour map. The roughness coefficient is a measure of roughness of surface on which the water flows. Standard values of this coefficient may be found in handbooks of hydrology. The higher the value of α, the faster the flow. Since it is the path of flow that is important in determining the concentration time, it would be

appropriate to compute a composite kinematic wave parameter averaged over length (Bras and Perkins, 1975)

$$\alpha = \frac{\sum_i \alpha_i L_i}{\sum_i L_i} \tag{3.13}$$

where α_i = kinematic wave parameter for the flow length, L_i.

An example will follow, illustrating the use of the urban catchment model.

3.2.2 Derived frequency curves of flood-volumes for Gray Haven

The chosen case study is Gray Haven, located seven miles east of Baltimore City in Maryland (Tucker, 1969). The catchment has a total area of 23.29 acres of which 52% of the area is impervious. It is an homogeneous residential type area containing group houses on lots of about 2000 to 3000 square feet.

A map of Gray Haven is shown in Figure 3.1, together with the sewer line. Five types of overland flow segments are identified on the map, namely: street, lawn, roof, backyard and alley. There are two basic types of drainage modules of the catchment which are shown in Figure 3.2. Water from roofs, after flowing over a pervious grass surface of approximately 40 feet, drains into alleys which feed triangular channels. The lawns and streets drain to gutters. After water reaches the gutters or channels, it all drains to the sewer, as shown on the map of Gray Haven. The average overland flow length for each segment is shown in Figure 3.2, with segment(s) classified into four different types given by T_1, T_2, T_3 and T_4.

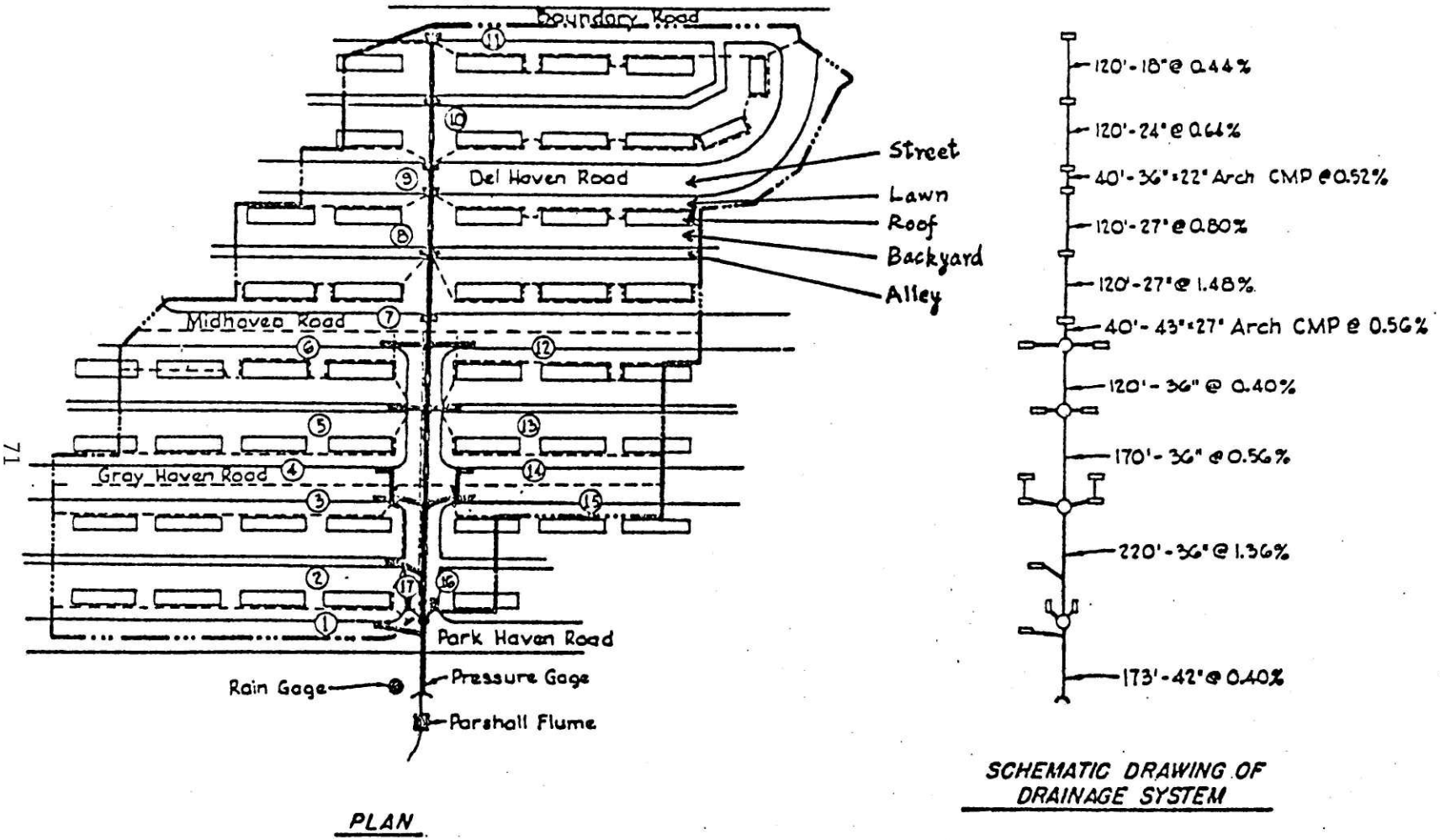

Figure 3.1: Map of the Gray Haven Urban Catchment

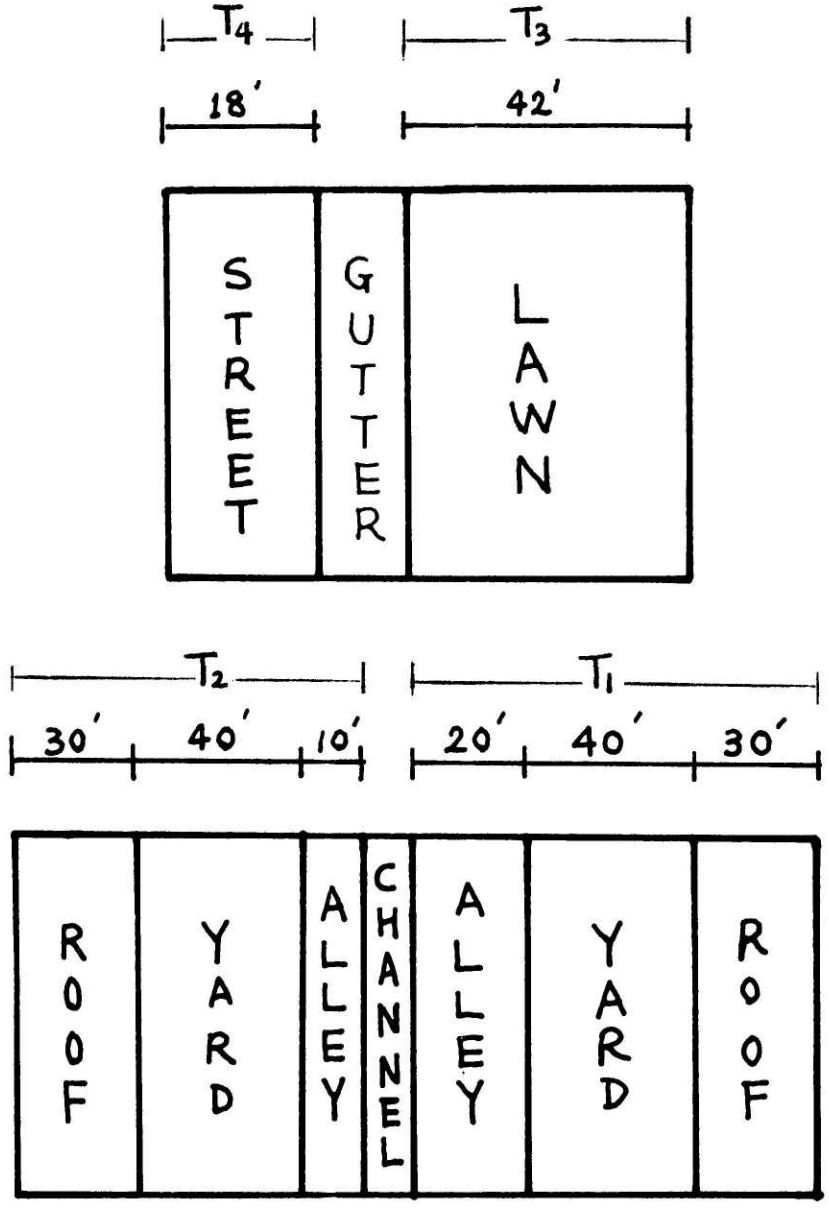

Figure 3.2: Basic Drainage Modules of the Gray Haven Catchment

Figure 3.3 gives a detailed map of gutter and channel flows. Table 3.1 gives values of relevant parameters (Leclerc and Schaake, 1973).

A detailed breakdown of the total area into segment types (Leclerc and Schaake, 1973) shows:

Type	Area (acres)
Street	3.433
Roof	4.476
Alley	2.238
Sidewalk	1.980
Lawn	5.193
Backyard	5.968

The sidewalk is added in because in the prototype it occupies a very narrow band of land in front of the lawn. Its inclusion allows the preservation of the imperviousness ratio of 0.52.

The catchment was gauged by the Johns Hopkins University Storm Drainage Research Project. Some synchronized rainfall and runoff data from 1963 to 1966 are available from Tucker (1969).

Since the catchment has a well-defined streamflow length (sewer line) and its area is more or less spread equally on both sides of the storm sewer, it seems reasonable to model the catchment into two equal rectangular blocks with (Bras and Perkins, 1975)

$$L_c = \frac{A}{2L_s} \tag{3.14}$$

where L_s = length of main storm sewer

L_c = equivalent length of overland flow

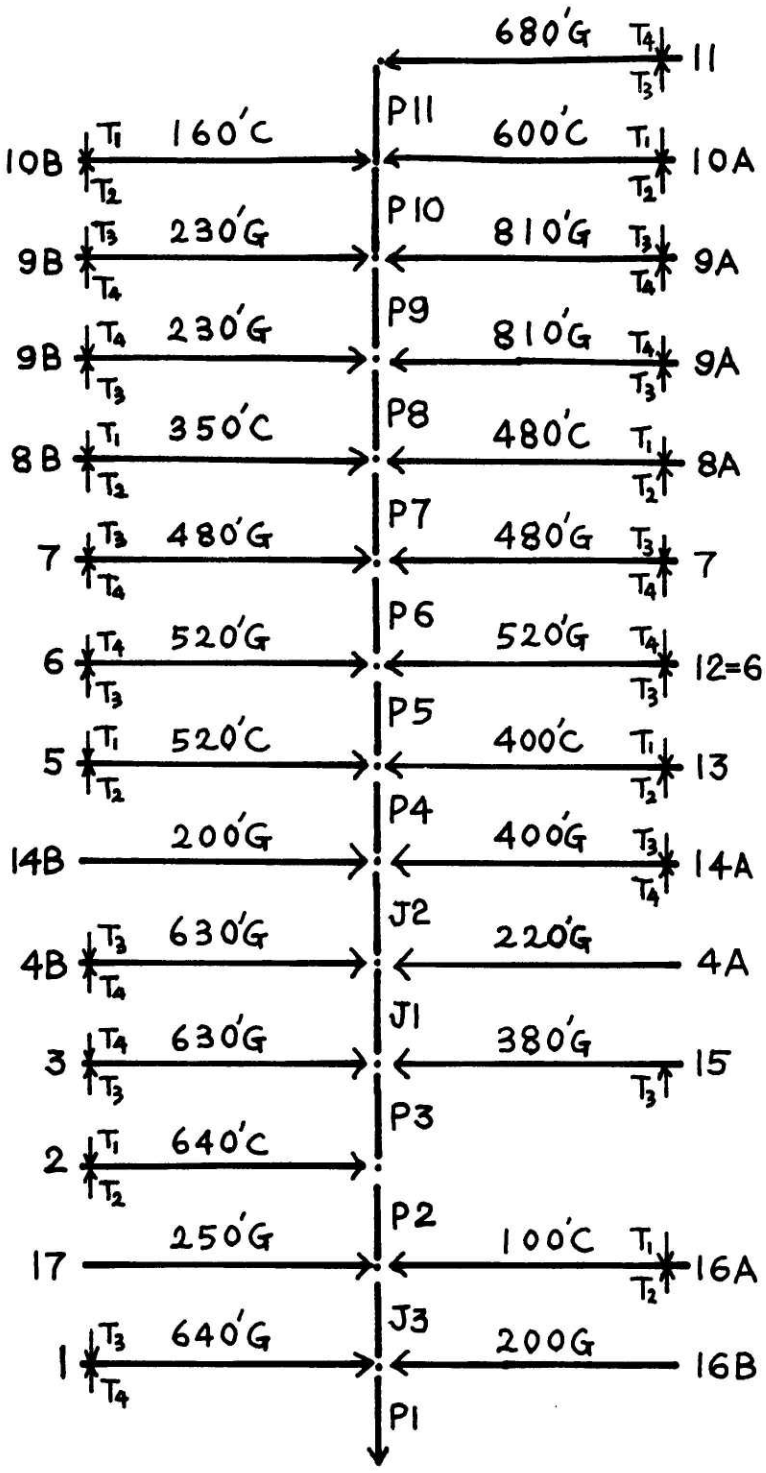

Note: C stands for channel
G " " gutter
T_1, T_2, T_3, T_4 are different types of overland flow segment

Figure 3.3 : Connectivity of the Gutters, Channels and Pipes for Gray Haven

Table 3.1

PARAMETERS OF THE DETAILED SEGMENTATION*

	Type	Length	Slope	Roughness
	overland flow (street)	18.	0.04	0.15
	overland flow (lawn)	42.	0.05	0.50
	overland flow (roof)	30.	0.05	0.15
	overland flow (backyard)	40.	0.05	0.50
	overland flow (alley)	10.	0.05	0.15
	overland flow (alley)	20.	0.05	0.15
11	gutter	680.	0.02	0.02
P11	pipe	120.		0.014
10A	triangular	600.	0.01	0.02
10B	triangular	160.	0.01	0.02
P10	pipe	120		0.014
9A	gutter	810.	0.01	0.02
9B	gutter	230.	0.01	0.02
P9	junction	0		
P8	pipe	160.		0.014
8A	triangular	480.	0.01	0.02
8B	triangular	350.	0.01	0.02
P7	pipe	120.		0.02
7	gutter	480.	0.01	0.02
P6	junction	0		
6	gutter	520.	0.01	0.02
P5	pipe	160.		0.014
13	triangular	400.	0.01	0.02
5	triangular	520.	0.01	0.02
P4	pipe	170.		0.014
4A	gutter	220.	0.01	0.02
4B	gutter	630.	0.01	0.02
14A	gutter	400.	0.01	0.02
14B	gutter	200.	0.01	0.02
J1	junction	0.		
J2	junction	0.		
3	gutter	630.	0.01	0.02
15	gutter	380.	0.01	0.02
P3	pipe	130.		0.014
2	triangular	640.	0.01	0.02
P2	pipe	80.		0.014
17	gutter	250.	0.01	0.02
16A	triangular	100.	0.01	0.02
16B	gutter	200.	0.01	0.02
J3	junction	0.		
1	gutter	640.	0.01	0.02
P1	pipe	173.		

Total area = 23.29 Imperviousness ratio = 0.52

*(Leclerc & Schaake, 1973)

A = total area of catchment.

In urban areas, overland flow is dominant. The concentration time for overland flow is usually much longer than that for streamflow, where streamflow is taken as flow in storm sewers. Therefore, it is further assumed that the flow, Q, at outlet of catchment, is equal to the overland flow rate per unit width (q_L) multiplied by the length of streamflow channel, L_s. That is,

$$Q = 2\ q_L\ L_s \tag{3.15}$$

This is a conservative assumption because it slightly overestimates the true streamflow rate. It implies that once the overland flow reaches the sewer, it will flow along the sewer to the outlet in no time.

Under the assumption of Equation (3.15), it follows that,

$$(V_{th})_s = (V_{th})_c .2\ L_s \tag{3.16}$$

and

$$(q_{th})_s = (q_{th})_c .2\ L_s \tag{3.17}$$

where subscript c stands for overland flow, s stands for streamflow; and V_{th}, q_{th} are given and explained in Chapter 2.

The runoff coefficient for each segment type is chosen as:

Type	C_i	A_i (acres)
Street	0.95	3.433
Roof	0.95	4.476
Alley	0.95	2.238
Sidewalk	0.95	1.980
Lawn	0.35	5.193
Backyard	0.47	5.968

The runoff coefficient for the backyard is based on the assumption that 80% of the backyard is lawn and 20%, impervious area. This is a reasonable assumption since in backyards, generally, there are concrete pathways and other works. This assumption also serves to increase the rainfall excess rate for conservative estimation of the flood-volume.

From the above data, a composite value of the runoff coefficient for the catchment is, from Equation (3.9)

$$C = \frac{\Sigma\, C_i\, A_i}{\Sigma\, A_i} = 0.69$$

An average value of the kinematic wave parameter, α, from Table 3.1, neglecting pipes and junctions, and from Figure 3.3, is computed as (using Equations (2.46) and (3.13))

$$\alpha_i = \frac{1.49}{n_i} (S_o)_i^{1/2}$$

and

$$\alpha = \frac{\Sigma\, \alpha_i\, L_i}{\Sigma\, L_i} = 6.4771 \text{ ft.}^{1/3}/\text{sec.}$$

The streamflow length is given by the length of storm sewer in Figure 3.1, i.e.,

$$L_s = 1243 \text{ ft.}$$

and the overland flow length, from (3.14), is

$$L_c = \frac{A}{2L_s} = 408 \text{ ft.}$$

The above representation of the catchment is simulated using the analytical solutions to the kinematic wave equations (2.52 through 2.63) for several storms. Results are shown on Figures 3.4 to 3.7. As it is expected, the simulated streamflow rate is generally higher than the actual flow rate because of the assumption that once the overland flow reaches the sewer, it will flow to the outlet in no time. This assumption also implies that the concentration time (defined as time to peak discharge) in the model is less than that of the actual catchment. Lowering the value of the runoff coefficient may force the two concentration times to meet, but then it will constantly underestimate the peak discharges of extreme events which are most important in the estimation of flood-volumes.

Since the area of the catchment is small (23.3 acres), the response of the catchment is fast. For this reason, any high sharp peak appearing in the rainfall event will produce a peak discharge which cannot be followed by the kinematic wave routing using an average uniform rainfall intensity. This effect is shown in the storm of August 1, 1963.

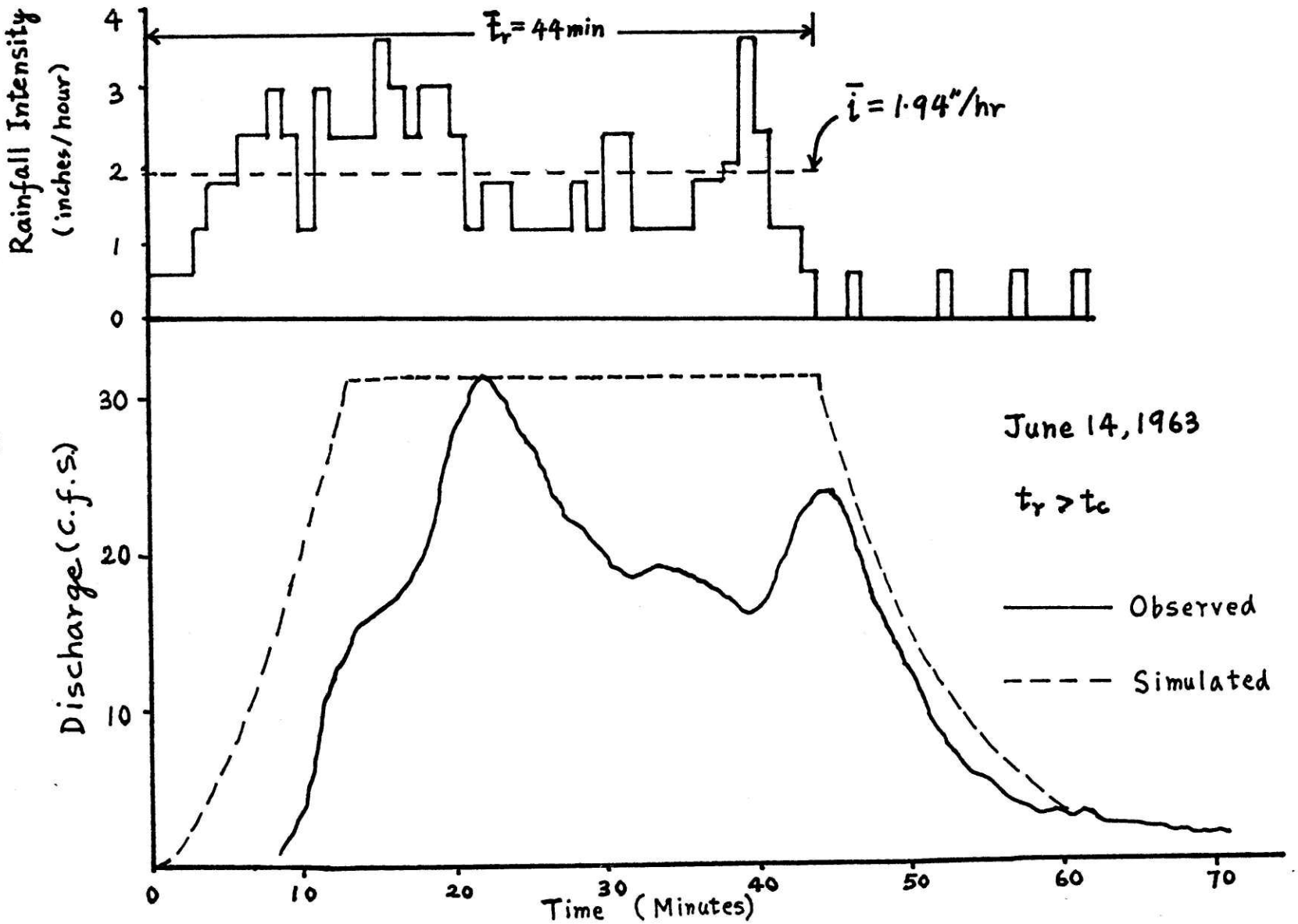

FIGURE 3.4: OBSERVED VS SIMULATED HYDROGRAPHS (STORM OF JUNE 14, 1963)

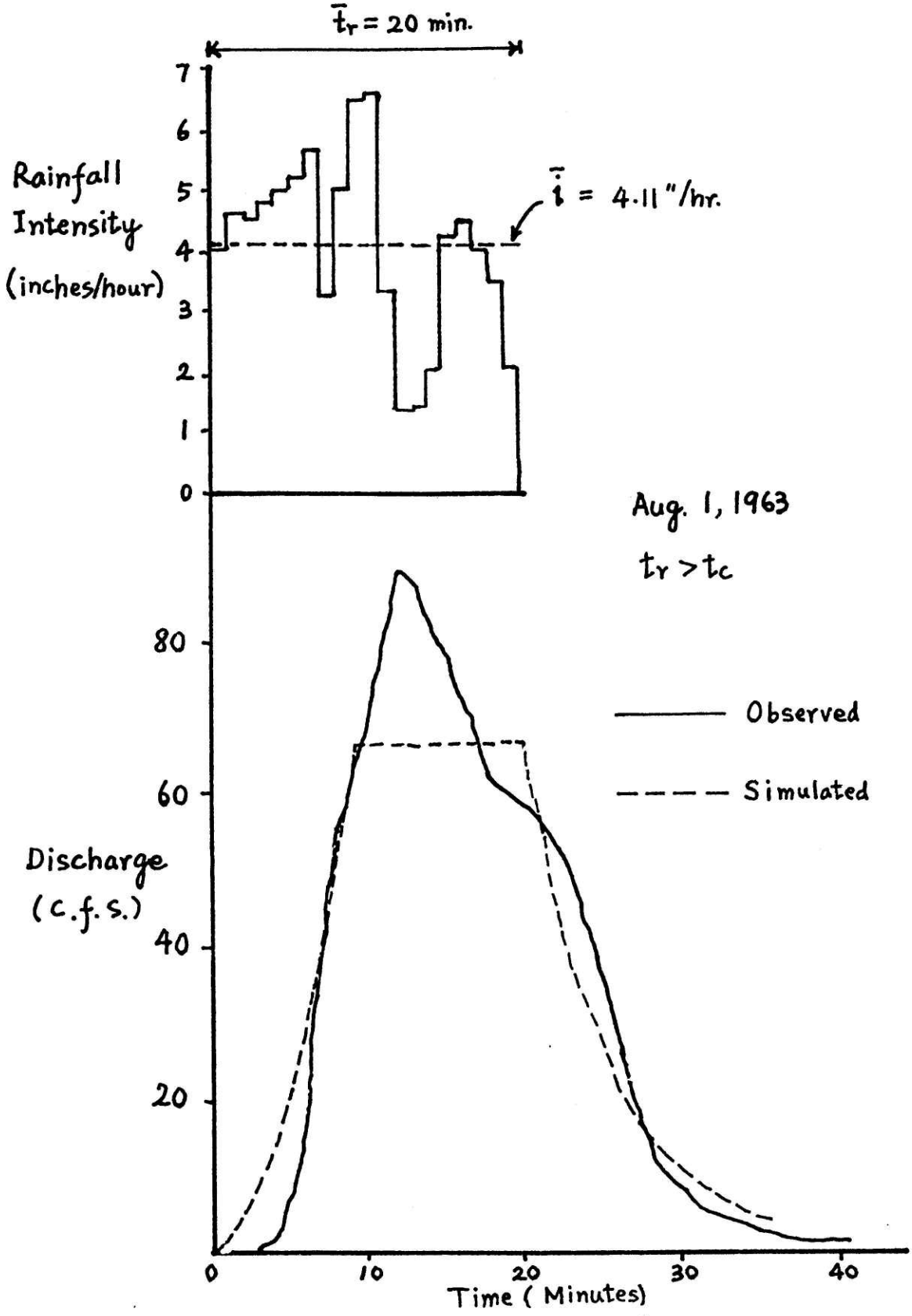

FIGURE 3.5: OBSERVED VS SIMULATED HYDROGRAPHS (STORM OF AUGUST 1,1963)

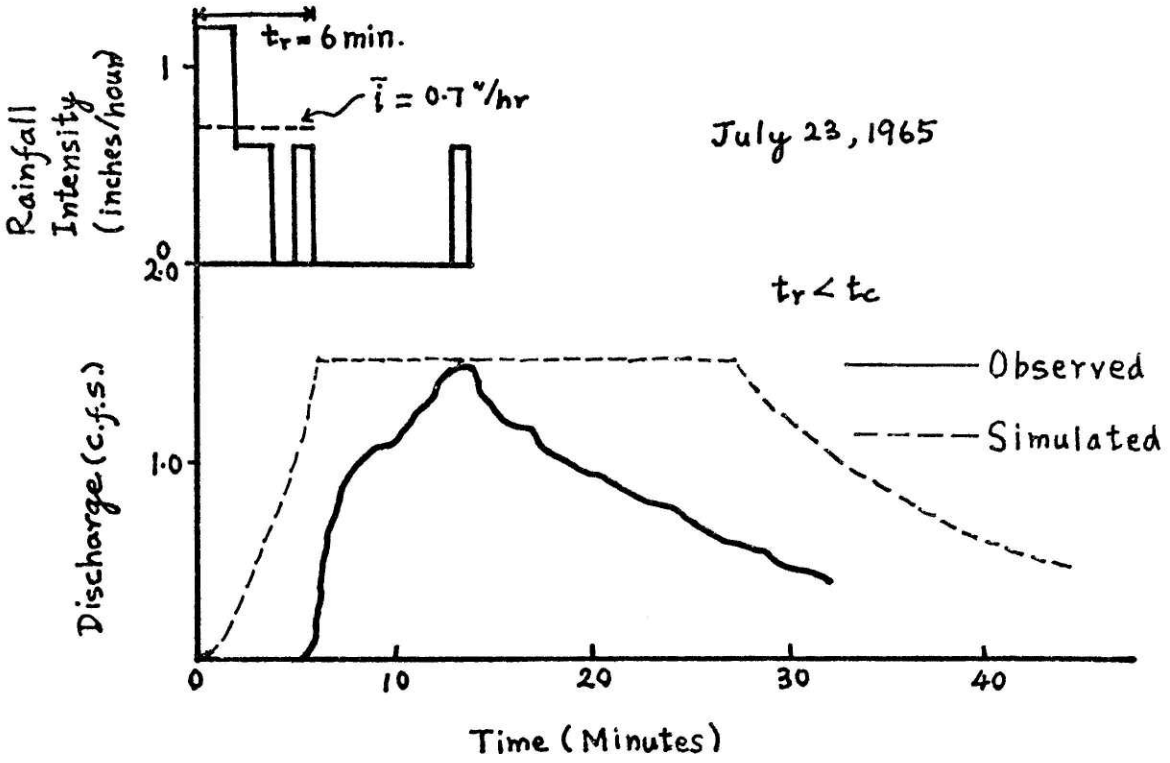

FIGURE 3.6: OBSERVED VS SIMULATED HYDROGRAPHS (STORM OF JULY 23,1965)

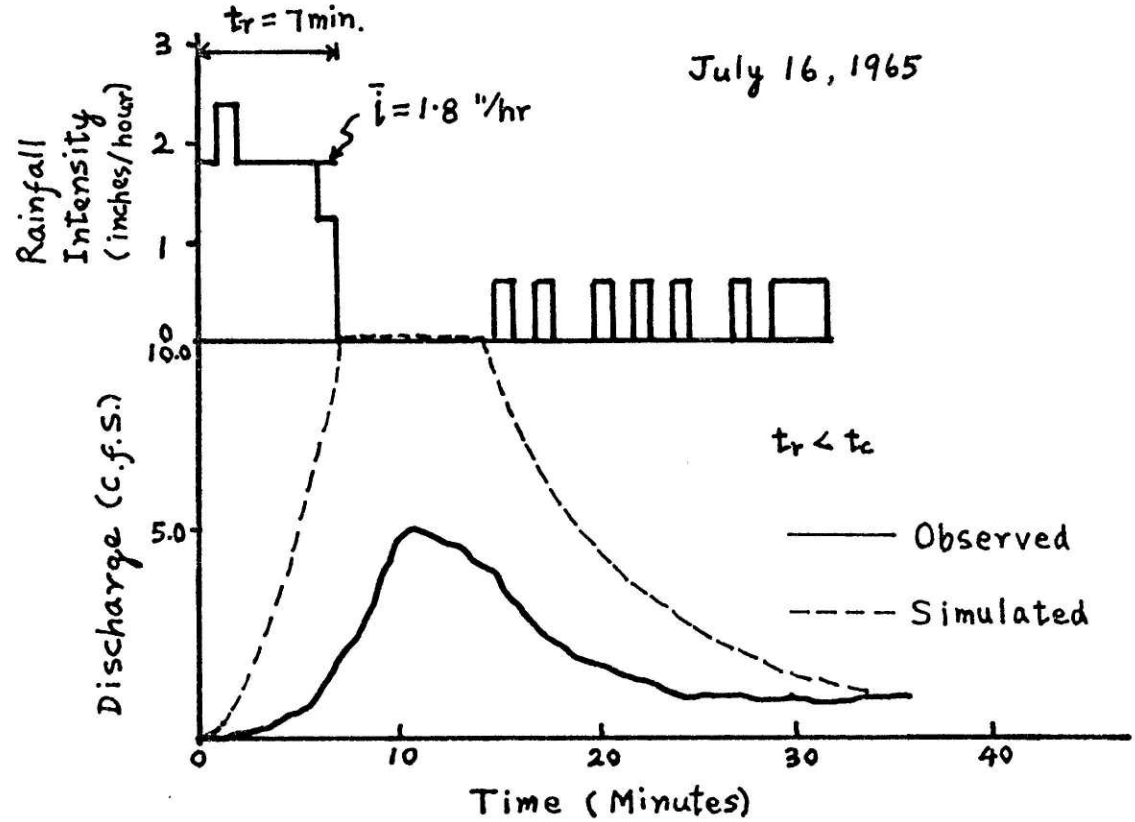

FIGURE 3.7: OBSERVED VS SIMULATED HYDROGRAPHS (STORM OF JULY 16,1965)

For high uniform rainfall intensities, the simulated catchment model matches the actual hydrograph reasonably well. Low rainfall intensities lead to overestimation of the flood-volumes. Nevertheless, the small volumes of water in such cases will have little effect on the accuracy of the distribution of the extreme events of interest.

It is felt that the approximate catchment model used will reasonably represent the order and frequency of the desired threshold volumes leading to a good c.d.f. Considering the approximations, the uniform rainfall intensity and the effortless fitting of parameters, the analytical solution does fairly well.

The catchment was gauged by the Johns Hopkins University Storm Drainage Research Project from 1959 to 1967. Only several years of rainfall and runoff records are easily available from Tucker (1969). In order to estimate the rainfall parameters, the rainfall data of Baltimore City in Maryland, which is seven miles west of Gray Haven, is used instead. Hourly rainfall data for the Custom House Gage, Baltimore, Maryland, is obtainable from U. S. W. B. Publications. The data for the period May 1948 to June 1970 were analyzed. Leclerc and Schaake (1973) summarized the results as shown in Figure 3.8 and Table 3.2. The parameters in the exponential distribution function of rainfall duration and intensity are computed as:

$$\lambda = 1/\text{mean of rainfall duration} \qquad (3.18)$$

$$\beta = 1/\text{mean of rainfall intensity} \qquad (3.19)$$

From Table 3.2 , the mean of rainfall duration is estimated to be 5.86 hours. (Using an equation similar to Equation 3.20)

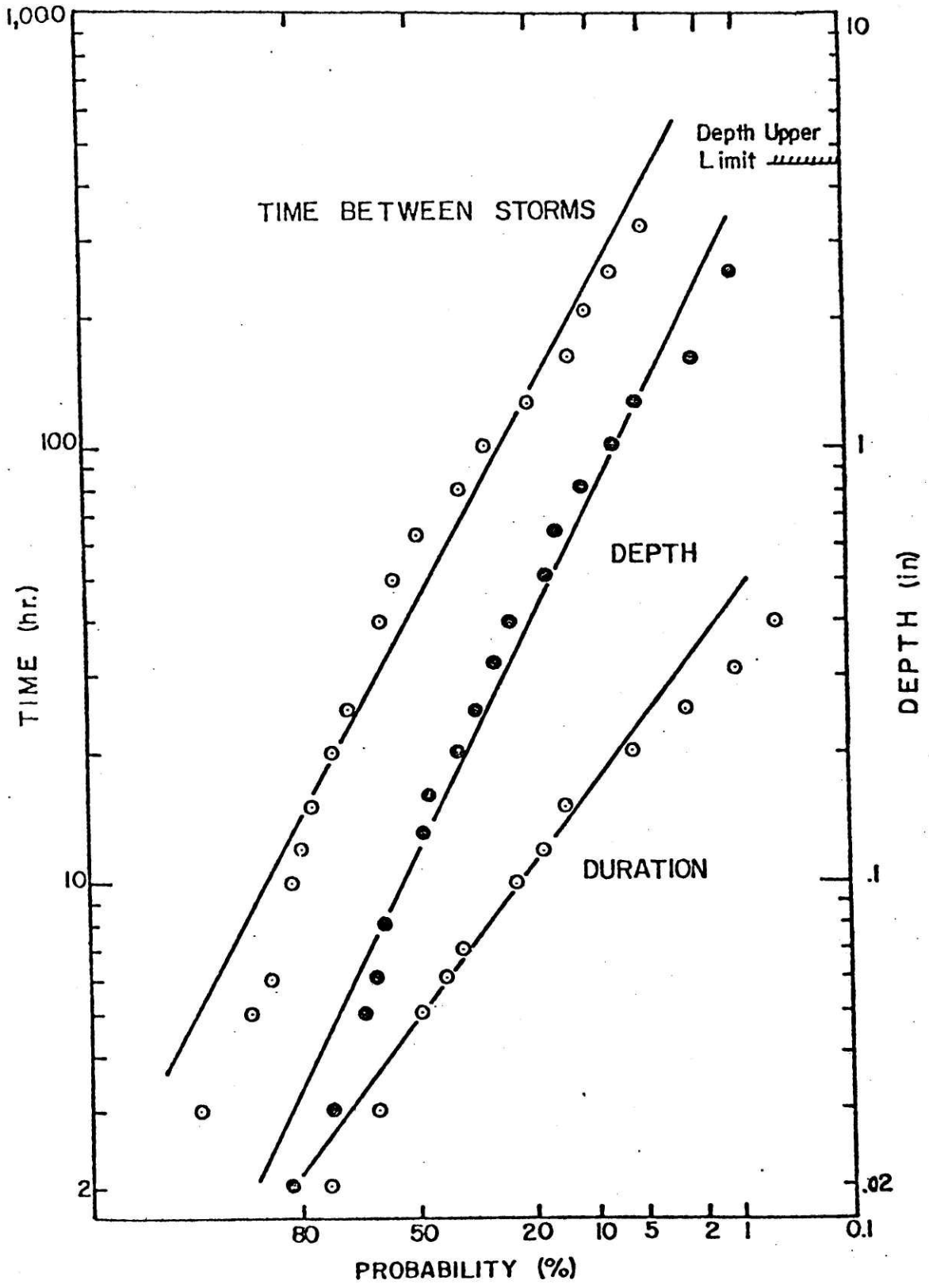

Figure 3.8 : Example Distribution of the parameters τ, d and t_r

(LECLERC AND SCHAAKE, 1973)

Table 3.2

MOMENTS OF STORM EXTERIOR PARAMETER DISTRIBUTIONS FOR BALTIMORE, MARYLAND
(Untransformed Data)

	Means				
Month	Time Between Storms (hrs.)	Storm Duration (hr.)	Storm Depth (in.)	Storm Intensity (in./hr.)	Number of Storms per Month
Jan.	90.7	7.54	.303	.040	8.32
Feb.	76.0	7.53	.346	.046	7.95
Mar.	77.2	7.42	.394	.053	9.38
Apr.	60.0	5.56	.286	.052	11.32
May	64.6	4.99	.322	.065	10.39
Jun.	75.1	4.28	.398	.093	9.09
Jul.	80.0	3.32	.390	.118	8.55
Aug.	69.4	4.09	.439	.107	9.14
Sep.	97.4	4.95	.409	.083	7.45
Oct.	109.9	5.83	.385	.066	6.19
Nov.	111.1	6.89	.377	.055	7.05
Dec.	95.1	9.07	.455	.051	6.86

From Table 3.2, the mean of rainfall intensity is estimated by the following:

$$\bar{i} = \frac{\sum_{j=1}^{12} n_j \, i_j}{\sum_{j=1}^{12} n_j} \tag{3.20}$$

where n_j = average number of storms for month j

i_j = average storm intensity for month j

The obtained result is,

$$\bar{i} = \frac{7.056}{101.69} = 0.0694 \quad \text{"/hr.}$$

The final step in deriving the flood-volume frequency curves requires the incorporation of the infiltration effect into Equation (3.6).

Starting with:

$$i_e = C \, \bar{i}_o \tag{3.7}$$

and

$$f(\bar{i}_o) = \frac{\beta}{K} e^{-\frac{\beta}{K} \bar{i}_o} \tag{2.20}$$

results in

$$f(i_e) = \frac{\beta}{KC} e^{-\frac{\beta}{KC} i_e} \tag{3.21}$$

By modeling the rainfall excess rate as a percentage of the average areal rainfall intensity (3.7), the duration of rainfall excess is simply the duration of the average areal rainfall intensity. Therefore,

$$f(t_{re}) = f(t_r) = \lambda e^{-\lambda t_{re}} \tag{3.22}$$

The joint density function of rainfall excess and duration of rainfall excess (assumed independent) now becomes

$$f(i_e, t_{re}) = \frac{\beta\lambda}{KC} \exp[-\frac{\beta}{KC} i_e - \lambda t_{re}] \tag{3.23}$$

Notice the only difference between (3.23) and (2.26) is the replacement of 'K' in (2.26) by 'KC' to obtain (3.23). The change of a constant by another constant does not affect the outcome of an integration. Thus, the final expression for the annual exceedance series of the flood volume is the same as Equation (3.6) but with the parameter K changed to KC. Equation (3.6) gives the recurrence interval for the flood-volume per unit width of overland flow. It is necessary to transform it into the flood-volume for the whole catchment.

From Equations (3.16) and (3.17),

$$(V_{th})_c = (V_{th})_s/2L_s$$
$$(q_{th})_c = (q_{th})_s/2L_s$$

Equation (3.6) becomes

$$\frac{1}{T_E} \cong n a_4 e^{-a_4 a_2 + \rho_2} \left\{ 2\sqrt{(a_1 + a_3)/a_4}\, K_1[2\sqrt{(a_1 + a_3)a_4}] - \Delta_2 E_2 \left[\frac{a_1 + a_3}{\Delta_2}\right] \right\} \tag{3.24}$$

where now

$$a_1 = F_1 \lambda (V_{th})_s/(2L_s) \tag{3.25}$$

$$a_2 = (q_{th})_s/(2L_s) \tag{3.26}$$

$$a_3 = F_2F_3\ \lambda L_c \left[\frac{(q_{th})_s}{2\alpha L_s}\right]^{1/m} \tag{3.27}$$

$$a_4 = \frac{F_4\ \beta}{KCL_s} \tag{3.28}$$

Selected parameter values for the case study are:

α = 6.477 ft.$^{1/3}$/sec., K = 1.0

L_c = 408 ft. L_s = 1243 ft.

λ = 0.1706/hr. β = 14.41 hr./in.

C = 0.69 n = 101.69 storms/year

$F_1 = 2.78 \times 10^{-4}$ $F_2 = 2.3 \times 10^{-5}$

F_3 = 12.0 F_4 = 1.0

The results of Equation (3.24) are shown in Figure 3.9 together with the more exact values given by Equation

$$\frac{1}{T_E} \simeq na_4 e^{-a_4 a_2} \int_0^\infty \exp - \left[\frac{a_1}{x} + \frac{a_3}{x + a_2} + a_4 x\right] dx \tag{3.29}$$

The information on Figure 3.9 may be used for designing the capacity of water treatment plant and storage tank if storm sewage needs to be treated. For example, if a recurrence interval of 25 years were chosen, a water treatment plant with a maximum capacity of 5 cfs (3.23 MGD) would require a storage volume of 115,000 cubic feet,with a possible failure of the whole system on the average once in 25 years.

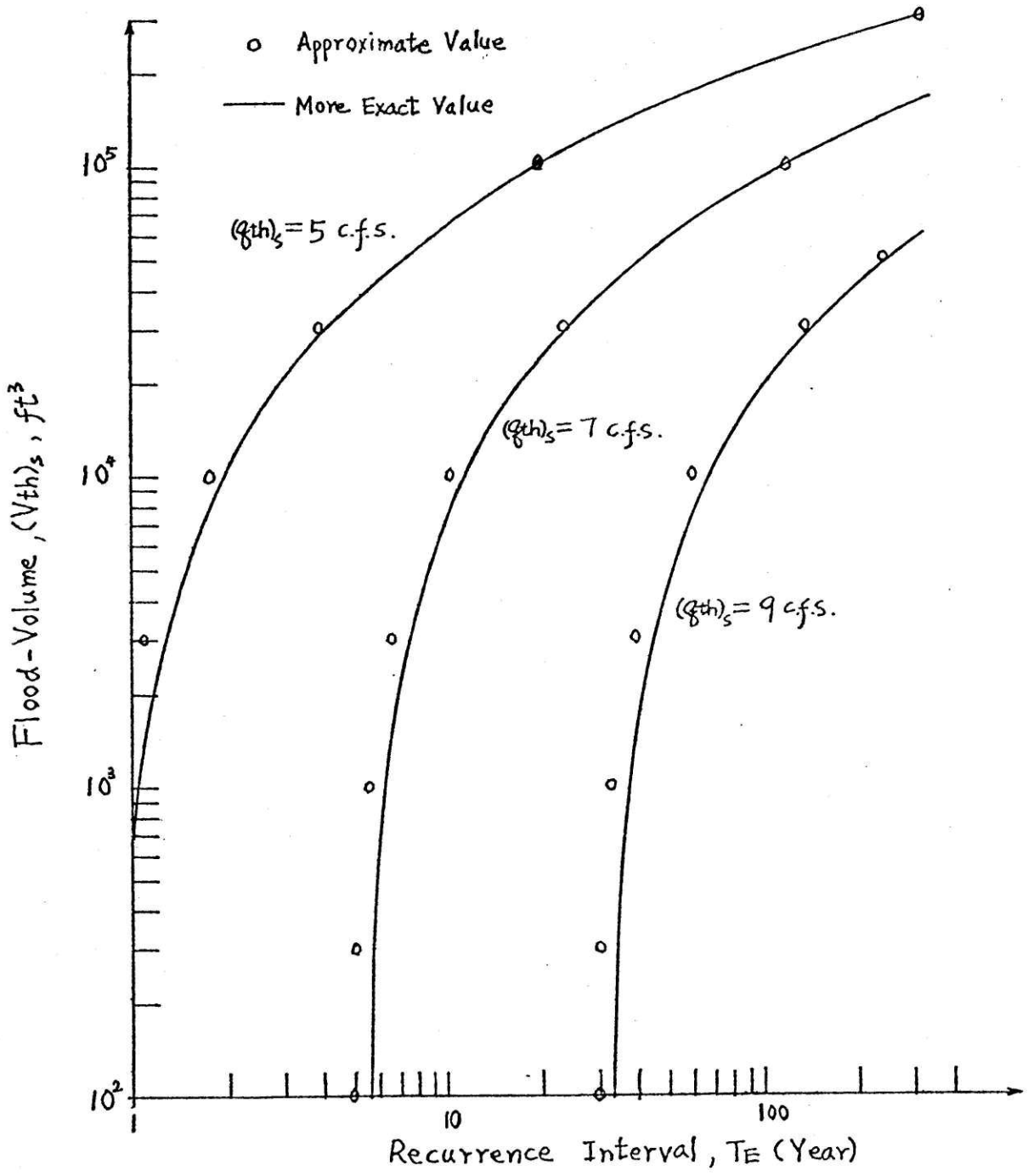

FIGURE 3.9: FLOOD-VOLUME FREQUENCY CURVES FOR THE GRAY HAVEN CATCHMENT

3.3 Conclusions

One of the main difficulties in judging the derived distribution approach for flood-volumes is the extreme scarcity of historical data adequate for comparisons. The determination of flood-volumes requires an entire hydrograph for each storm. In urban areas, continuous gaging records of runoff, even though some exist, are usually very short. Using historical records of less than ten years, the reliability of the comparison test is very much in doubt.

Another way of obtaining hydrograph data is by digital simulation. Hourly rainfall data for each storm is used as an input to a deterministic simulation model to reproduce an entire hydrograph so that the flood-volume for each storm can be determined. Since rainfall records are usually much longer than records of continuous discharge, it would be reliable to use the simulation approach to obtain the annual exceedance series of flood-volumes. But then, hundreds of storms have to be analyzed and the simulation cost would be enormous. At present, digital simulation seems to be the only mean by which an annual exceedance series of flood-volume can be obtained for comparison.

Since the model used is physically based, with reasonable parameters, there seems to be little doubt about the validity of this approach to small urban catchments. While at present better means of determining the distribution of flood-volumes are not available, the analytical, closed-form expression for the annual exceedance series of the flood-volumes will inevitably provide a fast, cheap, easy and

reliable means for the practitioners to make decisions on flood control measures in urban areas.

Chapter 4

STREAMFLOW MODEL

4.1 Introduction

Previous chapters have dealt with overland flow which usually governs urban areas. For large natural catchments in which streamflow is dominant, the single overland flow model is no longer adequate. In this chapter, a streamflow model will be considered. It consists of a uniform stream channel at the junction of two identical, plane catchments (Figure 4.1). The streamflow hydrograph may take many different forms, depending on the relative magnitudes of the duration of rainfall excess, overland concentration time and stream concentration times.

To solve the kinematic wave equations (4.1 and 4.2) for the streamflow case, the method of characteristics is theoretically preferred over the alternate finite difference methods since the former moves continuously along a characteristic curve in the space-time domain while the latter can only move from intersection to intersection on a finite difference grid in the same domain.

Few analytical solutions of the characteristic curves for the streamflow case are discussed in literature, mainly due to the mathematical difficulties encountered. Eagleson (1970) has presented a detailed analytical solution of the characteristic curves for a small stream for which $t_{re} < t_c$.

The main purpose of this chapter is to outline a procedure

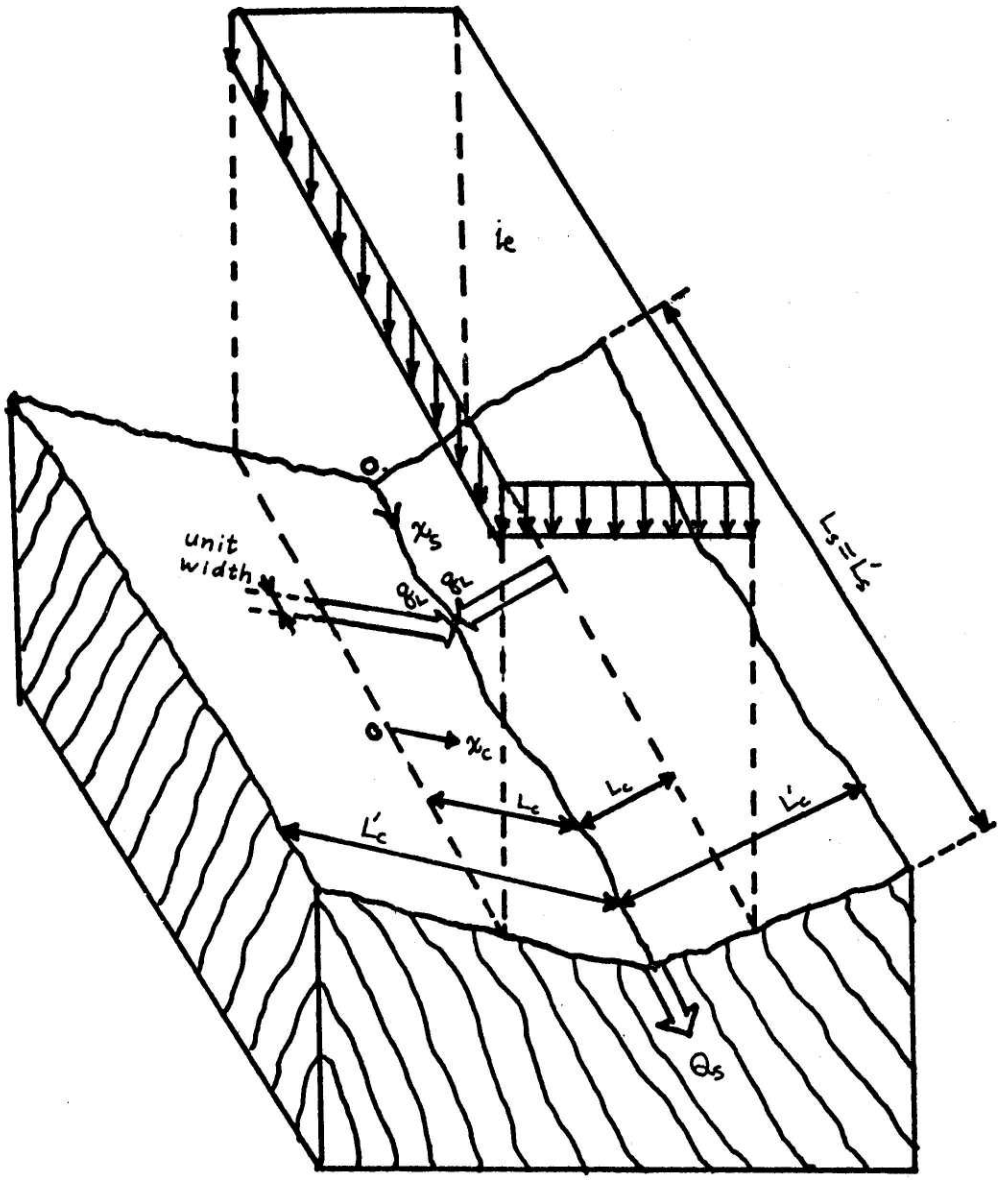

FIGURE 4.1: TYPICAL CATCHMENT-STREAM CONFIGURATION

for obtaining the cumulative density function (CDF) of the flood-volumes for the streamflow case. Some closed-form approximations to the analytical solutions of the kinematic wave equations in the streamflow case are offered.

4.2 Some Properties of the Kinematic Wave Model

Under uniform rainfall excess of duration t_{re}, overland flow response is one of the two cases, as seen in Chapter 2 (see Figure 4.2).

Case C.1: $t_{re} \geq t_c$

The discharge is increasing during the period $0 \leq t < t_c$, after which it will stay at its maximum for $t_c \leq t < t_{re}$. At $t = t_{re}$, the discharge begins to decline.

Case C.2: $t_{re} < t_c$

The discharge builds up during the period $0 \leq t < t_{re}$, after which it will stay at its maximum for $t_{re} \leq t < t_p$, where $(t_p - t_{re})$ is the time required for the initial disturbance to travel from its position at time t_{re} to $x = L_c$. At time t_p, the discharge begins to decline.

For the streamflow hydrograph, there are three general cases (Figure 4.3) to be considered, depending on the relative magnitudes of t_{re}, t_*. t_c, and t_s. t_* is the concentration time of the entire catchment and is defined as the sum of the overland flow concentration time, t_c, and the streamflow concentration time, t_s.

Case S.1: $t_{re} \geq t_* = t_c + t_s$

The discharge continues to build up until $t = t_*$, after which it will stay at its maximum value up to $t = t_{re}$. At $t = t_{re}$, the

FIGURE 4.2 CLASSIFICATION OF OVERLAND FLOW HYDROGRAPHS

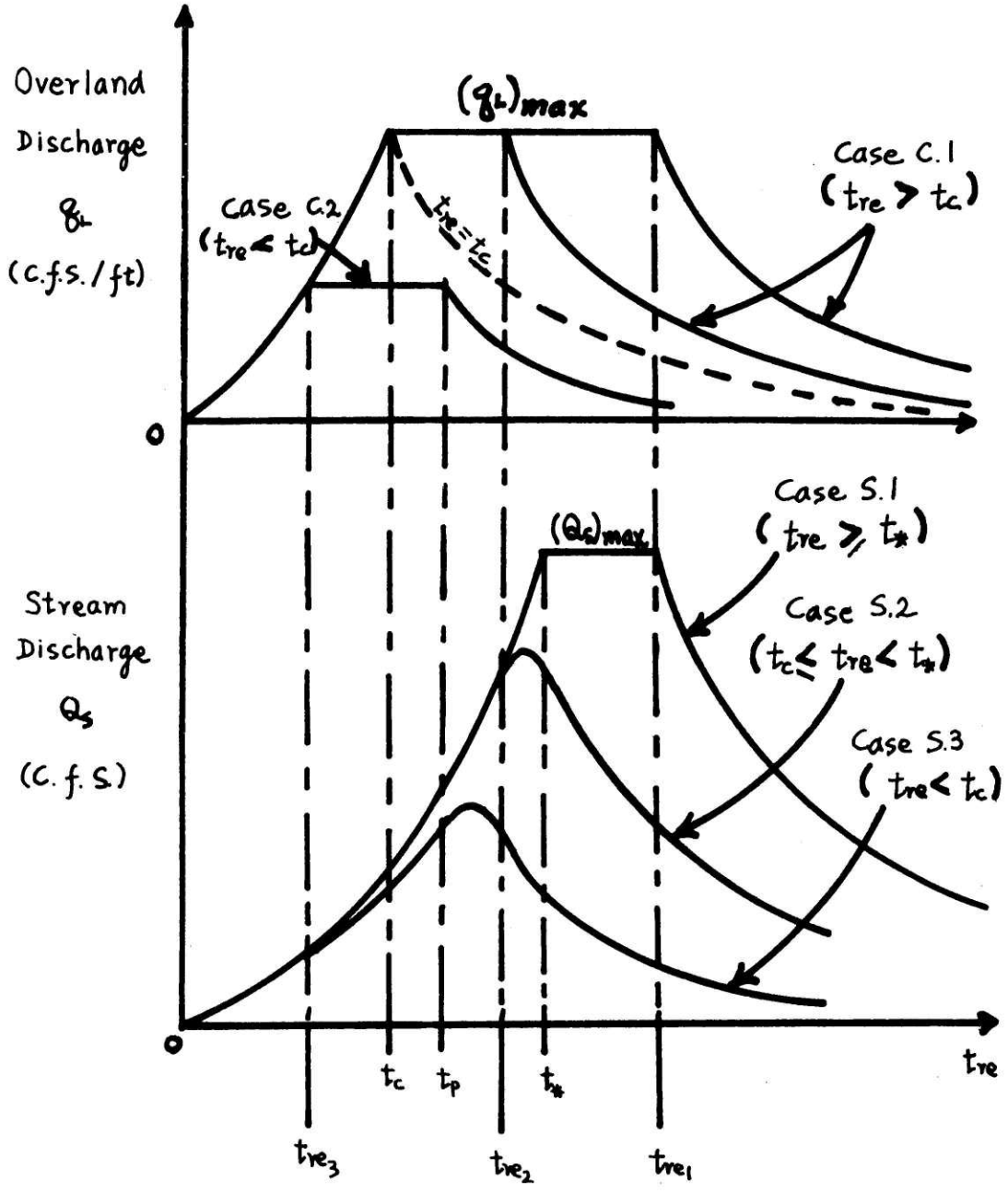

FIGURE 4.3 CLASSIFICATION OF STREAMFLOW HYDROGRAPHS

discharge begins to decline.

Case S.2: $t_c \leq t_{re} < t_*$

The discharge does not reach its maximum peak since $t_{re} < t_*$. It continues to grow beyond $t = t_{re}$ for a short while, after which recession begins.

Case S.3: $t_{re} < t_c$

The discharge continues to grow beyond $t = t_{re}$ but remains small. Recession begins shortly after $t = t_p$.

4.3 Relative Magnitudes of Concentration Time Constants in Natural Catchments

The equations representing the hydrographs of the streamflow case are extremely complex. They may take many alternative forms depending on the relative magnitudes of the time constants of the overland and stream segments. Comparing relative magnitudes of certain time constants and choosing the most probable events, it is possible to reduce the number of possible solutions to only three, one for each general hydrograph shape, (S.1, S.2, S.3) in Figure 4.3.

The derivation of the kinematic wave equations for the streamflow case is similar to those for the overland flow case, only that now the continuity equation becomes (Eagleson, 1970):

$$\frac{\partial A_s}{\partial t} + \frac{\partial Q_s}{\partial x_s} = 2q_L \qquad (4.1)$$

and the momentum equation becomes

$$Q_s = \alpha_s A_s^{m_s} \tag{4.2}$$

where Q_s = stream discharge at x_s

q_L = lateral inflow to stream along x_s

A_s = cross-sectional area of the stream channel at x_s

α_s = kinematic wave parameter for streamflow case

m_s = 3/2, for natural stream channel, trapezoidal shape.

Solving Equations (4.1), (4.2) by the method of characteristics (Harley, et.al., 1970) yields

$$\frac{dQ_s}{dt} = 2q_L . c_s \tag{4.3}$$

$$\frac{dA_s}{dt} = 2q_L \tag{4.4}$$

$$\frac{dQ_s}{dx_s} = 2q_L \tag{4.5}$$

$$\frac{dA_s}{dx_s} = 2q_L / c_s \tag{4.6}$$

Equations (4.3) through (4.6) are valid only along the characteristics,

$$\frac{dx_s}{dt} = c_s = \alpha_s m_s A_s^{m_s - 1} \tag{4.7}$$

These equations (4.2 to 4.7) define the shape of a streamflow hydrograph.

There are three important time constants to be considered:

t_c, t_s, t_s^*. t_c is the overland concentration time as defined in Chapter 2. The remaining time constants are defined as follows:

$t_s \equiv$ time for the water to travel from $x_s = 0$ at $t = t_c$ to $x_s = L_s$ under the condition that q_L is constant at its maximum value throughout $t_c \leq t \leq t_*$, given that $t_{re} \geq t_c + t_s$

$t_s^* \equiv$ time required for the water at $x_s = 0$, $t = 0$ to travel to L_s, irrespective of whether q_L is constant or not.

Referring to Figure 4.4, it can be seen that depending on the relative magnitudes of t_s^* with respect to t_c, t_p and t_{re}, different expressions and shapes for the streamflow hydrograph may result since whenever a characteristic curve starting at $x_s = 0$, $t = 0$ (limiting characteristic) crosses the lines $t = t_c$, $t = t_p$, $t = t_*$, $t = t_{re}$, the inflow to the stream channel, q_L, changes. The above leads to different equations for the characteristic curves.

All the possible paths leading to different hydrographs (corresponding to the situations given in Figure 4.4) are shown on Figure 4.5. Reduction of the number of paths is possible by identifying the most probable events. Since the wave velocity, c_s, is related to the cross-sectional area, A_s, and the streamflow discharge, Q_s, by

$$c_s = \frac{dx_s}{dt} \propto A_s^{1/2} \propto Q_s^{1/3} , \qquad \text{for } m_s = 3/2 \tag{4.8}$$

it follows that

$$t_s^* > t_s \tag{4.9}$$

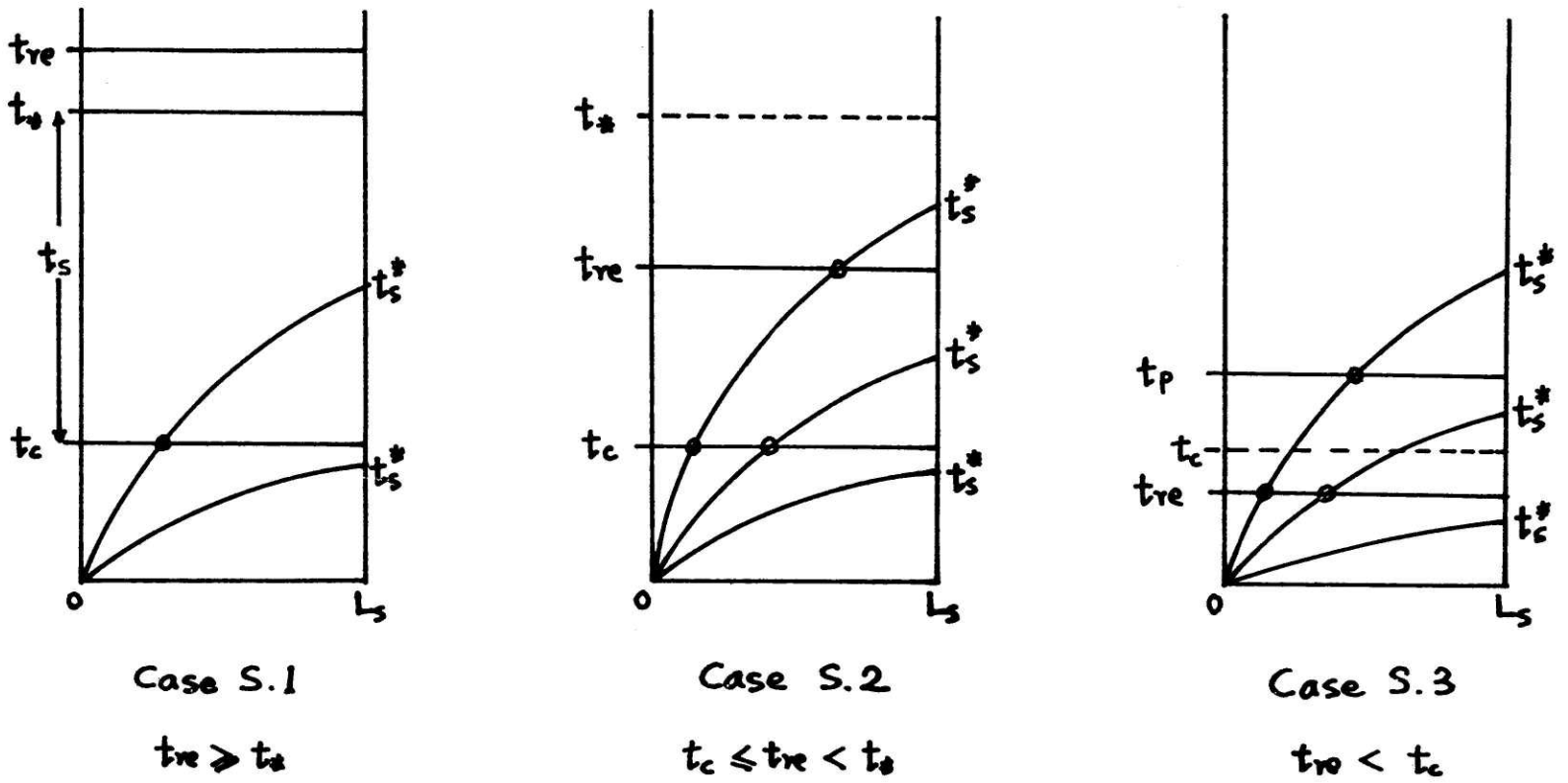

FIGURE 4.4: RELATIVE MAGNITUDES OF t_s^* WITH RESPECT TO t_c, t_p AND t_{re}

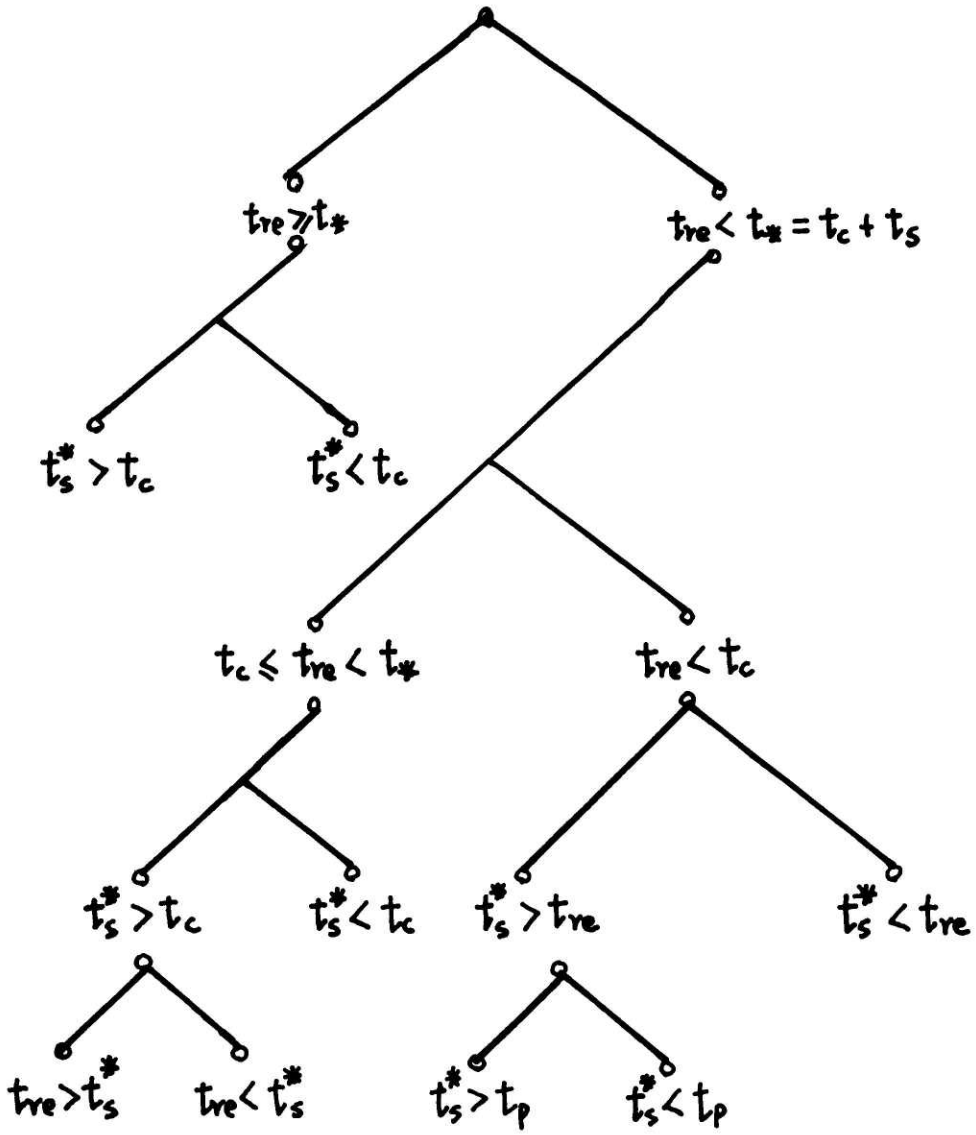

FIGURE 4.5: POSSIBLE PATHS LEADING TO DIFFERENT HYDROGRAPHS

For $t_{re} < t_c$, the kinematic wave equations also impose the condition,

$$t_c > t_p - t_{re} \quad \text{for} \quad 0.35 \leq \frac{t_{re}}{t_c} < 1 \tag{4.10}$$

Proof is shown below. Using Equations (2.61), (2.62), (2.73) and $m_c = 5/3$,

$$i_e(t_p - t_{re}) = \frac{3}{5}(i_e t_c^* - i_e t_{re}) , \qquad t_{re} < t_c$$

$$= \frac{3}{5}\left[\frac{L\, i_e}{\alpha(i_e t_{re})^{2/3}} - i_e t_{re}\right]$$

$$= \frac{3}{5}\left[\frac{\alpha(i_e t_c)^{5/3}}{\alpha(i_e t_{re})^{2/3}} - i_e t_{re}\right]$$

Dividing both sides by $i_e t_c$,

$$\frac{t_p - t_{re}}{t_c} = \frac{3}{5}\left(\frac{t_{re}}{t_c}\right)\left[\left(\frac{t_c}{t_{re}}\right)^{5/3} - 1\right] \tag{4.11}$$

A plot of $\frac{t_p - t_{re}}{t_c}$ against $\frac{t_{re}}{t_c}$ is shown in Figure 4.6, and it is found that, for $t_{re} < t_c$

$$\frac{t_p - t_{re}}{t_c} < 1 \quad \text{for} \quad 0.35 \leq \frac{t_{re}}{t_c} < 1$$

which leads to Equation (4.10).

The stream concentration time, t_s, is determined as follows: For q_L constant at its maximum value

$$q_L = L_c i_e$$

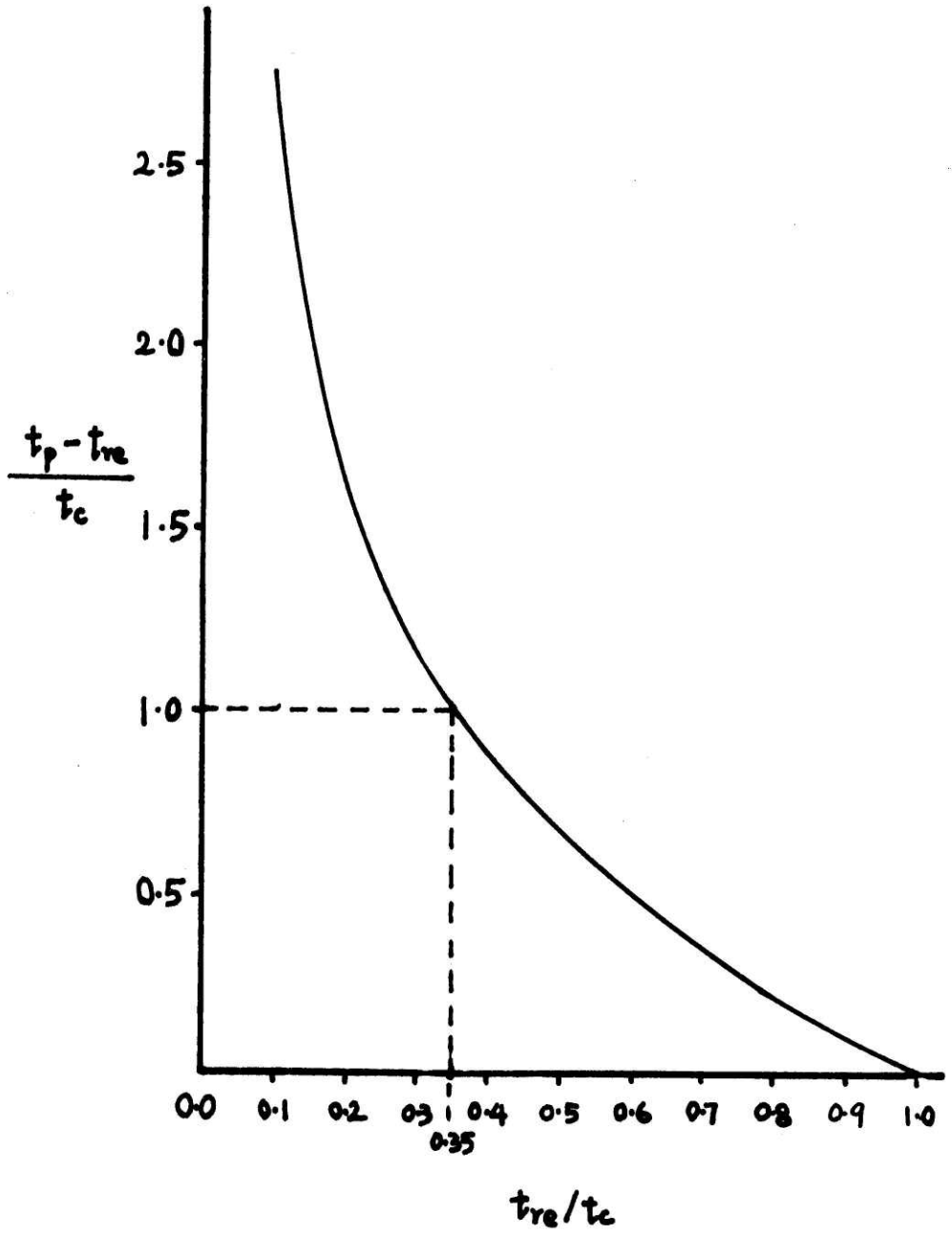

FIGURE 4.6: GRAPHICAL REPRESENTATION OF EQUATION 4.11 FOR $t_{re} < t_c$

from Equation (2.73). From Equations (4.6) and (4.7),

$$\frac{dA_s}{dx_s} = \frac{2q_L}{c_s} = \frac{2L_c i_e}{3/2\ \alpha_s\ A_s^{1/2}}$$

Integrating,

$$\int_{A(o,t_c)=0}^{A(x_s,t)} A_s^{1/2}\ dA_s = \frac{4}{3} \cdot \frac{L_c i_e}{\alpha_s} \int_0^{x_s} dx_s$$

or

$$[A(x_s,\ t)]^{1/2} = \left(\frac{2L_c i_e}{\alpha_s}\right)^{1/3} x_s^{1/3} \qquad (4.12)$$

Substitution into Equation (4.7) yields

$$\frac{dx_s}{dt} = \frac{3}{2}\ \alpha_s\ A_s^{1/2} = \frac{3}{2}\ \alpha_s \left(\frac{2L_c i_e}{\alpha_s}\right)^{1/3} x_s^{1/3}$$

which upon integration results in

$$\int_0^{L_s} x_s^{-1/3}\ dx_s = \frac{3}{2}\ \alpha_s \left(\frac{2L_c i_e}{\alpha_s}\right)^{1/3} \int_{t_c}^{t_c+t_s} dt$$

Finally, from the above

$$t_s = \left|\frac{L_s^2}{2L_c i_e\ \alpha_s^2}\right|^{1/3}, \qquad t_{re} \geq t_c + t_s \qquad (4.13)$$

From Equation (2.53), the concentration time for the overland segment is given by

$$t_c = \frac{L_c^{3/5}}{\alpha^{3/5}\, i_e^{2/5}} \quad , \qquad \text{for} \quad m_c = \frac{5}{3} \tag{4.14}$$

Comparing the magnitudes of t_s and t_c leads to, using Equation (4.13) and (4.14)

$$\frac{t_s}{t_c} = 0.7937 \left(\frac{L_s^{10}\, i_e\, \alpha_c^{9}}{L_c^{14}\, \alpha_s^{10}} \right)^{1/15} \tag{4.15}$$

The number of possible outcomes of the streamflow hydrograph may be reduced by studying the average value of t_s/t_c occurring in nature. This has to be done by relating the ratio t_s/t_c to the effective runoff contributing area A_r and the catchment area A_c. The runoff area is the portion of the catchment area which produces direct runoff.

In Figure 4.1,

$$A_r = 2L_c L_s \tag{4.16}$$

$$A_c = 2L_c' L_s' \tag{4.17}$$

Eagleson (1972), in deriving the distribution for peak stream discharge, assumes that A_r is a narrow band centered along the mainstream with a triangular distribution given by

$$f(A_r) = \frac{2}{A_r} \left[1 - \frac{A_r}{A_c} \right] , \qquad 0 \leq A_r \leq A_c \tag{4.18}$$

which is shown in Figure 4.7.

For geometrically similar natural catchments, the mean of the ratio A_c/L^2 is approximately given by (Eagleson, 1970)

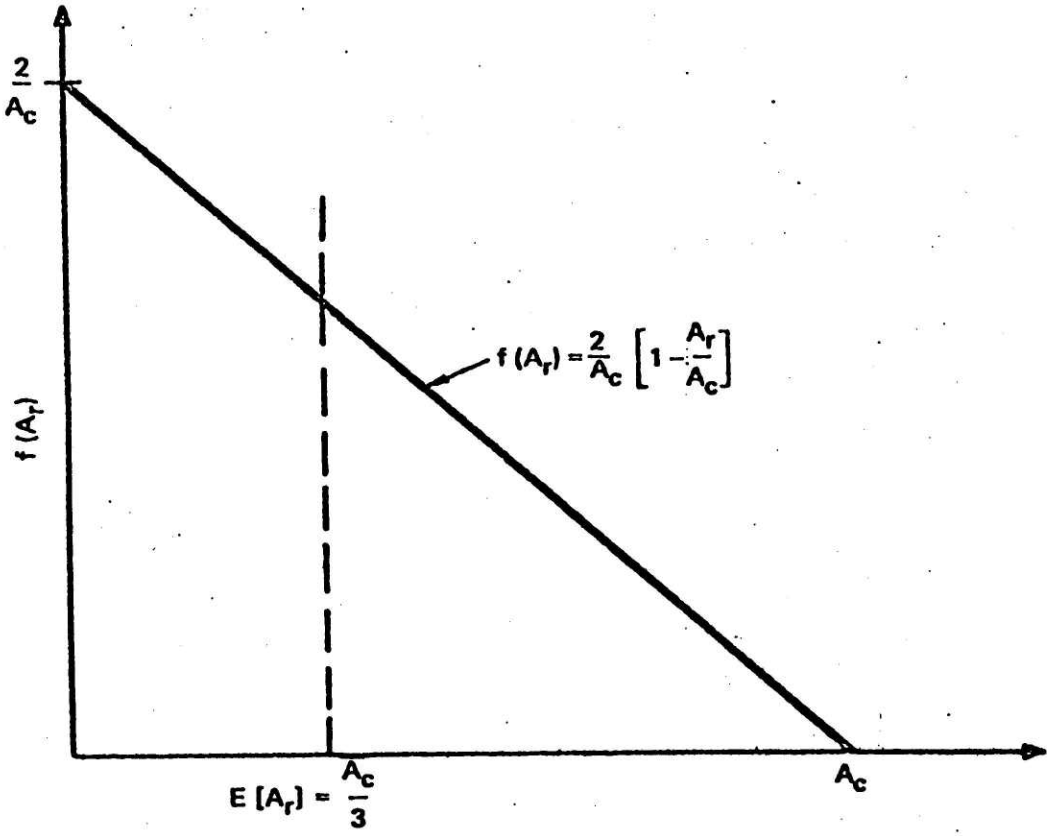

FIGURE 4.7 TRIANGULAR PROBABILITY DENSITY FUNCTION, $f(A_r)$

$$\frac{A_c}{L^2} = \frac{1}{3} \tag{4.19}$$

where A_c = total catchment area

L = length of the mainstream.

Therefore,

$$L_s' = L_s = (3A_c)^{1/2} \tag{4.20}$$

$$L_c' = \frac{1}{6} L_s' \tag{4.21}$$

for a rectangular catchment (see Figure 4.1).

And
$$L_c = \frac{A_r}{2L_s} = \frac{A_r}{2(3A_c)^{1/2}} \tag{4.22}$$

Substituting the above expressions in Equation (4.15) leads to

$$\frac{t_s}{t_c} = 3.65 \left[\frac{A_c^{12}\ \alpha_c^9\ i_e}{\alpha_s^{10}}\right]^{1/15} \cdot A_r^{-14/15} \tag{4.23}$$

Now,

$$E\left[\frac{t_s}{t_c} \mid i_e, A_c, \alpha_c, \alpha_s\right] = \int_0^{A_c} \frac{t_s}{t_c}(A_r) \cdot f(A_r)\, dA_r$$

$$= 3.65 \left[\frac{A_c^{12}\ \alpha_c^9\ i_e}{\alpha_s^{10}}\right]^{1/15} \cdot \frac{2}{A_c} \int_0^{A_c} A_r^{-14/15} \left(1 - \frac{A_r}{A_c}\right) dA_r$$

or

$$E\left(\frac{t_s}{t_c}\right) = 5.12\left(\frac{i_e^{1/15}\ \alpha_c^{3/5}}{\alpha_s^{2/3}}\right) A_c^{-2/15} \qquad (4.24)$$

where i_e = inches/hr.

A_c = square miles

α_c = $ft^{1/3}/sec$

α_s = sec^{-1}

The practical range of parameters reported in literature gives the approximate limits:

$$0.1 \leq \alpha_c \leq 10\ ft^{1/3}/sec$$

$$0.1 \leq \alpha_s \leq 1\ sec^{-1}$$

$$0.01 \leq i_e \leq 6"/hr$$

From the above values, the average value of the ratio $\frac{t_s}{t_c}$ is within the limits:

$$3.77A_c^{-2/15} < E\left|\frac{t_s}{t_c}\right| < 106.62A_c^{-2/15}$$

From this approximation, an important conclusion can be drawn,

$$\frac{t_s}{t_c} >> 1$$

i.e.,

$$t_s >> t_c \qquad (4.25)$$

for all practical catchment sizes.

When Equation (4.25) is combined with Equation (4.9) , it is reasonable to assume that

$$\text{Prob}[t_s^* \geq t_c] \cong 1 \tag{4.26}$$

The inequality, $t_* > t_{re} > t_c$ may be rewritten as (after dividing throughout by t_*)

$$1 > \frac{t_{re}}{t_*} > \frac{1}{1 + \frac{t_s}{t_c}} \tag{4.27}$$

where $t_* = t_c + t_s$.

Since the characteristic curves do not cross one another (assuming constant rainfall) and using Equation (4.9) , the following inequality holds,

$$t_* > t_s^* > t_s$$

Dividing throughout by t_*,

$$1 > \frac{t_s^*}{t_*} > \frac{1}{1 + \frac{t_c}{t_s}} \tag{4.28}$$

But, from Equation (4.25), $\frac{t_s}{t_c} >> 1$, or $\frac{t_c}{t_s} << 1$, implying that the lower limit of the ratio t_s^*/t_* is much closer to unity than that of the ratio t_{re}/t_* (see Equation (4.27)). From this, an additional assumption, which is only slightly less valid than Equation (4.26), is (compare Equations (4.27) and (4.28))

$$\text{Prob}[t_s^* > t_{re}] \cong 1, \quad \text{when} \quad t_{re} < t_* \tag{4.29}$$

For $t_{re} < t_c$, it is true that

$$t_{re} + t_c < 2t_c$$

Since $t_s >> t_c$, it would be most likely that

$$t_s \geq 2t_c > t_{re} + t_c \tag{4.30}$$

Combining Equations (4.9) , (4.10) and (4.30), it is also reasonable to assume that

$$\text{Prob}[t_s^* \geq t_p] \cong 1 \tag{4.31}$$

Finally, using Equations (4.26), (4.29) and (4.31), Figure 4.5 is reduced to Figure 4.8, which represents only three possible streamflow situations.

4.4 Defining Streamflow Hydrographs

In the last section, the most probable situations leading to streamflow hydrographs were identified (Figure 4.8). In this section, a qualitative analysis of those events will be followed.

The characteristic curves are defined by Equations (4.3) through (4.7), and the hydrograph is defined by Equation (4.2). There are only three cases to be considered, as shown in Figure 4.8.

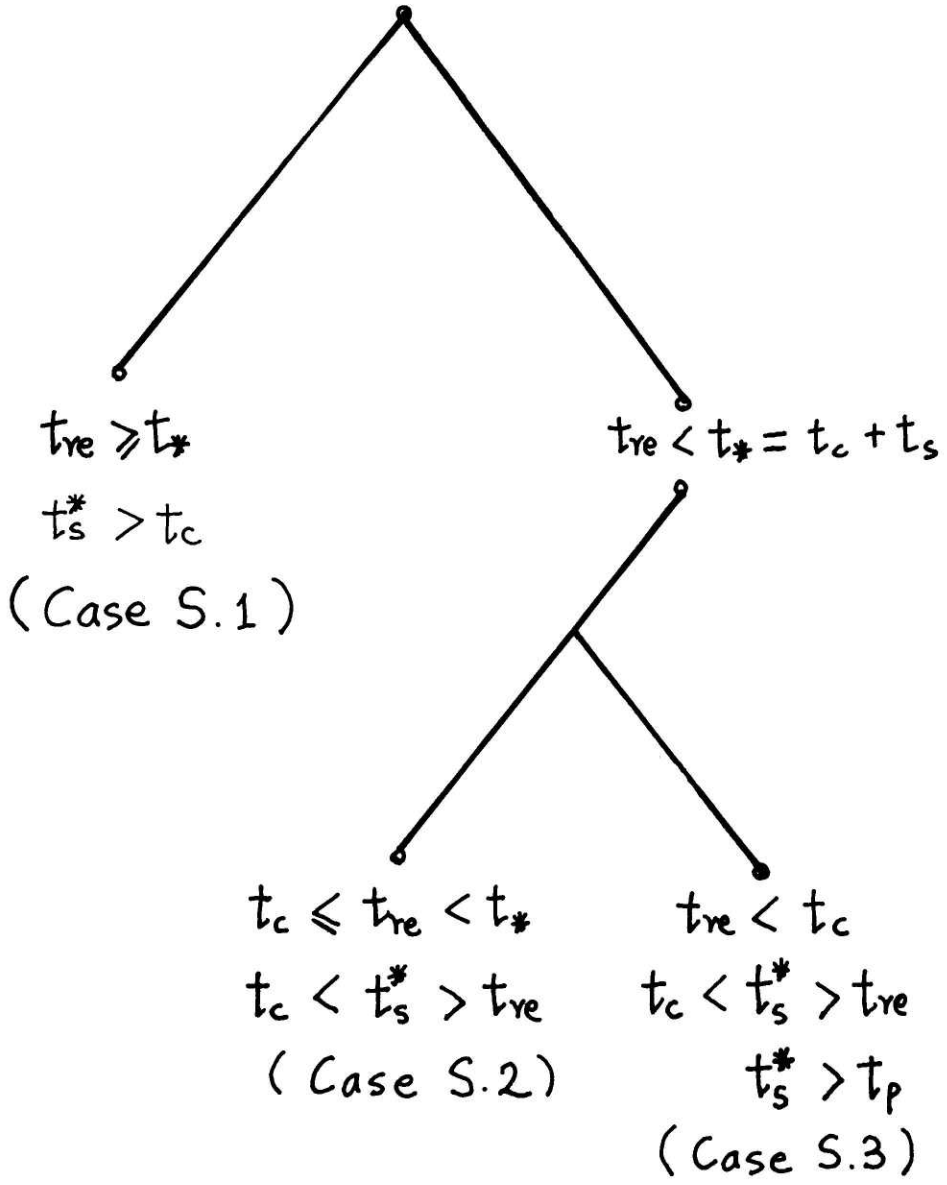

FIGURE 4.8: REDUCTION OF FIGURE 4.5

Case S.1: $t_{re} \geq t_* = t_c + t_s$

$t_s^* > t_c$

The characteristic curves and streamflow hydrograph are shown in Figures 4.9 and 4.10, respectively. In Figure 4.9, since it is known beforehand that $t_s^* > t_c$, an initial disturbance started at $x_s = 0$ will move along curve b reaching x_w ($x_w < L_s$) at $t = t_c$. It will continue to move along curve b until it reaches the stream outlet, L_s at $t = t_s^*$. Notice that when curve b crosses the line $t = t_c$, q_L changes. When q_L changes, the characteristic curve also changes. Thus, the portion of the curve b above or below t_c will be represented by different equations. The two equations will contain the variable x_w, which can be eliminated to form only one equation representing curve b. How this can be done will be demonstrated in Section 4.6.

Somewhere along the stream, there must exist a position x_1, at which an initial disturbance starts and reaches L_s at $t = t_c$. This is shown by curve a. Curve a envelopes a set of curves which start at x_s at $t = 0$ with $x_1 \leq x_s \leq L_s$ and end at L_s with $0 < t \leq t_c$. The characteristic curves do not cross each other. Since the equation of q_L is the same for all these curves and they all start at $t = 0$, they are all represented by one equation. This equation defines Region I in Figures 4.9 and 4.10.

All the curves that are bounded by curves b and a cross $t = t_c$ once and accordingly they can all be represented by the same equation. This defines Region II.

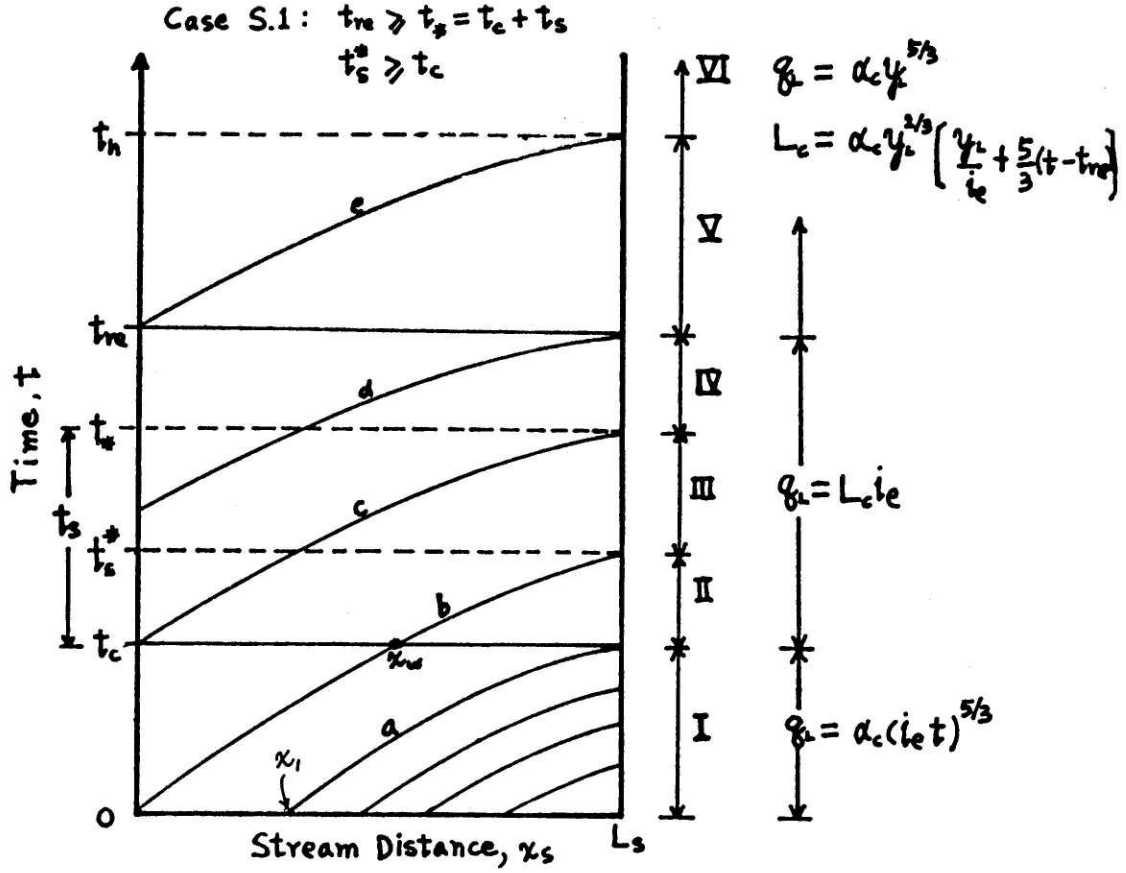

FIGURE 4.9: CHARACTERISTIC CURVES FOR CASE S.1

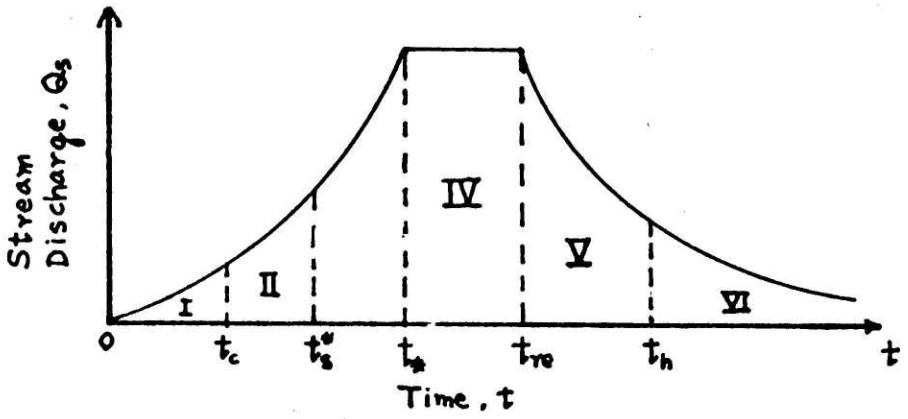

FIGURE 4.10: STREAMFLOW HYDROGRAPH FOR CASE S.1

All the curves that are bounded by curve c and b also cross $t = t_c$ once, at which the equation of q_L changes, but they all start at a time $t = t_o$ in which $0 < t_o < t_c$. Therefore, they are all represented by one equation which is different than the one for Region II. This equation defines Region III.

As can be seen from the figure, Regions IV, V, VI are all represented by different equations. t_h is defined as the time at which a disturbance started at ($x_s = 0$, $t = t_{re}$) reaches $x_s = L_s$.

The corresponding hydrograph is shown in Figure 4.10. It can be seen that in order to describe the entire hydrograph, six equations are needed, one for each region bounded by the dotted lines.

Case S.2: $t_c < t_{re} < t_*$

$t_c < t_s^* \geq t_{re}$

The characteristic curves and streamflow hydrograph are shown in Figures 4.11 and 4.12, respectively. An initial disturbance starts at ($t = 0$, $x_s = 0$) will cross the lines $t = t_c$ and $t = t_{re}$ before reaching L_s as shown by curve c. Curve c is represented by three equations since it crosses through two boundaries at which q_L changes. Elimination of x_w and x_w' reduces three equations to only one, where x_w and x_w' are the positions of the disturbance at $t = t_c$ and $t = t_{re}$, respectively.

Somewhere along the stream exist two positions, x_1 and x_2, where $x_2 > x_1$, from which disturbances start at $t = 0$ and reach L_s at $t = t_c$ and $t = t_{re}$, respectively.

The regions are shown on the figures. Each region is represented

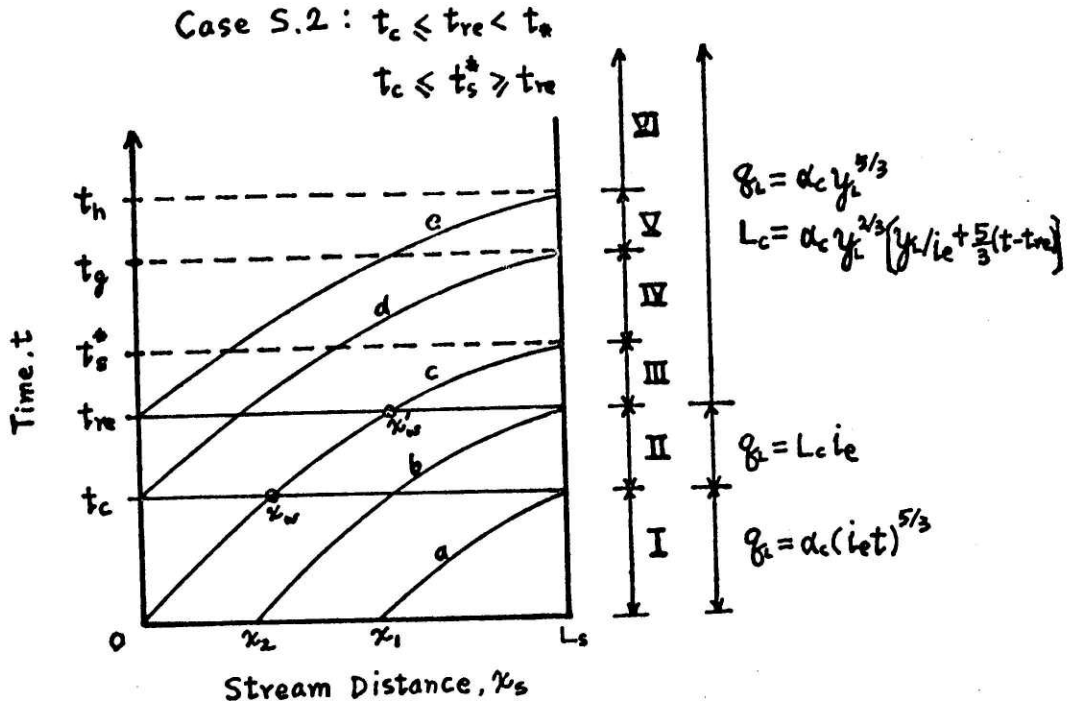

FIGURE 4.11: CHARACTERISTIC CURVES FOR CASE S.2

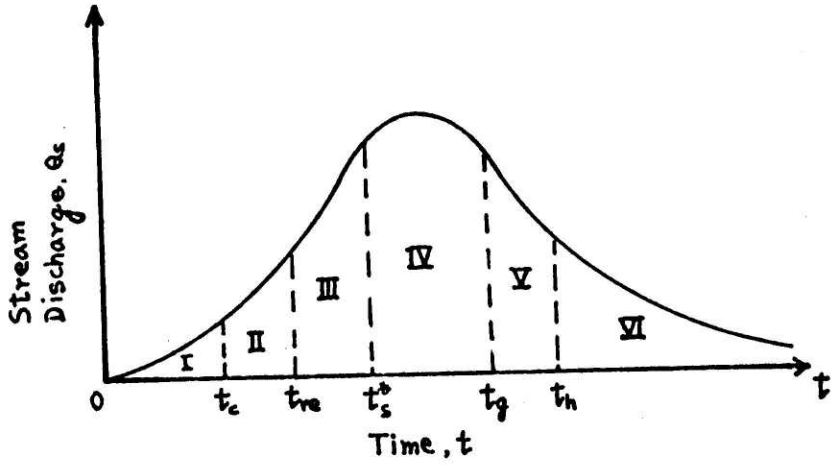

FIGURE 4.12: STREAMFLOW HYDROGRAPH FOR CASE S.2

by a different equation.

The peak discharge would most probably lie between t_s^* and t_g, where the increasing flow from upstream balances the effect of decreasing q_L. t_g is defined as the time at which a disturbance starting at ($x_s = 0$, $t = t_c$) reaches $x_s = L_s$.

Case S.3: $t_{re} < t_c$

$t_c < t_s^* > t_{re}$

$t_s^* > t_p$

The characteristic curves and streamflow hydrograph are shown in Figures 4.13 and 4.14, respectively. With $t_s^* > t_p$, an initial disturbance starting at ($t = 0$, $x_s = 0$) will have to cross the lines $t = t_{re}$ and $t = t_p$ before reaching L_s. Disturbances starting at x_1 and x_2 at $t = 0$ will reach L_s at t_{re} and t_p, respectively. In order to have some idea of when the peak discharge would occur, an additional stream concentration time, t_s'' has to be investigated first.

Let $t_s'' \equiv$ time for the water to travel from $x_s = 0$ at $t = t_{re}$ to $x_s = L_s$ for q_L constant at less than its maximum value given that $t_{re} < t_c$.

From Equation (4.8), it is true that

$$t_s'' > t_s \qquad (4.32)$$

Using Equations (4.10), (4.25), (4.32), it may be concluded that

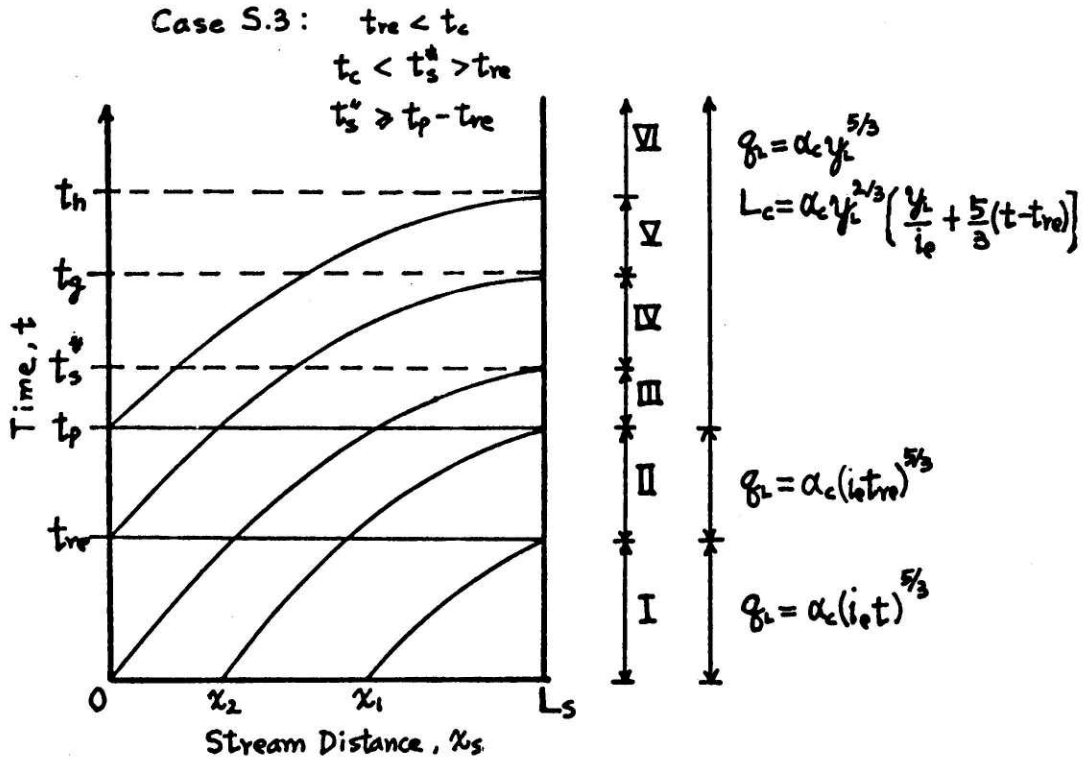

FIGURE 4.13: CHARACTERISTIC CURVES FOR CASE S.3

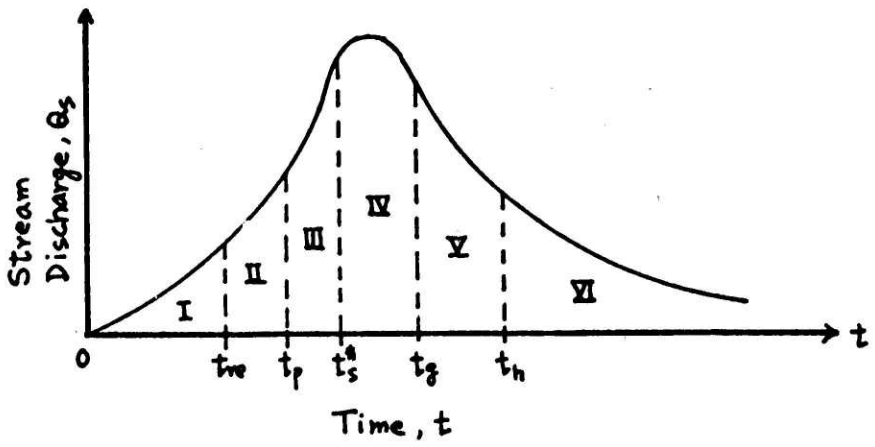

FIGURE 4.14: STREAMFLOW HYDROGRAPH FOR CASE S.3

$$\text{Prob}(t_s'' > t_p - t_{re}) \cong 1 \qquad (4.33)$$

The above condition insures that the peak discharge occurs at a time beyond t_p.

There are altogether six regions. The peak discharge would most likely occur between t_s^* and t_g, where the increasing flow from upstream balances the effect of decreasing q_L.

4.5 Procedure to Obtain the CDF of Flood-Volumes for the Streamflow Case

In order to obtain their CDF, flood-volume expressions must be determined. A look at Figure 4.15 for Case S.1 will indicate how complex the situation is for the streamflow case when compared to the overland flow case. There are three segments on the rising limb. Depending on which segment q_{th_s} cuts across, t_1 will be given by different expressions. Since there are two segments on the receding limb, t_2 may take two different forms. There are six possible expressions for the flood-volume, V_{th_s}, depending on the position of the given threshold discharge, q_{th_s}, where $q_{th_s} \leq Q_{max} = 2L_c L_s i_e$.

An examination of Case S.2 shows that it might have twelve possible expressions for the flood-volume, which is the same number as for Case S.3. If the equation for each segment of the hydrograph is known, it may be possible to eliminate some of the unlikely combinations.

The flood-volume is obtained in a way similar to that of the overland flow case in Chapter 2.

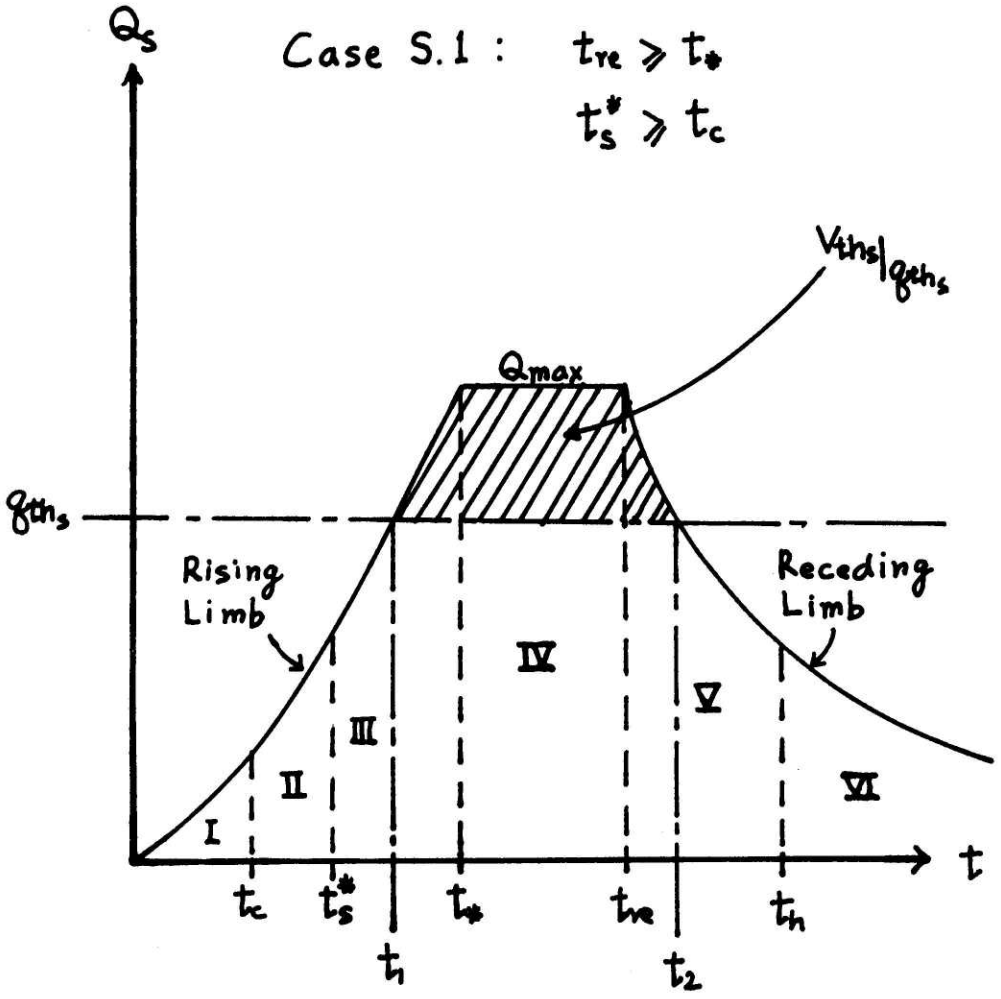

FIGURE 4.15: VOLUME ABOVE A GIVEN THRESHOLD DISCHARGE FOR CASE S.1

Take a simple example as shown in Figure 4.15. As q_{th_s} stands, the flood-volume is computed as follows:

$$V_{th_s}\Big|_{q_{th_s}} = \int_{t_1}^{t_*} Q_{III}(t)\,dt + Q_{max}(t_{re} - t_*) + \int_{t_{re}}^{t_2} Q_V(t)\,dt - q_{th_s}(t_2 - t_1) \qquad (4.34)$$

where $Q_{III}(t)$ = the discharge equation for segment III

$Q_V(t)$ = the discharge equation for segment V

After the flood-volume expression is obtained for each case S.1, S.2, S.3, the CDF of $V_{th_s}|q_{th_s}$ is obtained by

$$F_V(V_{th_s})\Big|_{q_{th_s}} = \int\int_{R_z} f(i_e, t_{re})\,di_e\,dt_{re} \qquad (4.35)$$

where R_z is the shaded region in Figure 4.16, in which all V_{th_s} are less than (V_{th_s}) given.

In the figure, the two dotted lines $t_{re} = t_c$ and $t_{re} = t_*$ separate three regions corresponding to three streamflow cases (S.1, S.2, S.3). The flood-volume expression for Case S.1 is given by $i_e = f_1(t_{re})$, or more correctly by $f_1(t_{re}, i_e, V_{th_s}, q_{th_s}) = 0$. Volumes for Cases S.2 and S.3 are given by $f_2(\cdot)$ and $f_3(\cdot)$, respectively.

4.6 Streamflow Hydrograph for Case S.1: $t_{re} \geq t_* = t_c + t_s^*$, $t_s^* > t_c$

The characteristic curves for this case are shown in Figure 4.17, which is essentially the same as Figure 4.9, except that more

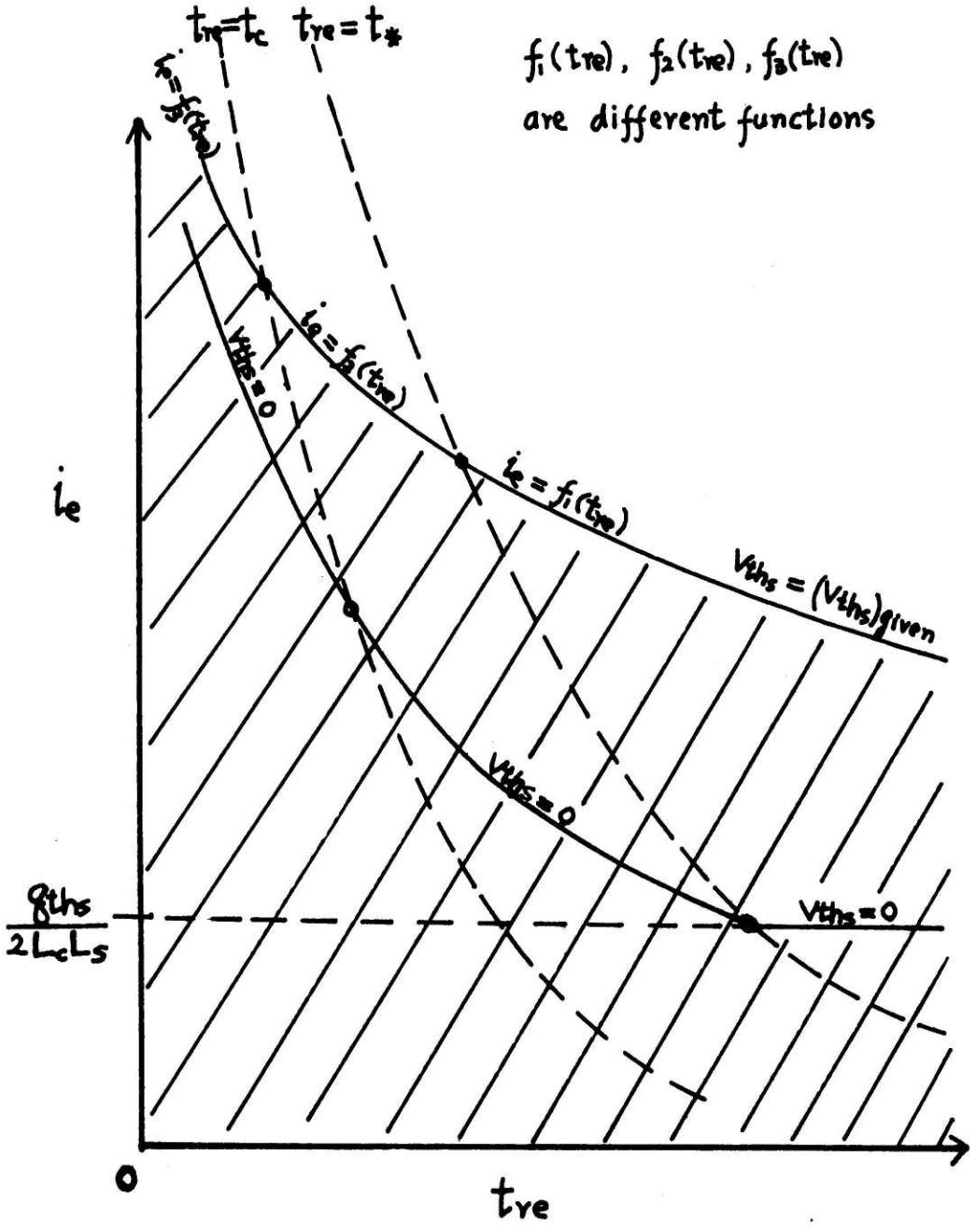

FIGURE 4.16: LINE OF CONSTANT EXCEEDANCE VOLUME AND REGION OF INTEGRATION FOR THE STREAMFLOW CASE

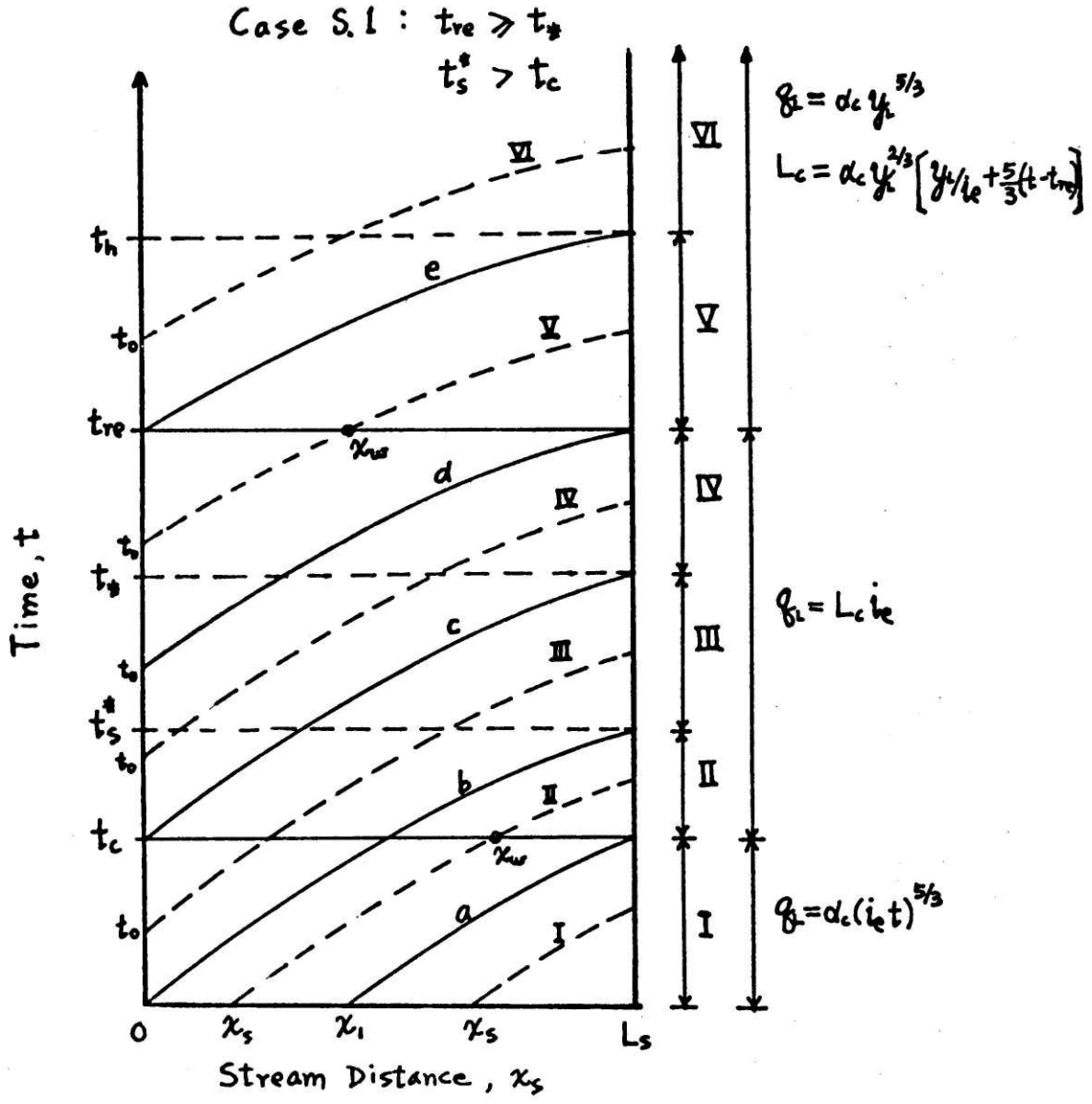

FIGURE 4.17: CHARACTERISTIC CURVES FOR CASE S.1

notations and dotted lines are added. The notations are defined as follows:

t_o = the time at which a disturbance starts at $x_s = 0$, where $t_o > 0$

x_w = the distance along the stream where the characteristic curve crosses the time when the equation of q_L changes.

The numerals stand for both the regions and the characteristic curves that end in those regions.

Since the streamflow hydrograph is given as:

$$Q_s(L_s, t) = \alpha_s A(L_s, t)^{3/2} \tag{4.36}$$

The cross-sectional area at L_s for all times must be evaluated. $A(L_s, t)$ will be obtained for the regions in ascending order. Equations (4.3) through (4.7) are reproduced here for convenience.

$$\frac{dQ_s}{dt} = 2q_L c_s \tag{4.3}$$

$$\frac{dA_s}{dt} = 2q_L \tag{4.4}$$

$$\frac{dQ_s}{dx_s} = 2q_L \tag{4.5}$$

$$\frac{dA_s}{dx_s} = 2q_L/c_s \tag{4.6}$$

$$\frac{dx_s}{dt} = c_s = \frac{3}{2} \alpha_s A_s^{1/2} \tag{4.7}$$

Region I: $0 \leq t \leq t_c$

The characteristic curves in this region are enveloped by curve a. From Equation (4.4), along curve I (dotted in Figure 4.17)

$$A(L_s, t) = \int_{A(x_s, 0) = 0}^{A(L_s, t)} dA = \int_0^t 2\alpha_c i_e^{5/3} t^{5/3} dt$$

or

$$A(L_s, t) = \frac{3}{4} \alpha_c i_e^{5/3} t^{8/3} \quad , \quad 0 \leq t \leq t_c \tag{4.37}$$

Region II: $t_c < t \leq t_s^*$

From Equation (4.4), along curve II, below t_c

$$A(x_w, t_c) = \int_{A(x_s, 0)=0}^{A(x_w, t_c)} dA = 2\alpha_c i_e^{5/3} \int_0^{t_c} t^{5/3} dt$$

or

$$A(x_w, t_c) = \frac{3}{4} \alpha_c i_e^{5/3} t_c^{8/3} \tag{4.38}$$

From Equation (4.4), along curve II, above t_c

$$\int_{A(x_w, t_c)}^{A(L_s, t)} dA = 2L_c i_e \int_{t_c}^{t} dt$$

Therefore,

$$A(L_s, t) = 2L_c i_e (t - t_c) + \frac{3}{4} \alpha_c i_e^{5/3} t_c^{8/3} \quad \text{for} \quad t_c < t \leq t_s^* \qquad (4.39)$$

Region III: $t_s^* < t \leq t_*$

From Equation (4.4), along curve III, below t_c

$$\int_{A(0, t_o)=0}^{A(x_w, t_c)} dA = 2\alpha_c i_e^{5/3} \int_{t_o}^{t_c} t^{5/3} \, dt$$

or

$$A(x_w, t_c) = \frac{3}{4} \alpha_c i_e^{5/3} (t_c^{8/3} - t_o^{8/3}) \qquad (4.40)$$

From Equation (4.4), along curve III, above t_c

$$\int_{A(x_w, t_c)}^{A(L_s, t)} dA = 2L_c i_e \int_{t_c}^{t} dt$$

Therefore,

$$A(L_s, t) = 2L_c i_e (t - t_c) + \frac{3}{4} \alpha_c i_e^{5/3} (t_c^{8/3} - t_o^{8/3}) \qquad (4.41)$$

The above equations both involve 't_o', which can be eliminated. 't_o' will appear in all the regions from now on and eliminating 't_o' will be one of the most difficult operations in solving the hydrograph analytically. A least square fitting technique will be employed in such a process. The following will show how this can be done.

From Equation (4.4), along curve III, below t_c,

$$A(x_s, t') = \int_{A(0, t_o)=0}^{A(x_s, t')} dA = \frac{3}{4} \alpha_c i_e (t'^{8/3} - t_o^{8/3}) \qquad (4.42)$$

where $0 < t_o \leq t' \leq t_c$, $0 \leq x_s \leq x_w$.

From Equation (4.7), along curve III, below t_c

$$x_w = \int_0^{x_w} dx = \frac{3}{2} \alpha_s \int_t^{t_c} [A(x_s, t')]^{1/2} \, dt'$$

Therefore,

$$x_w = \frac{3\sqrt{3}}{4} \alpha_s (\alpha_c i_e^{5/3})^{1/2} \int_{t_o}^{t_c} (t'^{8/3} - t_o^{8/3})^{1/2} \, dt'$$

$$= \frac{3\sqrt{3}}{4} \alpha_s (\alpha_c i_e^{5/3})^{1/2} \int_{t_o}^{t_c} t'^{4/3} \left[1 - \left(\frac{t_o}{t'}\right)^{8/3}\right]^{1/2} dt'$$

Let $y = \left(\frac{t_o}{t'}\right)^{8/3}$ where $0 < \frac{t_o}{t'} \leq 1$, $0 < \frac{t_o}{t_c} \leq 1$

then,

$$x_w = \left| \frac{9\sqrt{3}}{32} \alpha_s (\alpha_c i_e^{5/3})^{1/2} \, t_c^{7/3} \right| \left(\frac{t_o}{t_c}\right)^{7/3} \int_{\left(\frac{t_o}{t_c}\right)^{8/3}}^{1} \frac{(1 - y)^{1/2}}{y^{15/8}} \, dy$$

Let

$$Z = \frac{x_w}{b_o} \quad , \quad \text{where} \quad b_o = \frac{9\sqrt{3}}{32} \alpha_s (\alpha_c i_e^{5/3})^{1/2} \, t_c^{7/3} \qquad (4.43)$$

then

$$Z = \left(\frac{t_o}{t_c}\right)^{7/3} \int_{\left(\frac{t_o}{t_c}\right)^{8/3}}^{1} \frac{(1 - y)^{1/2}\, dy}{y^{15/8}} \quad , \quad 0 < \frac{t_o}{t_c} \leq 1 \qquad (4.44)$$

A plot of Z against $\left(\frac{t_o}{t_c}\right)$ is shown in Figure 4.18. There seems to be only one inflection point on the curve, therefore a third degree polynomial should be expected to fit the curve closely. This fit is also shown in the figure. The least squares fit is given by

$$\frac{t_o}{t_c} = b_1 + b_2 Z + b_3 Z^2 + b_4 Z^3$$

or

$$t_o = t_c\{b_1 + \frac{b_2}{b_o} x_w + \frac{b_3}{b_o^2} x_w^2 + \frac{b_4}{b_o^3} x_w^3 \} \qquad (4.45)$$

where

$$\begin{aligned} b_1 &= 0.9922 \\ b_2 &= -1.1235 \\ b_3 &= 1.2577 \\ b_4 &= -0.8592 \end{aligned} \qquad (4.46)$$

The next step is to eliminate x_w from Equation (4.45).

From Equation (4.4), along curve III, above t_c

$$\int_{A(x_w,\, t_c)}^{A(x_s,\, t')} dA = 2L_c i_e \int_{t_c}^{t'} dt'$$

where $t_c < t' \leq t_*$, $x_w < x_s \leq L_s$

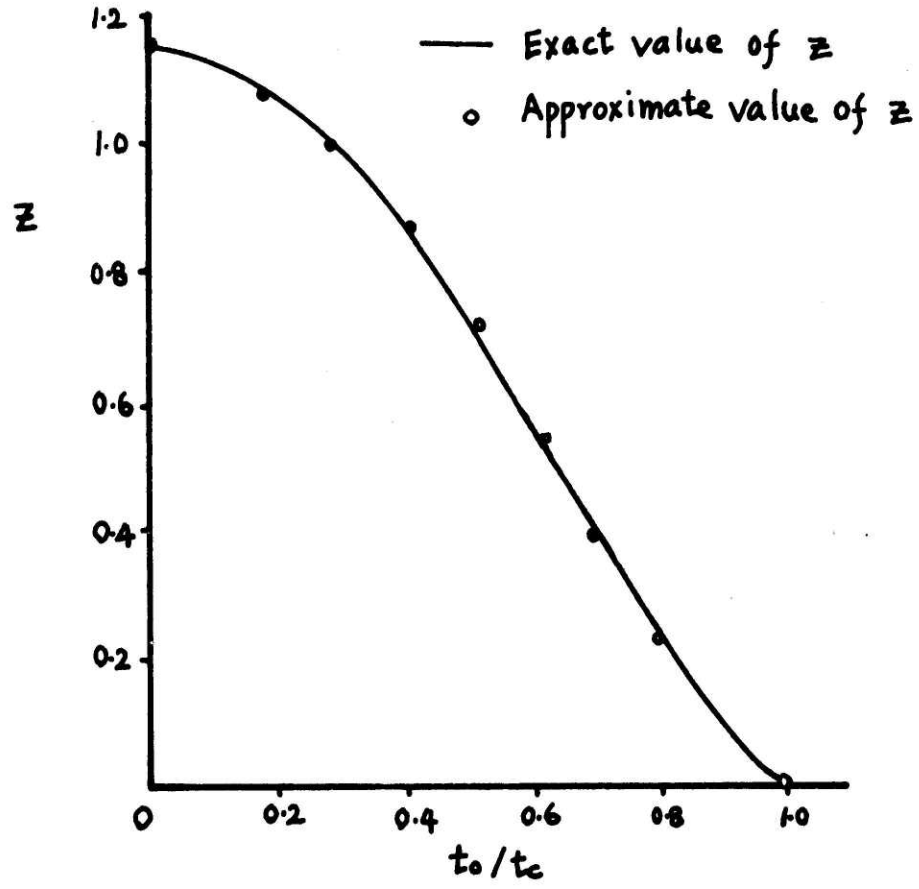

FIGURE 4.18: THIRD DEGREE POLYNORMIAL FIT OF EQUATION 4.44

Therefore,

$$A(x_s, t') = 2L_c i_e (t' - t_c) + A(x_w, t_c) \tag{4.47}$$

where, from Equation (4.40)

$$A(x_w, t_c) = \frac{3}{4} \alpha_c i_e^{5/3} (t_c^{8/3} - t_o^{8/3})$$

Therefore,

$$A(x_s, t') = c_1 t' + c_2 \tag{4.48}$$

where

$$c_1 = 2L_c i_e$$
$$c_2 = \frac{3}{4} \alpha_c i_e^{5/3} (t_c^{8/3} - t_o^{8/3}) - 2L_c i_e t_c \tag{4.49}$$

From Equation (4.7), along curve III, above t_c

$$\int_{x_w}^{L_s} dx_s = \frac{3}{2} \alpha_s \int_{t_c}^{t} (c_1 t' + c_2)^{1/2} \, dt'$$

$$L_s - x_w = \frac{\alpha_s}{c_1} [(c_1 t + c_2)^{3/2} - (c_1 t_c + c_2)^{3/2}]$$

or

$$x_w = L_s - \frac{\alpha_s}{c_1} [(c_1 t + c_2)^{3/2} - (c_1 t_c + c_2)^{3/2}] \tag{4.50}$$

Substituting x_w in Equation (4.45), an implicit relationship between t and t_o is obtained, as

$$f(t, t_o) = 0 \tag{4.51}$$

Using Equation (4.51), the expression for $A(L_s, t)$, (Equation (4.41)) is completely defined. Unfortunately, (4.51) cannot be expressed as $t_o = f(t)$, therefore t_o has to be solved by trial and error, given a value t for which $t_s^* < t \leq t_*$. Then both the value of t and t_o are substituted in (4.41) to obtain $A(L_s, t)$.

Region IV: $t_* < t \leq t_{re}$

In this region, the hydrograph is rather simple because $Q_s(L_s, t)$ is a constant at its maximum.

From (4.5),

$$\int_{Q_s(0, t_o)=0}^{Q_s(L_s, t)} dQ_s = 2L_c i_e \int_0^{L_s} dx_s$$

$$Q_s(L_s, t) = 2L_c L_s i_e \tag{4.52}$$

Region V: $t_{re} < t \leq t_h$

In this region, q_L has to be expressed explicitly as a function of t in order to carry on the integrations. q_L is given by (for $m_c = 5/3$)

$$q_L = \alpha_c y^{5/3} \tag{4.53}$$

and

$$L_c = \alpha_c y^{2/3}[y/i_e + \frac{5}{3}(t - t_{re})] \tag{4.54}$$

where y = overland flow depth at $x_c = L_c$ for time $t > t_{re}$

Equation (4.54) is written as

$$y^{m_c} + m_c i_e (t - t_{re})\, y^{m_c - 1} = \frac{L_c i_e}{\alpha_c} \tag{4.55}$$

Let

where

$$\left.\begin{aligned} y &= m_c i_e (t - t_{re}) Z = k_1 Z \\ k_1 &= m_c i_e (t - t_{re}) \end{aligned}\right\} \tag{4.56}$$

then (4.55) becomes

$$k_1^{m_c} Z^{m_c} + k_1 k_1^{m_c - 1} Z^{m_c - 1} = \frac{L_c i_e}{\alpha_s}$$

or

$$Z\left(1 + \frac{1}{Z}\right)^{1/m_c} = \frac{k_2}{(t - t_{re})} \tag{4.57}$$

where

and

$$\left.\begin{aligned} Z &= \frac{y}{m_c i_e (t - t_{re})} \\ k_2 &= \left(\frac{L_c i_e}{\alpha_c}\right)^{1/m_c} / m_c i_e \end{aligned}\right\} \tag{4.58}$$

Equation (4.55) is reduced to (4.57), a dimensionless form in which the least square fitting technique may be employed.

In Equation (4.57), let

$$\lambda = Z(1 + \frac{1}{Z})^{3/5} = k_2/(t - t_{re}), \text{ for } m_c = 5/3 \qquad (4.59)$$

An examination of the properties of λ shows that when

$$Z << 1 , \quad \lambda \cong Z(\frac{1}{Z})^{3/5} = Z^{2/5} \qquad (4.60)$$

and when

$$Z >> 1 , \quad \lambda \cong Z(1 + \frac{3}{5} \cdot \frac{1}{Z})$$

$$= Z + 3/5 \qquad (4.61)$$

An approximation of Equation (4.59) in the form $Z = f(\lambda)$ is desired so y can be expressed explicitly as a function of t,

$$Z = f(\lambda)$$

or

$$y = mi_e(t - t_{re})\ f\left(\frac{k_2}{t - t_{re}}\right) \qquad (4.62)$$

and

$$q_L = \alpha_c y^{5/3} = \text{function of t explicitly}$$

y is important when $(t - t_{re})$ is small, because that is the time when the recession just begins. When $(t - t_{re})$ is large, y approaches zero and at this portion of the hydrograph, y has hardly any contribution to the flood-volume. When $(t - t_{re})$ is small, Z is large. Therefore, Equation (4.61) is chosen for further manipulation.

A plot of Z versus λ for (4.59) and (4.61) is shown in Figure 4.19.

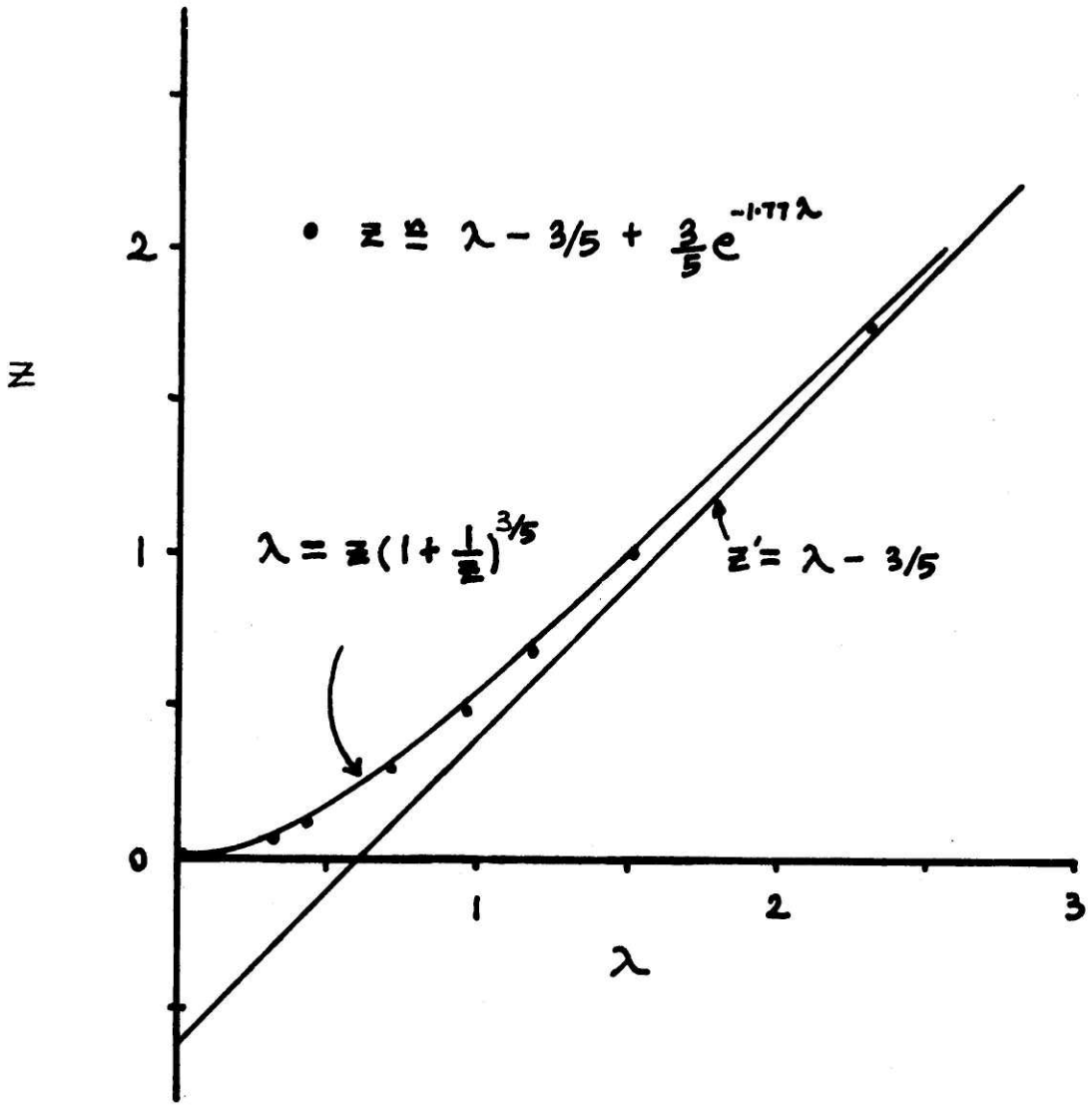

FIGURE 4.19: APPROXIMATION TO EQUATION 4.59

In the figure, Z' is always smaller than Z. When Z is large, the difference between Z and Z' is very small. When Z is small, something has to be added to Z' to correct the error.

Let

$$Z \cong \lambda - \frac{3}{5} + g(\lambda) \tag{4.63}$$

$g(\lambda)$ should be a rapidly decreasing function so that when Z is large, $g(\lambda) \to 0$ and when $Z \to 0$, $g(\lambda) \to 3/5$. An exponential function fulfills all the requirements of $g(\lambda)$, so let

$$g(\lambda) = \frac{3}{5} e^{-\gamma\lambda} \tag{4.64}$$

From Equations (4.63) and (4.64)

$$\gamma\lambda = -\ell n[1 + \frac{5}{3} (Z - \lambda)] \tag{4.65}$$

A plot of λ against $-\ell n[1 + \frac{5}{3} (Z - \lambda)]$ for $0 < Z < 1$ gives the best value of the slope, $\gamma = 1.77$. For $Z > 1$, the difference between Z' and Z is small and $g(\lambda)$ is small too. Therefore, the equation

$$Z \cong \lambda - \frac{3}{5} + \frac{3}{5} e^{-1.77\lambda} \tag{4.66}$$

satisfies the entire range of λ.

Converting back to its original symbols, Equation (4.66) becomes

$$y \cong \left(\frac{L_c i_e}{\alpha_c}\right)^{3/5} - i_e(t - t_{re}) \left|1 - \text{EXP}\left(-\frac{1.77(L_c i_e/\alpha)^{3/5}}{m i_e (t - t_{re})}\right)\right| \tag{4.67}$$

and

$$q_L \cong \alpha_s y^{5/3} \tag{4.68}$$

Some of the graphs for y and q_L are shown in Figure 4.20, 4.21.

Since the purposes of this chapter are to lay out the procedures for obtaining the flood-volume distribution for the streamflow case, and to demonstrate how the hydrographs may be solved analytically by using the least squares fitting technique, it is beyond the scope of this work to solve the entire set of hydrographs. The rest of the regions for Case S.1 (Regions V and VI) will remain to be solved in future work.

4.7 Conclusions

The necessary procedures for obtaining the flood-volume distribution for the streamflow case have been discussed in detail. Methods for obtaining the hydrographs analytically have also been demonstrated. There seems to be little doubt that analytical solution for the flood-volume distribution can be derived, but only with tremendous efforts.

The analytical solutions for the hydrographs, after they have been derived should be compared to the hydrographs obtained by numerical methods so as to test on the goodness of approximations. The properties of these analytical solutions should also be studied, so as to reduce the number of flood-volume expressions to a minimum.

Although the flood-volume distribution has not yet been derived in this work, when done, it will undoubtedly be one of the most useful tools in the design of flood control measures in large basins.

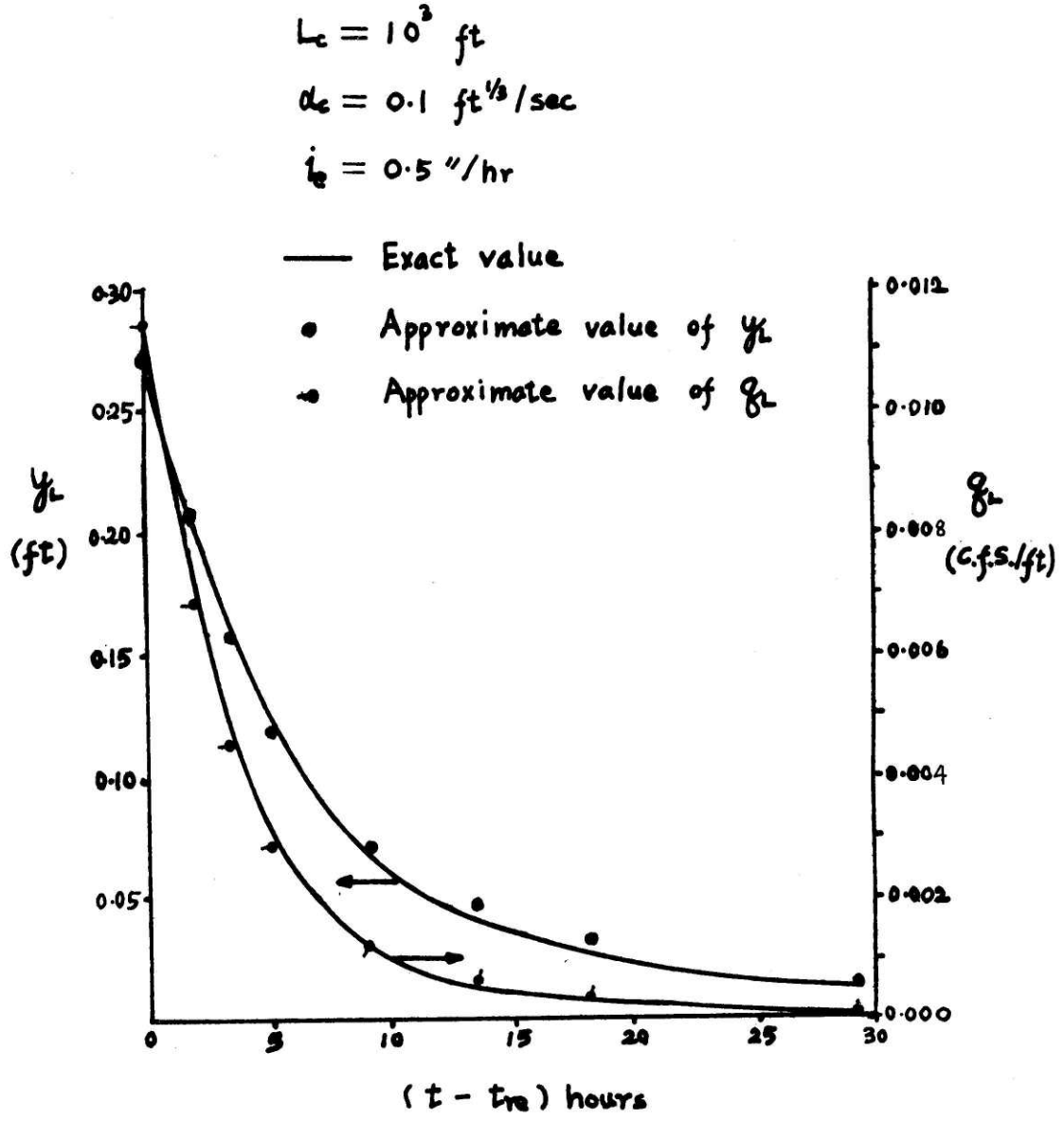

FIGURE 4.20: APPROXIMATIONS TO OVERLAND FLOW DEPTH y_L AND DISCHARGE q_L (I)

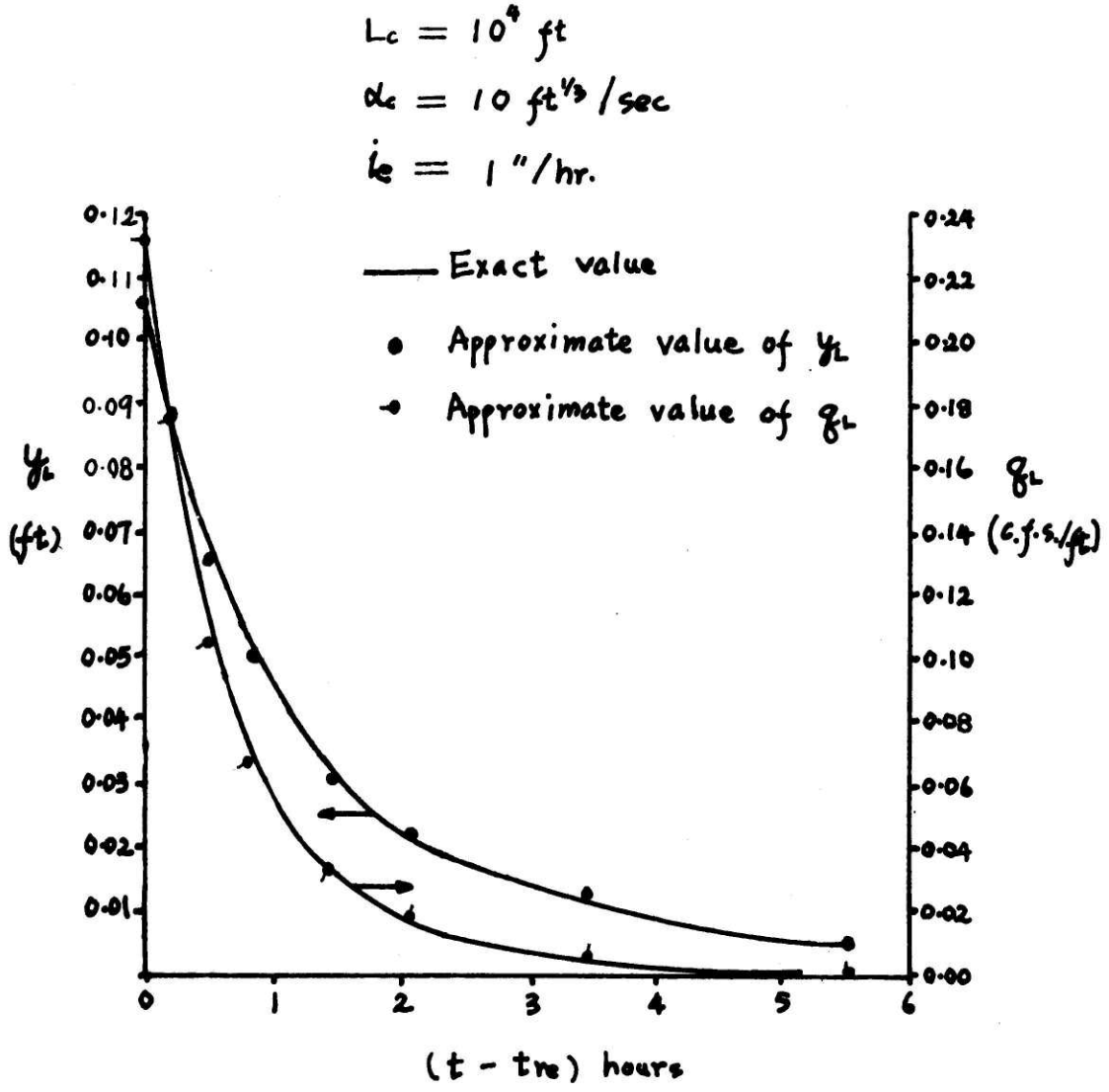

FIGURE 4.21: APPROXIMATIONS TO OVERLAND FLOW DEPTH y_L AND DISCHARGE q_L (II)

Chapter 5

CONCLUSIONS AND RECOMMENDATIONS FOR FUTURE WORK

In this work, the applicability of the derived distribution technique in urban storm drainage problems has been demonstrated. The theoretical, physically-based distribution of the volume of water above a given threshold discharge for the overland flow case is given in a closed, analytical form with few hydrologic and catchment parameters. Application of this distribution function to a small urban catchment, Gray Haven, for flood-control design is shown in Chapter 3. The simplicity of the results allows its general application to any small urban catchment. The procedures for obtaining the flood-volume distribution for the streamflow case have also been outlined.

There seems to be little doubt about the validity of applying the flood-volume distribution function to small urban catchments because the expression is physically-based with catchment parameters computed on a rational basis.

Suggested future work is well defined. It includes, for the overland flow model:

1) Using digital simulation to obtain the annual exceedance series of the flood-volume for comparison for a number of small urban catchments.
2) Developing standard procedures for applying this model to large urban drainage systems.

For the streamflow model:

1) Solving the hydrographs analytically for cases $t_{re} \geq t_*$, $t_c \leq t_{re} < t_*$ and $t_{re} < t_c$

2) Reducing the number of possible flood-volume expressions to a minimum.

3) Deriving the flood-volume distributions of the streamflow case for different regions of threshold discharges in closed-analytical forms.

4) Testing the validity of applying this model to large basins by simulation.

The streamflow model, when completed, should also be applied to large urban catchments to obtain results comparable to those of the overland flow model, hopefully corroborating the validity of using the overland flow model in those situations.

As a solution to the problems of environmental pollution and local flooding caused by combined sewage overflows, the detention by storage method is the best alternative yet conceived. The distribution function of the overflow volumes derived in this work provides a mean for designing the storage volume of interest. Increased urbanization in cities with existing combined sewage overflow problems demands the need for information of this storage volume. Thus, this work will be of great value in solving the environmental pollution and local flooding problems in those cities.

REFERENCES

1. American Society of Civil Engineers, "Design and Construction of Sanitary and Storm Sewers," Manuals and Reports on Engineering Practice, No. 37, New York, N. Y., 1969.

2. American Public Works Association, "Report on Problem of Combined Sewer Facilities and Overflows," Water Pollution Control Research Series WP-20-11, Federal Water Pollution Control Administration, 1967.

3. Benjamin, J. R. and Cornell, C. A., Probability, Statistics and Decision for Civil Engineers, McGraw-Hill Book Company, 1970.

4. Bras, R. L. and Perkins, F. E., "Effects of Urbanization on Catchment Response," Proc. ASCE, Journal of the Hydraulics Division, Vol. 101, No. HY3, March 1975, pp. 451-466.

5. Crawford, N. H. and Linsley, R. K., "Digital Simulation in Hydrology," Stanford Watershed Model IV Technical Report No. 39, Stanford, Calif., Dept. of Civil Engineering, Stanford University, 1966.

6. Cywin, A. and Rosenkranz, W. A., "Advances in Storm and Combined Sewer Pollution Abatement Technology," Paper presented at the 4th Annual Conference of the Water Pollution Control Federation, San Francisco, California, Oct. 3-8, 1971.

7. Daily, J. W. and Harleman, D. R. F., Fluid Dynamics, Addison-Wesley Publishing Company, Inc., Mass., 1966.

8. Eagleson, P. S., Dynamic Hydrology, McGraw-Hill Book Company, 1970.

9. Eagleson, P. S., "Dynamics of Flood Frequency," Water Resources Research, Volume 8, No. 4, 1972.

10. Field, R. and Lager, J. A., "Urban Runoff Pollution Control - State-of-the-Art," Proc. ASCE, Journal of the Environmental Engineering Division, Vol. 101, No. EE1, February, 1975, pp. 107-125.

11. Fleming, G. and Franz, D. D., "Flood Frequency Estimating Techniques for Small Watersheds," Proc. ASCE, Journal of the Hydraulics Division, Vol. 97, No. HY9, September 1971, pp. 1441-1460.

12. Harley, B. M., Perkins, F. E. and Eagleson, P. S., "A Modular Distributed Model of Catchment Dynamics," MIT, Ralph M. Parsons Laboratory for Water Resources and Hydrodynamics, Technical Report No. 133, 1970.

13. Leclerc, G. and Schaake, J. C., Jr., "Derivation of Hydrologic Frequency Curves," MIT, Ralph M. Parsons Laboratory for Water Resources and Hydrodynamics, Technical Report No. 142, 1972.

14. Leclerc, G. and Schaake, J. C., Jr., "Methodology for Assessing the Potential Impact of Urban Development on Urban Runoff and the Relative Efficiency of Runoff Control Alternatives," MIT, Ralph M. Parsons Laboratory for Water Resources and Hydrodynamics, Technical Report No. 167, 1973.

15. Lighthill, M. J. and Whitham, G. B., "On Kinematic Waves. 1 - Flood Movement in Long Rivers," Proc. of the Royal Society of London, Series A, Vol. 229, May 1955, pp. 281-316.

16. Perkins, F. E., "Flood Plain Modeling," Water Resources Research, Vol. 6, No. 3, 1970.

17. Wood, E. F., "An Analysis of the Effects of Parameter Uncertainty in Deterministic Hydrologic Models," Water Resources Research, Vol. 12, No. 5, October, 1976.

18. Wooding, R. A., "A Hydraulic Model for Catchment-Stream Problem," "I. Kinematic-Wave Theory," Journal of Hydrology, Vol. 3, Nos. 3/4, 1965, pp. 254-267.
"II. Numerical Solutions," Journal of Hydrology, Vol. 3, Nos. 3/4, 1965, pp. 268-282.
"III. Comparison with Runoff Observations," Journal of Hydrology, Vol. 4, 1966, pp. 21-37.

19. Tucker, L. S., "Availability of Rainfall-Runoff Data for Sewered Drainage Catchments," ASCE Urban Water Resources Research Program, Technical Memorandum No. 8, ASCE, 1969.

20. U. S. Weather Bureau, "Rainfall Intensity Frequency Regime, 1-5, Technical Paper 29, Washington, D. C., 1957-1960.

APPENDIX A*

Description of Area	Runoff Coefficents
Business	
Downtown	0.70 to 0.95
Neighborhood	0.50 to 0.70
Residential	
Single-family	0.30 to 0.50
Multi-units, detached	0.40 to 0.60
Multi-units, attached	0.60 to 0.75
Residential (suburban)	0.25 to 0.40
Apartment	0.50 to 0.70
Industrial	
Light	0.50 to 0.80
Heavy	0.60 to 0.90
Parks, Cemeteries	0.10 to 0.25
Playgrounds	0.20 to 0.35
Railroad yard	0.20 to 0.35
Unimproved	0.10 to 0.30

Character of Surface	Runoff Coefficients
Pavement	
Asphaltic and Concrete	0.70 to 0.95
Brick	0.70 to 0.85
Roofs	0.75 to 0.95
Lawns, sandy soil	
Flat, 2 percent	0.05 to 0.10
Average, 2 to 7 percent	0.10 to 0.15
Steep, 7 percent	0.15 to 0.20
Lawns, heavy soil	
Flat, 2 percent	0.13 to 0.17
Average, 2 to 7 percent	0.18 to 0.22
Steep, 7 percent	0.25 to 0.35

The coefficients in these two tabulations are applicable for storms of 5- to 10-year frequencies. Less frequent, higher intensity storms will require the use of higher coefficients because infiltration and other losses have a proportionally smaller effect on runoff. The coefficients are based on the assumption that the design storm does not occur when the ground surface is frozen.

*(ASCE, 1969)